Contaminant Transport in Groundwater for Environmental Performance Assessment

by

Yoram Rubin
Dept. of Civil and Environmental Engineering
University of California, Berkeley
Berkeley, CA 94720

TECHNICAL COMPLETION REPORT

Project Number UCAL-WRC-W-836
October, 1997

GEOTECHNICAL ENGINEERING

DEPARTMENT OF CIVIL AND ENVIRONMENTAL ENGINEERING

UNIVERSITY OF CALIFORNIA • BERKELEY

Contaminant Transport in Groundwater for Environmental Performance Assessment

by

Yoram Rubin
Dept. of Civil and Environmental Engineering
University of California, Berkeley
Berkeley, CA 94720

TECHNICAL COMPLETION REPORT

Project Number UCAL-WRC-W-836
October, 1997

The research leading to this project was supported by the University of California Water Resources Center, as part of Water Resources Center Project UCAL-WRC-W-836

Contaminant Transport in Groundwater for Environmental Performance Assessment

Project Number W-836

Investigator: Yoram Rubin and Mark Cushey

Key Words: Groundwater and Groundwater Hydrology, Groundwater management and modeling.

Project Summary

A methodology for simulating 3-D flow and reactive solute transport through statistically anisotropic heterogeneous porous media was developed and demonstrated. First, a method for generating 3-D flow fields in statistically anisotropic heterogeneous porous media was presented. Sample flow fields were generated and analyzed to demonstrate the method and examine the characteristics of 3-D subsurface flow. This stochastic technique was then coupled with a mobile-immobile domain model for simulating the sorption processes. Model results for the spatial moments of the solute plume were shown to capture the major trends observed in the field-scale experiment performed at Borden. These simulations were based on basic site information and independent laboratory data was used to determine the sorption parameters. In a second application of the model, a series of simulations was completed to investigate the coupled effects of heterogeneities of subsurface hydraulic properties and nonequilibrium processes on reactive solute concentrations undergoing transport in three-dimensional natural porous formations. From these analyses, the following observations and conclusions were made:

- The generated velocity fields exhibited the specified spatial correlation structure and mass continuity was observed on a block-by-block level. Cross sectional planes of sample flow fields illustrated the extent and direction of velocity correlations which conformed with previous derivations and theory.
- The method for generating the 3-D flow fields was shown to be computationally efficient in terms of its CPU requirements which increase linearly with the number of velocities or nodes. For the analysis in Chapter 3, 2500 realizations of the flow field were generated whereas previous studies of the site had only reported results from several realizations. In Chapter 4, 350 to 500 realizations of 3-D flow fields were generated for each of the field conditions and parameter settings considered to determine full statistical distributions of local solute concentrations. No other studies at this scale for this number of realizations have been reported in the literature.
- The coupling of the stochastic approach for modeling advective transport with a mobile-immobile model for simulating sorption processes captured the major trends observed in the field data for PCE at the Borden site. This included nearly identical values for the zero and first spatial moments of the plume. The observed second spatial moments were within the predicted 95% confidence intervals. The model results more closely resembled the field data than previous studies reported in the literature.
- The results presented in Chapter 3 also indicate that proper selection of model input parameters is vital. Equilibrium distribution

coefficients must be based on experiments were sufficient time was allowed for equilibrium. The assumption of $f=\phi$ for modeling purposes does not appear to be valid. An alternative is to estimate f based on batch equilibrium experiments or surface area measurements.

- The combined effects of subsurface heterogeneities and nonequilibrium processes associated with sorbing solutes were shown to be non-additive. Sorption processes are rate-limited and their influence at a particular location depends on the time that each portion of the solute plume arrives which can be controlled by the spatial variability of subsurface hydraulic properties.
- As has been reported previously for non-reactive solutes in 2-D formations and instantaneously adsorbing solutes, the distributions for non-reactive solute (tracer) concentrations are non-Gaussian in 3-D statistically isotropic and anisotropic formations.
- In statistically isotropic formations, the concentration distribution for reactive solutes subject to nonequilibrium processes which have characteristic times on the order of advective transport processes were found to resemble truncated normal distributions.
- In statistically anisotropic formations (e=0.1), reactive solutes subject to nonequilibrium processes were found to have log-normal distributions under most conditions considered.

As discussed in Chapter 3, the importance of using only laboratory data for the input parameters should be noted. Many of the mechanisms which can influence the transport of reactive contaminants can be modeled in similar

mathematical forms. Fitting parameters to these models based on observed data does not confirm that the controlling mechanisms have been identified but merely that the true controlling mechanisms can be represented by a similar mathematical form.

The model, in the form presented here, is designed for the simulation of the field-scale transport of dissolved nonpolar organic solutes. It should be noted that for other types of dissolved contaminants such as ionic and/or polar organic compounds and metals, the sorption process may be limited by other mechanisms such as surface reaction kinetics. If these processes are represented by first-order expressions then the model presented here could be utilized by redefining the nondimensional parameters as discussed in Chapter 4. For incorporating other types of kinetic models, accounting for the presence of nonaqueous phase liquids (NAPL), or including continuous sources, eqn 3-1 would have to be modified and new expressions derived for eqns 3-5 through 3-9 using different boundary conditions, if applicable. The technique though would remain the same.

Finally, the relative importance of the potential controlling mechanisms will depend on the type of solute, the properties of the aquifer material, and the scale of the analysis. For field-scale applications, the utilization of a mobile-immobile domain model within the framework of 3-D stochastic groundwater model was shown to simulate the transport of dissolved nonpolar organic compounds and results corresponded directly with site data. The unmapped heterogeneities of the subsurface hydraulic properties, physical and chemical nonequilibrium processes, and the non-ergodic nature of a plume can all be important factors in

assessing the field-scale transport of reactive solutes. In general, the efficiency of the 3-D flow field generator allows for the simulation of the large number of realizations necessary to fully analyze field-scale problems in a probabilistic framework. This combined with the presented approach for modeling reactive nonequilibrium processes provides a means to investigate the impacts and inter-relationships of advective and reactive transport mechanisms and develop a better understanding of the migration of contaminants in the subsurface.

Table of Contents

Table of Contents (continued)

Appendices:

CHAPTER 1

Introduction

The release and transport of contaminants from underground storage tanks, industrial plants, waste disposal sites, and agriculture facilities is a major environmental concern due to the potential for contamination of drinking water supplies and environmentally sensitive aquifers. The transport of these solutes in groundwater is primarily controlled by advection, diffusion and sorption processes as well as chemical and biological transformations. The importance of these individual mechanisms depends on the type of solute, the properties of the aquifer material, and the scale of the analysis. The three scales typically considered are the pore, field, and regional scales which represent formations on the order of less than a meter, ten to hundreds of meters, and tens of kilometers, respectively (Dagan, 1986).

For non-reactive solutes, the spreading of solutes in field experiments has been found to be orders of magnitude larger than predicted values based on laboratory experiments (Gelhar, 1986; Dagan, 1987). This enhanced spreading has been attributed to the spatial variations in the subsurface water velocities which result from the natural large scale heterogeneities of the hydraulic properties of the aquifer. The scale of these heterogeneities is much larger than the pore scale and cannot be measured in a laboratory setting. From a modeling perspective, a deterministic approach would require detailed sampling of all of the subsurface hydraulic properties to account for these heterogeneities. As an alternative, the stochastic approach models these hydraulic properties as spatial random processes. Typically, the hydraulic conductivity (K) is modeled as a

spatially random process or field, while other properties are treated as uniformly distributed.

For reactive solutes, in addition to encountering large scale heterogeneities in hydraulic properties, the solutes are also subject to subsurface chemical and physical processes. These processes can occur instantaneously (relative to advective processes) or can be rate limited. For example, for nonpolar organic solutes, sorption is usually the primary controlling mechanism which retards its migration. Sorption, as referred to here, includes partitioning into soil organic matter and/or physical adsorption. For nonpolar organic compounds, this process is typically considered to occur instantaneously at the water-sorbent interface. In the field, though, since sorption sites are also present within regions of the soil where the fluid is immobile, such as intra-aggregate or dead-end pores, it has been recognized that the sorption process can be rate limited due to mass transfer resistances to and from these immobile regions within the soil. For other types of solutes, the sorption process itself may be rate limited and subject to soil surface reaction kinetics.

One field of research of particular interest is the transport of dissolved nonpolar organic compounds through saturated heterogeneous porous media at the field-scale. Nonpolar (or weakly polar) organic compounds such as tetrachloroethylene (PCE), carbon tetrachloride (CTET), polynuclear aromatic hydrocarbons (PAHs), and hydrocarbons associated with petroleum products or used as solvents are of particular interest since these compounds are widely used in industrial applications and many are known or suspected carcinogens (Patrick et. al., 1987). The field-scale transport of nonpolar organics is not

presently fully understood. In addition, field-scale analysis is applicable to most sites of regulatory concern. Models for these transport processes must be able to account for the heterogeneities and statistical anisotropy common in 3-D natural porous formations. The methodology and discussion presented here focuses of this area of research but many of the findings and analysis are applicable to other areas as noted throughout the text.

The remainder of this introductory chapter provides an overview of the organization of this report and provides a review of the environmental regulatory perspective on contaminant transport modeling. Reviews of the current theoretical and scientific understanding of flow and transport processes are given at the beginning of each of the applicable chapters and are only briefly summarized in the next section.

1.1 Overview

This report is divided into five chapters (including this introduction) and five appendices for additional detailed information. Chapters 2-4 are the primary chapters and each of these includes a separate abstract, introduction and/or background, methodology, results and discussion, and conclusion sections. In Chapter 2, a methodology is developed and demonstrated for simulating 3-D fluid flow in statistically anisotropic heterogeneous aquifers. Next, in Chapter 3, the field-scale transport of dissolved reactive solutes subject to first-order physical (or chemical) nonequilibrium processes are incorporated into the methodology and model results for the spatial moments of the plume are compared with site data. In Chapter 4, the approach is used to analyze the

effects of these transport processes on local solute concentration statistics and distributions. Chapter 5 provides a summary of the conclusions drawn from this analysis. A review on the modeling of the sorption of nonpolar organics onto soils is also included as Appendix C. Each of these chapters and the appendices are discussed below in more detail.

The first portion of this report concerns the development of a rapid technique for simulating 3-D flow fields. This technique is designed to fully simulate 3-D fluid flow in natural porous formations and account for the spatial heterogeneities and statistical anisotropy of subsurface hydraulic properties. Most stochastic modeling efforts have been limited to analysis utilizing two dimensional (2-D) flow fields. Simulations of 3-D flow in heterogeneous porous media have become more common in the literature during the last several years but most of this work has been either limited by the number of realizations which were generated or by their restricted applicability. The primary hindrance to expanding 2-D analysis to 3-D and to generating a greater number of realizations is the computational requirements for applying these techniques. The methodology developed and demonstrated here is different from the more traditional techniques and can rapidly generate 3-D fluid flow fields while maintaining the spatial correlation structure of the subsurface velocities and mass continuity. Chapter 2 provides the details behind the development and testing of this rapid technique. Appendix A provides additional information regarding the procedures utilized.

The next chapter addresses the issues relating to field-scale transport of reactive solutes. As noted above, the transport of organic solutes at the field-scale is

currently not fully understood. The results of the field experiment at the Canadian Air Forces Base in Borden, Ontario indicated that the movement of a nonpolar organic solute plume decelerates with time and undergoes enhanced spreading relative to tracers injected at the same location (Roberts et. al., 1986). Initial efforts to model these observations utilizing a linear equilibrium model to represent the sorption process were unsuccessful (Curtis et. al., 1986). Since then a number of researchers have considered various mechanisms to explain this observed behavior (see Chapter 3). None of these models have adequately reproduced the field observations without fitting model parameters directly to the observed data. To address field-scale transport of dissolved nonpolar organic compounds, an approach is developed which utilizes the methodology for generating 3-D flow fields discussed in Chapter 2 (to account for the spatial variability of the physical subsurface properties on the movement of solutes) and incorporates the additional effects due to the sorption of the solute and rate limited mass transfer processes. Chapter 3 describes the development of this methodology. The model is presented through an analysis of the transport of tetrachloroethylene (PCE) at Borden and results are compared to those from the field experiment. The reaction coefficients are modeled as constant values and are selected independent of the field study by utilizing results from laboratory experiments reported in the literature. These results are compared to the site data, analytical solutions, and previous studies. Additional details regarding the procedures utilized are given in Appendix B. A more general review on the modeling of sorption processes is included as Appendix C. The determination of sorption parameters from laboratory tests is discussed in Chapter 3 with calculations listed in Appendix D.

Lastly, in Chapter 4, the combined effects of the heterogeneities of subsurface hydraulic properties and nonequilibrium processes on local solute concentrations are analyzed for statistically isotropic and anisotropic formations. Most of the prior research in the field of modeling of contaminant and tracer transport processes has focused on determining the ensemble mean concentration of solutes in natural porous formations. Less effort has been devoted to the areas of concentration uncertainty and probability distribution functions (PDF) of concentrations. As a result, estimates are usually limited to the mean and variance of solute concentrations at points of interest. Unless its distribution is known (e.g., Gaussian), solute concentrations are not fully characterized by their first two moments. Previous efforts in this area indicate that the distributions are non-Gaussian. In a two-dimensional analysis, Bellin et. al. (1994) found that the PDF of tracer concentrations were non-Gaussian except when averaged over large areas. Kabala and Sposito (1994) expanded on this work to consider instantly adsorbing reactive solutes and made similar conclusions. Chapter 4 expands on these previous efforts and considers reactive solutes which are subject to physical or chemical nonequilibrium processes. These processes can include intraparticle diffusion, diffusion within the solid matrix, or surface reaction kinetics. The model developed in Chapters 2 and 3 is used to analysis local solute concentrations under a variety of field conditions and for a range of sorption parameters.

Chapter 5 summarizes the conclusions drawn from the analysis presented here. References for all chapters and appendices are included as Chapter 6. The Appendices A-D provide additional detailed information for the modeling procedures and analysis as noted above.

1.2 Regulatory Perspective

Beyond the applications presented here, there are regulatory motivations for developing probabilistic contaminant transport models. The increasing complexity of environmental regulations both at the state and federal level has made it essential to generate estimates in a probabilistic rather than deterministic framework. Models to estimate only average concentrations are no longer completely adequate. The appropriate type and form of model output required is often designated or implied by the applicable regulation(s). In some instances, standards specify the exact form of statistical output. Typical examples are minimum exceedance probabilities for a given concentration criterion and contaminant travel time statistics. In other cases, a probabilistic approach is not directly specified but is implied by the standard's compliance criteria. The following discussion highlights the usefulness of a probabilistic transport modeling approach, like the one developed here, under the current regulatory structure.

As noted above, more recent regulations have directly adopted probabilistic limits. For example, the U.S. EPA has promulgated specific exceedance probabilities and contaminant travel times limits for high level nuclear waste disposal. The EPA rules include a containment requirement that the facility must be designed to assure that the probability of exceeding a radionuclide-specific cumulative release limit is less than 1 in 10 and the probability of exceeding ten times this limit is less than 1 in a 1000 over a 10,000 year period (U.S. EPA, 1986a).

Regulations pertaining to the remediation or clean-up of hazardous waste sites provide an example where a statistical approach is implied rather than strictly stipulated (e.g., state regulations under the Carpenter-Presley-Tanner Hazardous Substance Account Act (CA Superfund) and federal regulations under the Comprehensive, Environmental Response, Compensation and Liability Act (CERCLA)). Feasibility studies or remedial action plans typically require the completion of a risk assessment. Preparation of a risk assessment for a site must include an evaluation of the potential exposure pathways. Transport modeling is an important part of this evaluation (often referred to as an exposure assessment). One purpose of this exposure assessment is to provide input for other portions of the risk assessment in the form of estimated concentrations. These estimates should be in a format consistent with the dose-response information (U.S. EPA, 1986a; U.S. EPA, 1988; Reichard et al. 1990). The type of output required may include mean concentrations, statistical moments, estimated time of exposure, or any number of other formats depending on the form of the dose-response data. These data may be in a variety of formats and may apply to short or extended periods of exposure (Hallenback and Cunnigham, 1986). Transport models should be flexible and provide concentration estimates in a variety of formats to accommodate the risk assessment process. In general, the risk assessment process encourages the use of stochastic formats and the U.S. EPA guidelines suggest the development of percentiles of concentrations whenever possible (U.S. EPA, 1986b).

Similarly, other state environmental regulations imply the use of a probabilistic approach. Many of these regulations include compliance criterion to prevent

"significant" exposure to humans, drinking water supplies, or the environment. For example, several regulations require that the potential for the migration of hazardous constituents to a drinking water source must be shown to be insignificant. The Hazardous Waste Control Act includes such a provision for land treatment units and the Porter-Cologne Water Quality Act includes a similar provision for disposal of waste on land near waterways (Denny et al., 1989). In the case of Proposition 65 (The Safe Drinking Water and Toxic Enforcement Act of 1986), the reference to "significant" exposure is in terms of exemptions to the Act. The basis for exemption is demonstrating that the discharge of a listed chemical will either be at non-detectable levels or will cause "no significant risk" to any source of drinking water (Jennings, 1990; Denny et. al., 1989; Carrick, 1987). Otherwise, the discharge is prohibited. These discharges include both direct discharge into water or onto land where constituents may migrate to drinking water sources. Transport modeling can provide a useful tool for analyzing both of these exemptions. For the former exemption, transport modeling capable of assessing low probability scenarios is necessary. For the second exemption, transport modeling can be used in conjunction with other analyses. Much effort has already been expended to account for "no significant risk" at the exposure point (Jennings, 1990; Carrick, 1987; Griffin and North, 1987). Much of this work has focused on the dose-response portion of a risk assessment, but the importance of the exposure pathways, and therefore the exposure assessment, should not be underestimated. Exposure assessment defines who or what part of the environment will be exposed, at what level the exposure will occur, and for what length of time. The exposure assessment is crucial to the overall assessment and should not be overlooked (Griffin and North, 1987).

Probabilistic transport modeling can help better define the potential for exposure at specific locations and, therefore, determine the extent to which dose-response analyses is necessary to determine "no significant risk".

These regulatory trends are reflected in many recent studies involving contaminant transport modeling. Varshney et. al. (1993) developed a framework for determining exceedance probabilities to analyze the transport of pesticides in groundwater. Their results are presented as exceedance probabilities versus pesticide concentration at a given time and location. Sitar et. al. (1987) and Jang et. al. (1994) applied methods of first-order and second-order reliability analysis to contaminant transport problems for estimating the probability of exceeding specified performance criteria. Massmann and Freeze (1987a,b) and Massmann et. al. (1991) developed a risk-cost-benefit approach and decision analysis procedure which account for the probability of failing to meet regulatory requirements. Examples are given for designing a landfill facility, selecting extraction well pumping rates for removing a contaminant plume, and designing a leachate collection system for a soil remediation facility. McBean and Rovers (1992) analyzed the effect of the assumed distributions for input parameters on the resulting exceedance probabilities utilized in a risk assessment format. Helton (1993) developed a conceptual model to determine complementary cumulative distribution functions (CCDF) to indicate the probability of exceeding individual consequence values as defined by the EPA release limits for high level nuclear waste depositories. Likewise, Campbell and Cranwell (1988) specify the need for results from flow and transport models to be in a probabilistic format to facilitate incorporation with other models to develop a CCDF of the release limit (or summed ratios) as part of a performance

assessment for a proposed site. Lastly, Rautman and Treadway (1991) and Rubin and Dagan (1992a) present their approach to account for geological uncertainties as part of an overall model to generate probability density functions (PDF) of travel times for a nuclear waste repository to address Nuclear Regulatory Commission requirements.

Based on the present form of environmental regulations, it has become necessary to establish transport modeling techniques which can indicate results in a probabilistic format. A study by the National Research Council (1990) has indicated the importance of probabilistic methods for modeling groundwater systems as part of the overall assessment procedure. It is apparent that purely deterministic approaches to transport modeling can no longer supply the necessary information for regulatory analysis. The more appropriate forms of model output include exceedance probabilities over a range of concentrations and complete distributions in the forms of CDF or PDF for concentrations, mass releases, travel times and exposure times. Model results shown here in Chapters 3 and 4 are primarily in the form of spatial moments with confidence intervals and complete distribution functions in the forms of CDF or PDF for local solute concentrations.

CHAPTER 2

Generation of Three-Dimensional Groundwater Flow Fields in Heterogeneous Porous Media

A methodology for generating three dimensional (3-D) flow fields for statistically anisotropic heterogeneous porous media is presented and demonstrated. The simulated flow fields are shown to exhibit the input spatial correlation structure and observe mass continuity. Sample flow fields are presented in the form of cross sectional slices of the 3-D formation. These cross sections demonstrate visually the characteristics of subsurface flow. The method was found to be faster than traditional techniques in terms of its computational requirements. Given this method, it is possible to generate a large number of realizations of a velocity field which is necessary to compute high order statistics in transport problems.

2.1 Introduction

To better assess the movement of contaminants in the subsurface environment, it has become necessary to develop techniques which can fully simulate 3-D fluid flow in subsurface porous media. These techniques must be able to account for the heterogeneities and anisotropy common in geological formations. In general, the physical properties which control fluid flow vary irregularly and unpredictably in subsurface aquifers. Measuring, estimating or mapping these properties in a detailed or deterministic manner is neither feasible nor justifiable. This has lead to the development of stochastic techniques which model these properties as space random functions.

Until recently, though, most stochastic contaminant transport models have been limited to analysis utilizing two dimensional (2-D) flow fields. Simulations of 3-D flow in heterogeneous porous media have appeared in the literature more frequently during the last several years. Unfortunately, most of this work has been either limited by the number of realizations which were generated (Burr et. al, 1994; Robin et al. 1993; Tompson and Gelhar, 1990) or by their restricted applicability (e.g., analysis for isotropic medium only by Chin and Wang, 1992). For the most part, the primary hindrance to expanding 2-D analysis to 3-D and to generating a greater number of realizations is the computational requirements for applying these techniques. A common example is the traditional approach of generating an anisotropic hydraulic conductivity field followed by the computation of fluid velocities utilizing a finite difference or finite element method. This technique can be applied in 3-D but the computational effort becomes excessive given the high resolution required to reproduce reliably the effects of heterogeneity on flow and transport. The method presented here is an alternative to these previous approaches and requires less computational effort without loss of accuracy.

The remainder of this chapter is divided into five sections. The first discusses the methodology used to generate the flow fields. The second assesses the ability of the model to reproduce a spatially correlated field and maintain mass continuity on an individual block basis. The next section presents the results for several sample flow fields in a visual format. This is followed by a section discussing the computational requirements for the model.. The last section presents the conclusions based on this analysis.

2.2 Methodology

The fluid velocity is modeled as a space random function (cf., Dagan, 1984; McComb, 1990) that exhibits a spatially correlated structure attributable to the spatial variability of the hydraulic conductivity. Rather than initially generating a hydraulic conductivity field prior to each iteration (as is typically done in most numerical applications), this method utilizes Gaussian conditioning to generate the fluid velocities directly. The conditioning is based on the spatial correlations of the velocity field which can be derived using Darcy's Law and the flow equation.

The basis of this methodology follows from several important geostastical principles, including :

1. The seemingly irregular behavior observed for fluid velocities in heterogeneous porous media is attributable to the spatially variability of the hydraulic conductivity;

2. For a given spatial structure of the hydraulic conductivity and specified boundary conditions, the spatial correlation structure of the velocity can be derived using Darcy's law and the flow equation. Analytical solutions have been derived for steady state conditions (Rubin and Dagan, 1992b; Rubin, 1990; and Zhang and Neuman, 1992), for a uniformly-recharged field (Rubin and Bellin, 1994), and

for a nonstationary logconductivity field (Rubin and Seong, 1994; Indelman and Rubin, 1995). Numerical solutions have also been developed for steady state conditions (Bellin et. al., 1992 and Levin et. al., 1992);

3. For the quite prevalent case of aquifers with normally distributed logconductivities (Hoeksema and Kitanidis, 1985) and a relatively small logconductivity variance, the fluid velocity is Gaussian and can be fully characterized by its expected value and spatial covariances; and

4. The prediction of the velocity at a generic point x can be carried out using Gaussian conditioning (Mood and Graybill, 1963), which is mathematically analogous to kriging.

Given these principles, a methodology was developed in which all the traditional interim steps are bypassed and the fluid velocity is computed directly at each node using Gaussian conditioning. These velocities include the longitudinal, transverse, and vertical transverse velocities with respect to the mean flow direction and are referred to here as v_1 , v_2 , and v_3 , respectively, or as the velocity vector **v**. This approach has been used to generate two-dimensional flow fields in Bellin et. al (1994) and Rubin et. al (1994).

The Gaussian conditioning equations used to compute the conditional mean and variance of the velocity are given below. Boldface letters denote vectors.

$$U_i^c(\mathbf{x}_N) = U_i + \sum_{k=1}^{m}\sum_{j=1}^{N-1}\lambda_{k,j}^{i}(\mathbf{x}_N)\left[v_k(\mathbf{x}_j) - U_k\right] \qquad \text{for i = 1, ..., m} \qquad (2\text{-}1)$$

$$v_{ij}^c(\mathbf{x}_N) = v_{ij}(\mathbf{x}_N) - \sum_{k=1}^{m}\sum_{j=1}^{N-1}\lambda_{k,j}^{i}(\mathbf{x}_N)v_{kp}\left(\mathbf{x}_N,\mathbf{x}_j\right) \qquad \text{for i, p = 1, ..., m} \qquad (2\text{-}2)$$

where U_i^c = conditional mean velocity in direction i

U_i = unconditional mean velocity in direction i

m = number of dimensions

N = number of conditioning nodes in the search neighborhood

$\lambda_{k,j}^{i}$ = conditioning coefficient, conditions velocity i on velocity k at node j

v_k = velocity in direction k

j = vector of coordinates of node j

v_{ip}^c = conditional variance – covariance tensor

v_{ip} = unconditional variance – covariance tensor

These equations are utilized to calculate the conditional means and variances at each node for each realization of the field. The procedure for generating random deviates based on these conditional statistics and applying these to individual nodes is included in Appendix A. The coefficients ($\lambda_{k,j}^{i}$) in eqns 2-1 and 2-2 are the solution of the linear system of equations:

$$\sum_{k=1}^{m}\sum_{j=1}^{N-1}\lambda_{k,j}^{i}(\mathbf{x}_N)v_{k,p}\left(\mathbf{x}_j,\mathbf{x}_q\right) = v_{ip}\left(\mathbf{x}_N,\mathbf{x}_q\right) \quad \text{for i, p = 1,..., m and q = 1,..., N – 1} \qquad (2\text{-}3)$$

Eqn 2-3 is presented in matrix form and discussed further in Appendix A.

The overall method entails computing the conditional mean and variance of the velocity at a given point (equations 2-1 and 2-2, respectively) which are then used for generating its random deviates. The velocity **v** at a given node x_N (where **x** is a vector representing a location in 3-D space) is conditioned on a subset of the velocities previously generated, $\mathbf{v}(x_1)$ to $\mathbf{v}(x_{N-1})$. This subset is referred to as the search neighborhood. Only a subset is required since the most influential data are those closest to node x_N. This is analogous to *screening* in geostastical analysis and greatly reduces the computational effort without any consequence to the result (Journel and Hujibregts, 1978). A sample of a search neighborhood is shown in Figure 2-1. The open circle represents the node N while the grid intersection points represent the nodes 1 to N-1. The conditioning coefficients utilized are the solution of the kriging system of equations (see equation 2-3). These coefficients do not depend on the actual values at each node but only on the spatial configuration of the nodes relative to the node of interest. Once a set of coefficients is determined for computing $\mathbf{v}(x_N)$ it can be reused to compute the velocities at node x_{N+1} provided that the new set of conditioning nodes has the same spatial configuration (without rotation) as those used to compute $\mathbf{v}(x_N)$. In addition, once a coarse grid of velocities is generated, a refined grid with smaller spacing can be computed utilizing the same technique. A new set of conditioning coefficients is required for each configuration of the search neighborhood utilized in the refinement. For the results shown in this chapter, three configurations were utilized for each level of refinement. The step-by-step procedure for generating a coarse and subsequent refined grids is included in Appendix A.

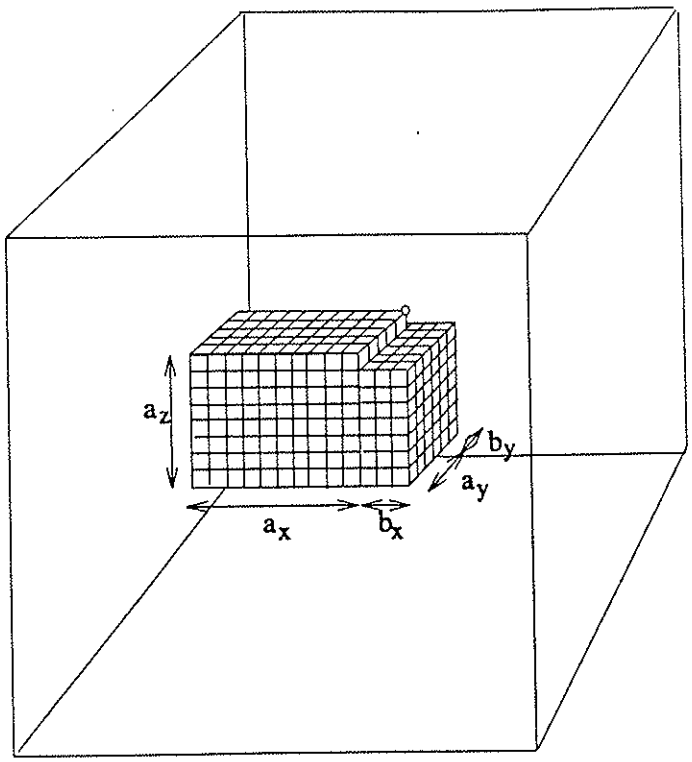

Figure 2–1: Sample Search Neighborhood

The results presented in this chapter are for the case of mean flow in the horizontal direction in a heterogeneous formation which exhibits an anisotropic exponential correlation in the log-conductivity field. The spatial covariance of the velocities used in the present application were determined using a set of quasi-analytical algorithms derived for this case by Rubin and Dagan (1992b) under the assumptions of an unbounded flow domain, small σ_Y^2, steady state conditions, and uniform average flow. The anisotropy of the formation is represented by the ratio of the integral scale of the log-conductivity in the vertical direction ($I_{Y,V}$) over the integral scale in the horizontal direction ($I_{Y,H}$). This is designated as e where $e = I_{Y,V} / I_{Y,H}$.

2.3 Spatial Statistics and Mass Balance Considerations

A series of simulations was undertaken to determine the most efficient size and configuration of the search neighborhood and to analyze the model's ability to reconstruct the appropriate spatial statistics. Figure 2-2 compares the spatial covariances of the velocities for a set of simulated fields with the quasi-analytical solutions for $e = 1$. For the simulated fields, the velocity spatial covariance $v_{ij}(\mathbf{r})$ was defined as:

$$v_{ij}(\mathbf{r}) = \left\langle \left[v_i(\mathbf{x}) - \langle v_i \rangle \right] \left[v_j(\mathbf{x}+\mathbf{r}) - \langle v_j \rangle \right] \right\rangle \quad \text{for } i,j = 1,2,3 \tag{2-4}$$

The vector $\mathbf{r}$ represents the separation distance between the nodes with r_1, r_2, and r_3 being the separation distances in the x, y, and z directions, respectively. The covariances in Figure 2-2 have been non-dimensionalized by the unconditional mean velocity (U) and normalized by the logconductivity

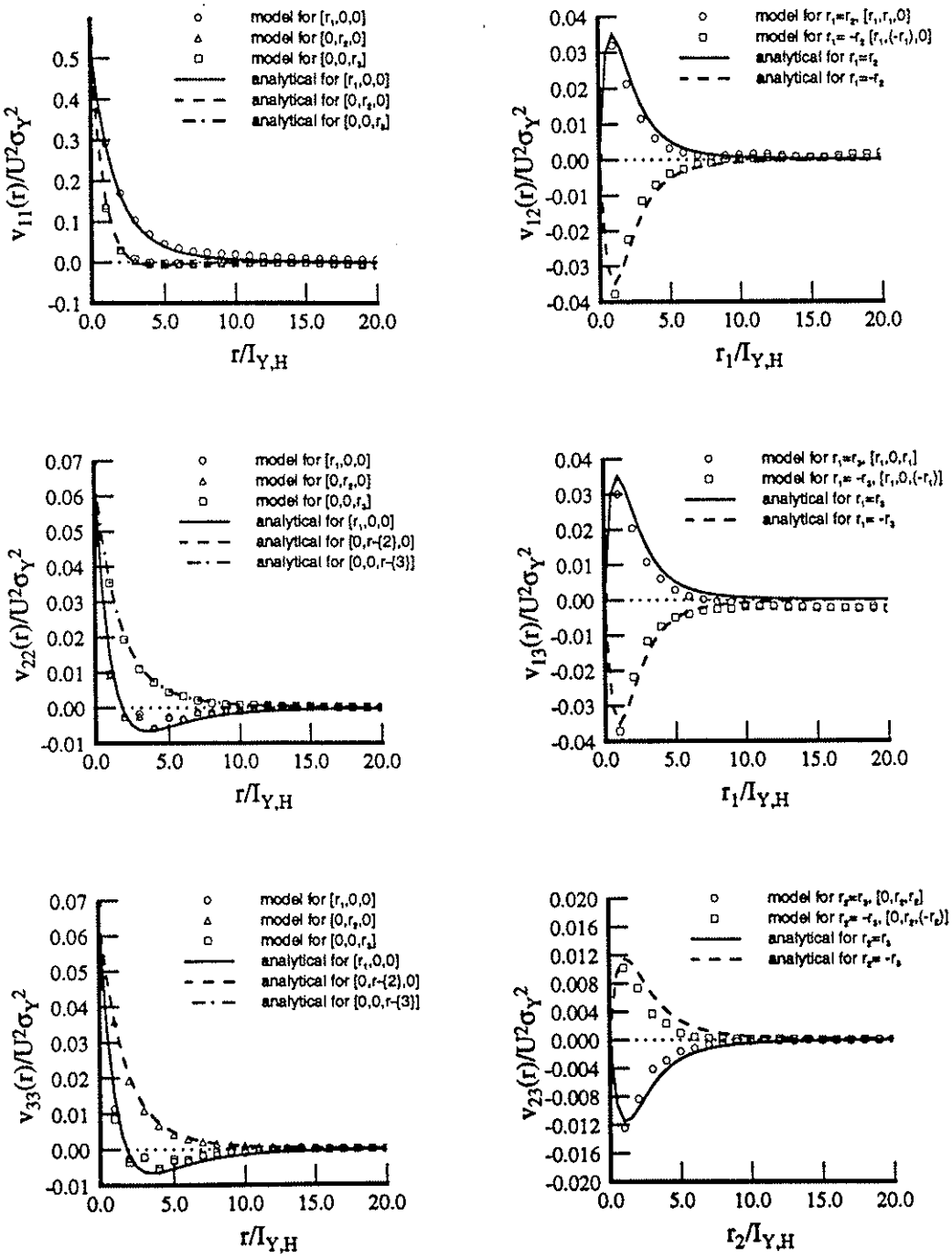

Figure 2-2: Velocity spatial covariances with symbols representing model results and lines representing quasi-analytical solutions from Rubin and Dagan (1992b)

variance (σ_Y^2). As can be seen, the model correctly reproduces the spatial correlation structure. The results shown are for 10 realizations of a 80 $I_{Y,H}$ x 80 $I_{Y,H}$ x 80 $I_{Y,V}$ grid with an initial coarse spacing of $\Delta = 2\ I_Y$ which was refined to $\Delta = 1\ I_Y$. The velocities were conditioned over a volume 14 $I_{Y,H}$ x 14 $I_{Y,H}$ x 6 $I_{Y,V}$ (search neighborhood). The corresponding lengths as shown in Figure 2-1 are $a_x = 10\ I_{Y,H}$, $b_x = 4\ I_{Y,H}$, $a_y = 10\ I_{Y,H}$, $b_y = 4\ I_{Y,H}$, $a_z = 6\ I_{Y,V}$.

The results of these simulations were also analyzed in terms of the mass balance error on a block-by-block basis. Mass conservation is implicit in the velocity spatial covariance algorithms utilized to compute the conditioning coefficients. This derivation ensures that, for a point, the flow is divergence free. The generation of velocities over a 3-D grid, though, will result in some error when considering the mass balance over individual blocks. The theoretical mean of this error can be shown to be zero (Bellin et al., 1992) but the variance of this error will be non-zero. The mass balance error ($M_{e,i}$) was calculated as follows:

$$M_{e,i} = q_{in,i} - q_{out,i} \tag{2-5}$$

where $q_{in,i}$ and $q_{out,i}$ are the volumetric inflow and outflow, respectively, for block i. The mean and variance of this error were calculated over the entire grid for single realizations. The variances are shown for different grid spacing in Figure 2-3. Bellin et. al (1994) derived an expression for the variance of the mass error for 2-D flow. A similar derivation for 3-D indicates that the variance should decrease linearly with Δ^4. Figure 2-3 illustrates the variance of the error per unit area (variance divide by $\Delta^4\ U^2$) for different spacing.

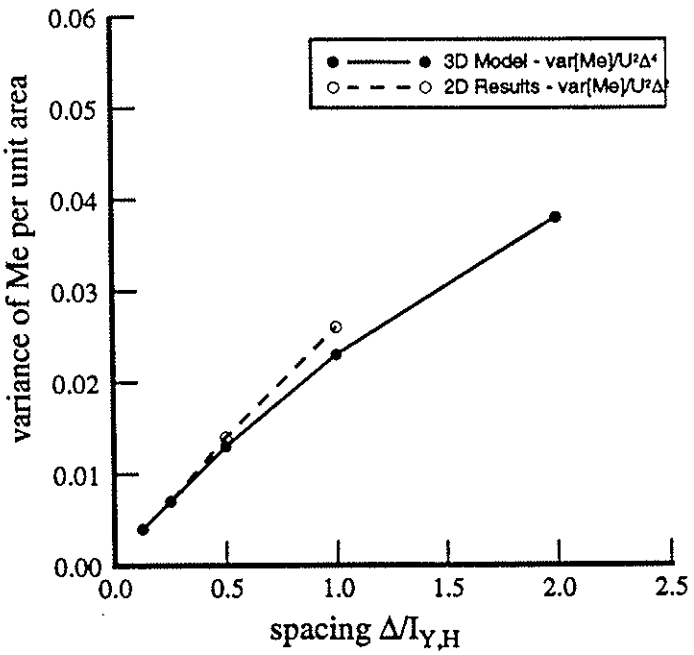

Figure 2-3: Variance of the mass balance error. $\Delta=\Delta_x=\Delta_y=\Delta_z$ and $I_{Y,H}=I_{Y,V}$

2D results from Bellin et al. 1994

The results are nearly linear for the three smallest spacings considered and the intercept, extrapolated from these points, passes close to the origin. These results indicate that the model conforms with its theoretical basis, and furthermore, that the error can be controlled by varying Δ.

Another way of measuring the mass balance error is to consider the absolute percentage error observed for each block. This error (α_i) was defined as follows:

$$\alpha_i = \frac{q_{in,i} - q_{out,i}}{\bar{q}_i} \tag{2-6}$$

where $\bar{q}_i$ is the mean flow through block i. Figure 2-4 illustrates the mean absolute percent mass error calculated for various spacing. These results indicate that the mass error decreases as the grid spacing decreases. Also, the average absolute error can be expected to be less than 2 % when a grid spacing of 0.25 or less is utilized.

Figures 2-2 to 2-4 indicate that the generated flow fields exhibit the specified spatial covariance structure and observe mass continuity on a block-by-block level.

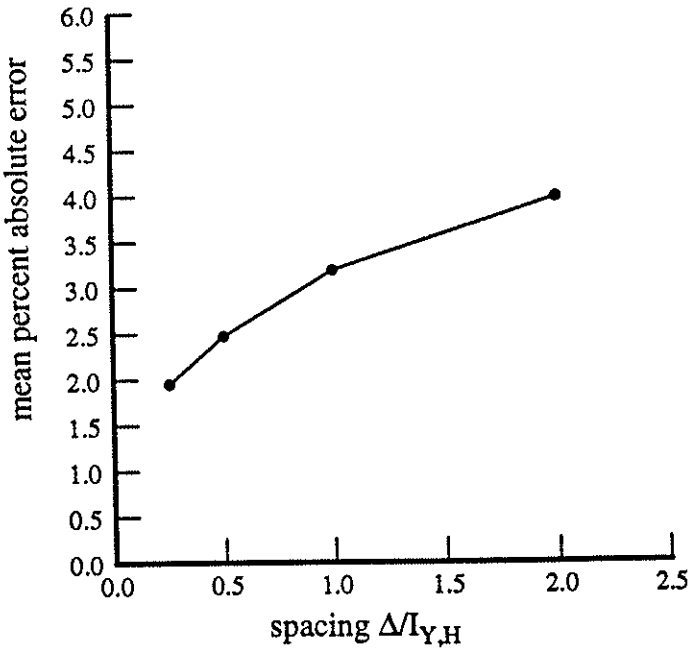

Figure 2-4: Percent absolute mass balance error. $\Delta=\Delta_x=\Delta_y=\Delta_z$ and $I_{Y,H}=I_{Y,V}$

2.4 Sample Flow Fields

Model output includes velocities in three directions at each node of a 3-D grid. These velocities are displayed in the form of cross sectional slices of the flow field to illustrate the direction and extent of their correlation within heterogeneous isotropic and anisotropic porous media.

A series of flow fields (single realizations) were generated for a grid with dimensions 40 $I_{Y,H}$ x 40 $I_{Y,H}$ x 20 $I_{Y,V}$ with a spacing of $\Delta = 0.25\ I_{Y,H}$ in the x and y direction and $\Delta = 0.25\ I_{Y,V}$ in the z direction. The scenarios considered included two values for the log-conductivity variance ($\sigma_Y^2 = 0.2$ and 1.0) and an isotropic ($e = 1$) and anisotropic ($e = 0.1$) formation. For comparison purposes, the same set of random numbers were used for each scenario (single realizations only) so that observed differences would be attributable only to the input parameters. Figure 2-5 illustrates the 3-D grid and identifies the cross sectional planes which are displayed in later figures.

The longitudinal velocity (v_1) for the xy plane is shown in Figures 2-6(a) and 2-6(b) for an isotropic structure with $\sigma_Y^2 = 0.2$ and 1.0, respectively. The extreme values, indicated by the lightest and darkest shading, are more prevalent for the higher log-conductivity variance case indicating greater variability in the velocity field, as would be expected. Figure 2-6 also illustrates the direction of and extent of the spatial correlation for v_1. The light and dark sections are longest in the x direction which corresponds with the integral scale of v_1 being greater in the longitudinal than the transverse

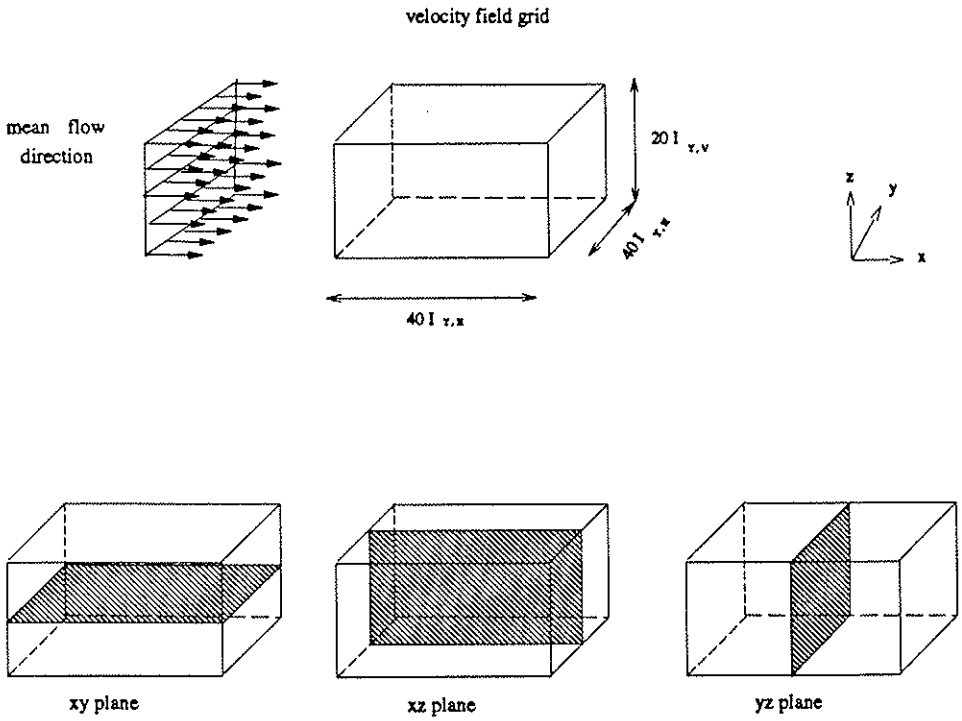

Figure 2–5: Orientation of cross sectional planes within a velocity field grid

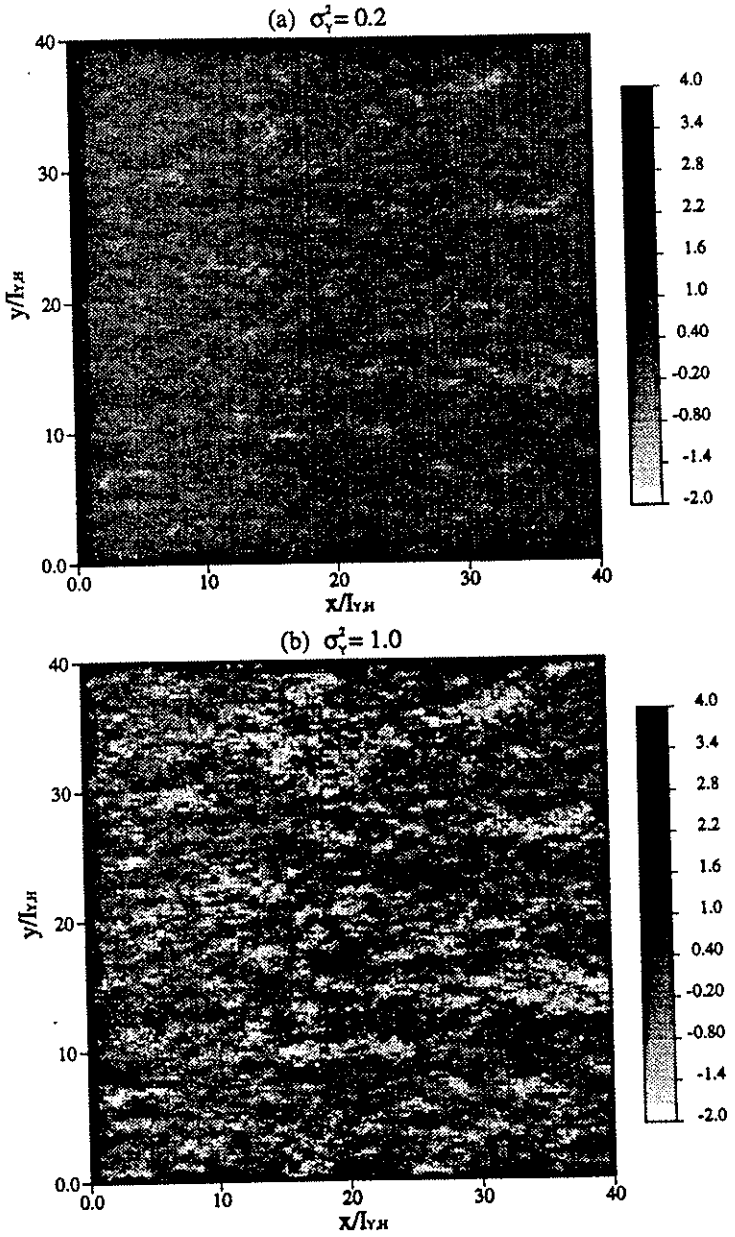

Figure 2-6: Longitudinal velocities (v_1) in a xy plane cross section for (a) σ_Y^2=0.2 and (b) σ_Y^2=1.0
Velocities are non-dimensionalized by the mean flow U.

direction. This is better illustrated in Figure 2-7 which displays the velocity v_1 in three ranges indicating high, average, and low velocities. For these figures the correlation structure is more distinct and indicates that regions of high or low velocities for v_1 can exhibit correlations on the order of 10 to 20 I_Y in the longitudinal direction. The correlations are much less pronounced in the transverse direction but can still be 2 or 3 I_Y. The significance of these figures is in demonstrating that the velocity varies more smoothly in space compared to the logconductivity. The smaller variability reflects the constraint imposed on the velocity by the boundary conditions and mass conservation and was mentioned recently by Glimm et al. (1993) as a possible explanation fro the robustness of the linear theory used here at large σ_Y^2.

Figure 2-8 shows the cross sectional slices for the velocities v_2 and v_3 in the xy, xz, and yz planes. In the xy plane (Figures 2-8(a) and 2-8(b)), the velocity v_2 exhibits its strongest correlation along the diagonal as indicated by the light and dark cross-hatching while the velocity v_3 is most strongly correlated in the y direction. This is reversed in the xz plane (Figures 2-8(c) and 2-8(d)). In the yz plane (Figures 2-8(e) and 2-8(f)), v_2 and v_3 are correlated primarily in the z and y directions, respectively. The correlation of v_2 is at its maximum along the vertical transverse direction (z-axis) and minimum along the longitudinal and transverse direction (x-axis and y-axis) and v_3 is at its maximum along the y-axis and minimum along the x-axis and z-axis (see Figure 2-2).

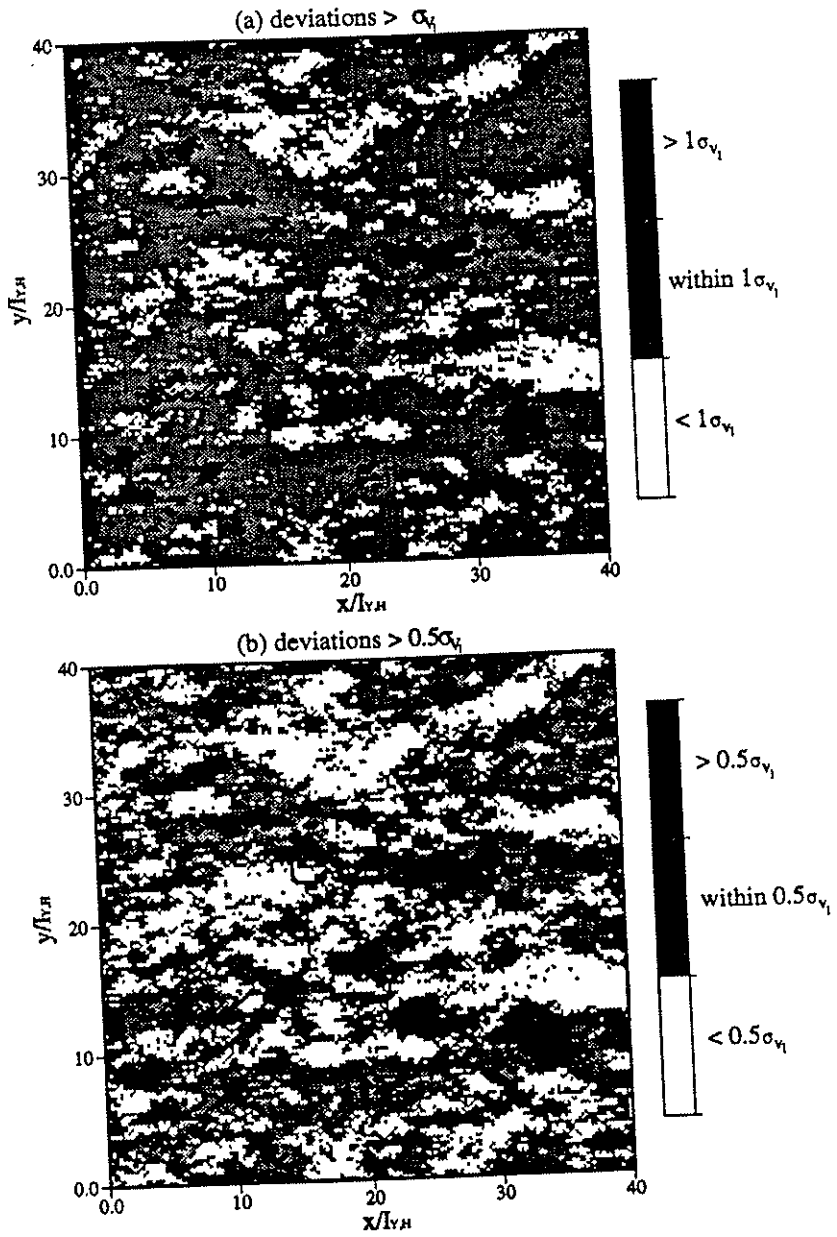

Figure 2-7: Deviations in the longitudinal velocities (v_1) from its mean in a xy plane cross section.

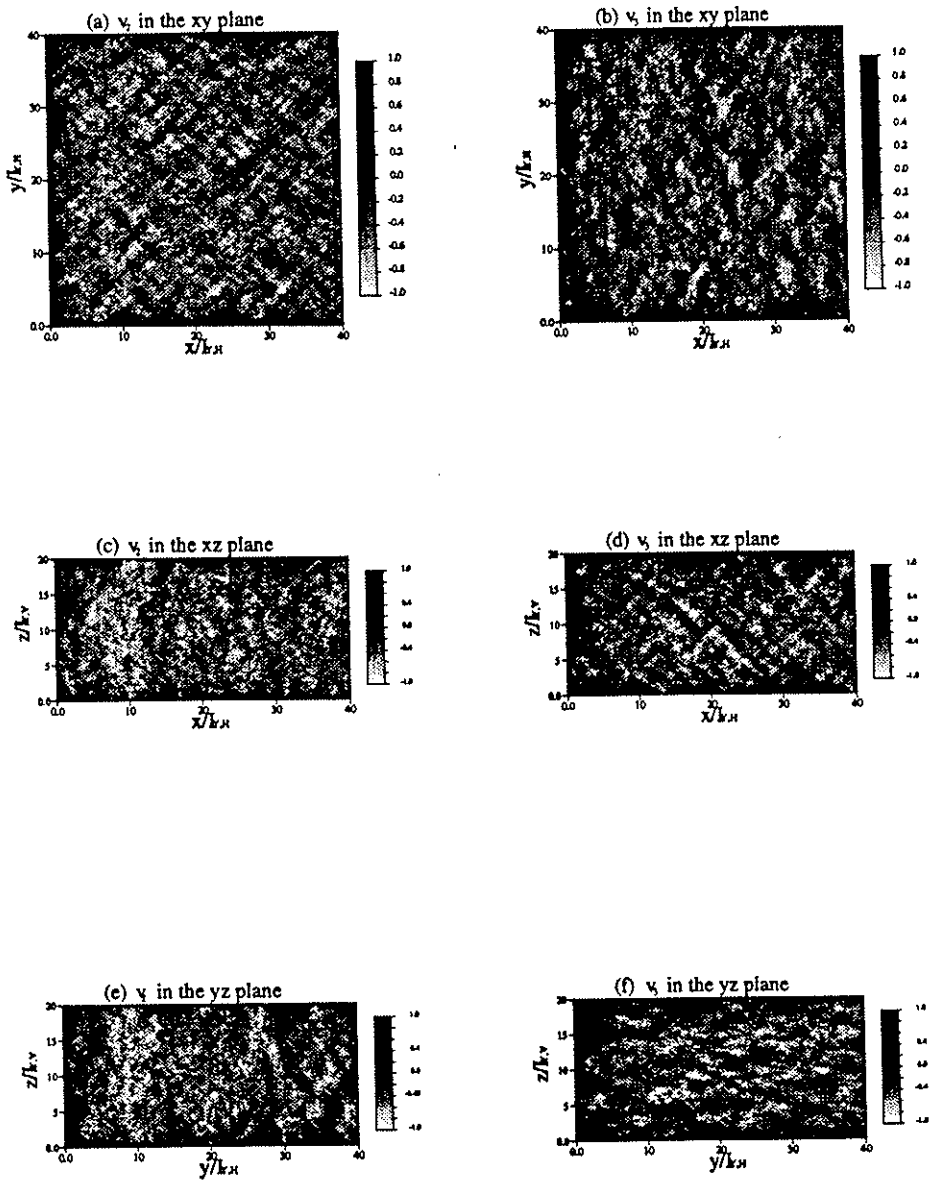

Figure 2-8: Transverse and vertical transverse velocities (v_2 and v_3) in three cross sectional planes. Velocities are non-dimensionalized by the mean flow U.

Figure 2-9 illustrates the effect of anisotropy. Figure 2-9(a) shows an anisotropic case where $I_{Y,H}$ is ten times greater than $I_{Y,V}$ (e = 0.1). There is less correlation along the longitudinal direction for the anisotropic case because there is greater opportunity for a streamline to circumvent low conductivity zones as well as deviate from preferential flow paths. This corresponds with the quasi-analytical solutions derived for e = 0.1 where the v_1 variance was higher and the covariance curve was steeper than those for the e = 1 case (Rubin and Dagan, 1992b).

2.5 Computational Requirements

The CPU requirements for the model are listed in Table 2-1 and compared with a finite element method for 2-D flow generation. The computational efficiency of this method is advantageous for two reasons. First, large flow fields can be generated in a relatively short period of time allowing for extensive monte carlo analysis. Second, flow fields can be generated using workstations with modest computational capacity.

The CPU time is listed in two parts. The first indicates the time required to generate all of the conditioning coefficients (for the coarse and refined grids). One linear system of equations must be solved to compute the conditioning coefficients for the coarse grid while three systems are required for the conditioning coefficients for each level of refinement. The application package LAPACK was used to directly solve these matrices (Anderson, 1992). These calculations need only be performed once and can be considered an

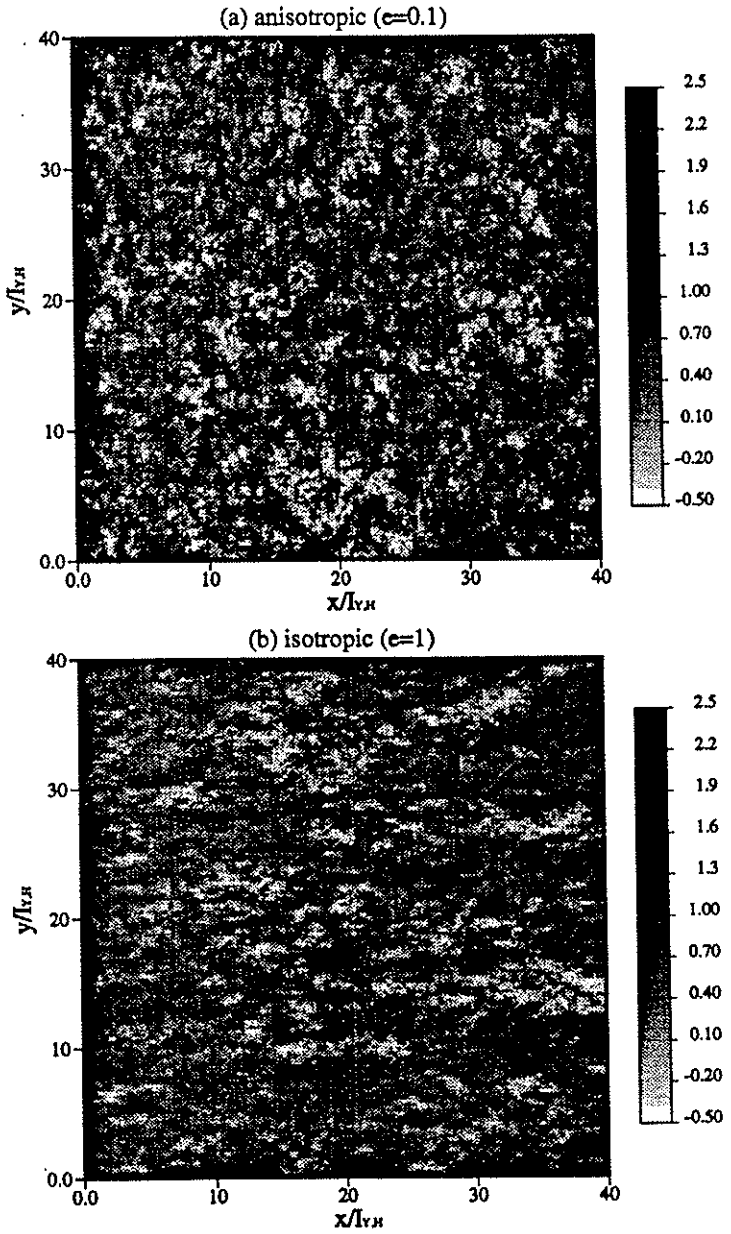

Figure 2-9: Longitudinal velocities (v_1) in a xy plane cross section for (a) anisotropic and (b) isotropic formations. Velocities are non-dimensionalized by the mean flow U.

initial preparation step. The second value listed in the table is the CPU time required to generate one realization of the flow field.

Table 2-1: Computational Requirements for Generating Flow Fields
All runs performed on a IBM RISC 6000 model 530

Grid Spacing[a]	Levels of Refinements	Number of Velocities Generated	CPU Time for Calculating Coefficients (seconds)	CPU Time for Generating One Flow Field (seconds per replicate)
3-D Grids[b]:				
$\Delta = 2$	0	14,553	82	7
$\Delta = 1$	1	105,903	361	51
$\Delta = 0.5$	2	807,003	641	405
$\Delta = 0.25$	2	6,298,803	747	3285
2D Grids[c]:				
$\Delta = 0.25$	1	42,050	388	14
Finite Element $\Delta = 0.25$	-	42,050	286 [d]	68

[a] $\Delta = \Delta_x = \Delta_y = \Delta_z$ with Δ_x , Δ_y in $I_{Y,H}$ and Δ_z in $I_{Y,V}$
[b] 40 $I_{Y,H}$ x 40 $I_{Y,H}$ x 20 $I_{Y,V}$
[c] 36 $I_{Y,H}$ x 36 $I_{Y,H}$
[d] CPU time for computation of the matrix geometry

As can be seen, the computational requirements increase as the grid spacing size decreases. For calculating the coefficients, the CPU time is independent of the field size and the observed increase is attributable primarily to the number of matrices to be solved which increases with each level of refinement. For the generation of the flow field, the CPU time

increases because velocities must be generated at more nodes. The CPU time for generating a flow field increases linearly with the number of velocities (or nodes) in the field. Figure 2-10 illustrates this relationship. For comparison purposes, Table 2-1 also lists the CPU requirements to generate a 2-D flow field for the present method and a Galerkin finite element method with triangular elements and linear shape functions (see Bellin et. al, 1992). The present method requires more initial preparation time but less CPU time per replicate. This is beneficial in Monte Carlo analysis where hundreds or thousands of grids are typically required. The present method is more economical after only 2 realizations.

2.6 Conclusions

This chapter presented a method for generating 3-D flow fields in statistically anisotropic heterogeneous porous media. Sample flow fields were generated and analyzed to demonstrate the method and examine the characteristics of 3-D subsurface flow. From this analysis, the following observations were made:

- the generated velocity fields exhibited the specified spatial correlation structure;
- mass continuity was observed on a block-by-block level and the variance of the mass balance error was shown to decrease with grid spacing;
- cross sectional planes of sample flow fields illustrated the extent and direction of velocity correlations which conformed with previous derivations and theory;

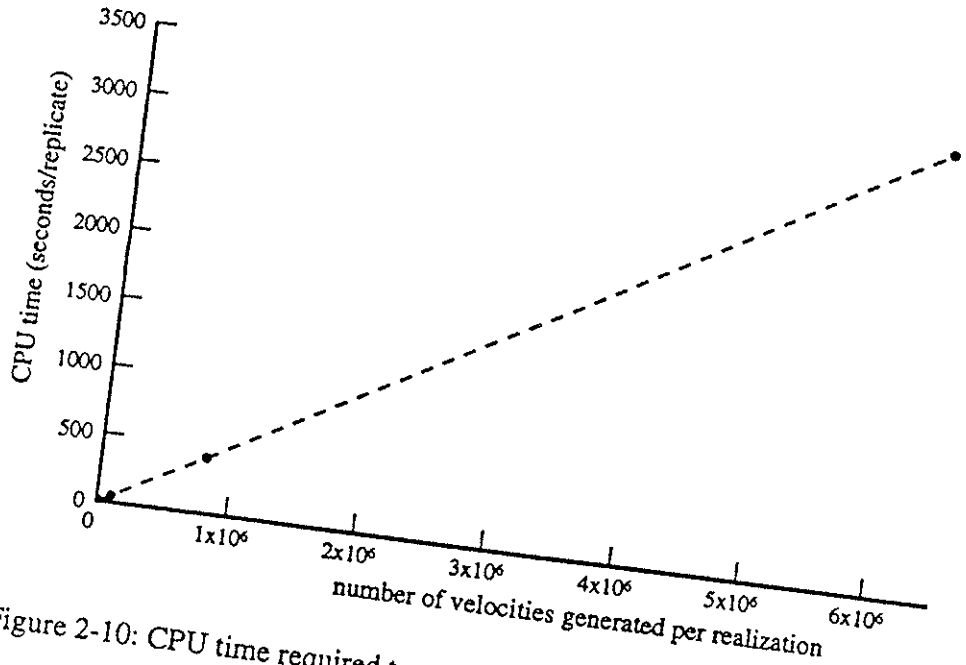

Figure 2-10: CPU time required to generate one realization of a 3D flow field

- the effects of the magnitude of the log-conductivity variance and anisotropy could be examined visually; and
- the method was shown to be computationally efficient in terms of its CPU requirements which increase linearly with the number of velocities or nodes.

Given these observations, the method can be utilized as the basis for 3-D models of contaminant transport in anisotropic heterogeneous aquifers. Its computational efficiency makes it an effective means to generate large fields since the required CPU time increases linearly as the field size is expanded. This efficiency also enables the generation of a large number of realizations which is required in many regulatory and hydrogeological applications. The significance of the computational savings is that it will facilitate the development of tools which can more realistically model contaminant transport.

CHAPTER 3

Modeling the Field-Scale Transport of Nonpolar Organic Compounds: Methodology and Comparisons with Site Data

Field experiments have indicated that reactive solute plumes released in natural porous media decelerate with time and undergo enhanced spreading. To analyze these and other unresolved transport issues, a methodology is presented to simulate the field-scale transport of dissolved nonpolar organic compounds in 3-D heterogeneous aquifers. This includes the development of a model which couples a stochastic technique for generating 3-D flow fields with a mobile-immobile domain model to account for sorption and intraparticle mass diffusion. The methodology is presented through the analysis of the transport of tetrachloroethylene (PCE) at the Borden site, and model results are compared to field data, analytical solutions, and other studies. The input parameters are based on laboratory data reported in the literature. The interpretation of this data is discussed and the required experimental procedures are identified. The model results for the expected displacement of the plume's centroid (first spatial moment) are nearly identical to those observed in the field and capture the trends in the field data more accurately than previous studies. The observed second spatial moments of the plume are within the 95% confidence intervals generated by the model (based on 2500 realizations). In general, the behavior of the plume can be attributed to the large-scale heterogeneities in the subsurface hydraulic properties, the non-ergodic nature of the plume, the sorption of the solute within the soil matrix, and mass transfer resistances within the aqueous phase.

3.1 Introduction

The release and subsequent subsurface transport of contaminants from underground storage tanks, industrial plants, waste disposal sites, and agriculture facilities is a major environmental concern due to the potential for contamination of drinking water supplies and environmentally sensitive

aquifers. Nonpolar (or weakly polar) organic compounds such as tetrachloroethylene (PCE), carbon tetrachloride (CTET), polynuclear aromatic hydrocarbons (PAHs), and hydrocarbons associated with petroleum products or used as solvents are of particular interest since these compounds are widely used in industrial applications and many are known or suspected carcinogens (Patrick et. al., 1987). The transport of these solutes in groundwater is primarily controlled by advection, diffusion and sorption processes as well as chemical and biological transformations. The importance of these individual mechanisms depends on the type of solute, the properties of the aquifer material, and the scale of the analysis. The three scales typically considered are the pore, field, and regional scales which represent formations on the order of less than a meter, ten to hundreds of meters, and tens of kilometers, respectively (Dagan, 1986). This analysis focuses on the transport of dissolved nonpolar organic compounds at the field-scale.

Currently, the transport of organic solutes at the field-scale is not fully understood. The results of the field experiment at the Canadian Air Forces Base in Borden, Ontario (referred to here as Borden) indicate that the movement of a nonpolar organic solute plume decelerates with time and undergoes enhanced spreading relative to tracers injected at the same location (Roberts et. al., 1986). The observed retardation factors increased as the plume migrated through the formation and more than doubled during the study period. Initial efforts to model these observations utilizing a linear equilibrium model to represent the sorption process were unsuccessful (Curtis et. al., 1986). Since then a number of researchers have considered various mechanisms to explain this observed behavior. For the Borden site,

these modeling efforts can be classified by their treatment of sorption processes and advective transport mechanisms. For the modeling of sorption processes, researchers have considered several types of rate-limited sorption as the primary controlling mechanism. These include intraparticle mass transfer limitations (Goltz and Roberts, 1988; Burr et. al., 1994), soil surface reaction kinetics (Burr et. al., 1994; Cvetkovic and Dagan, 1994; Ptacek and Gilham, 1992), and a combination of these mechanisms (Brusseau, 1992). Other models have also considered the incorporation of spatial variability of the soil sorption distribution coefficient (K_d) by correlating it with variations of the hydraulic conductivity (Burr et. al., 1994). For the advective transport mechanisms, some of the models utilized numerical or analytical stochastic approaches (Burr et. al., 1994; Cvetkovic and Dagan, 1994) while others have used effective dispersivity coefficients determined by either fitting site data or from the analysis of tracer spreading (Goltz and Roberts, 1988; Ptacek and Gilham, 1992). None of these models have adequately reproduced the field observations without fitting model parameters directly to the observed data.

For non-reactive solutes, the spreading of solutes in field experiments has been found to be orders of magnitude larger than predicted values based on laboratory experiments (Gelhar, 1986; Dagan, 1987). This enhanced spreading has been attributed to the spatial variations in the subsurface water velocities which result from the natural large scale heterogeneities of the hydraulic properties of the aquifer. The scale of these heterogeneities is much larger than the pore scale and can not be measured in a laboratory setting. From a modeling perspective, a deterministic approach would require detailed sampling of all of the subsurface hydraulic properties to account for these

heterogeneities. As an alternative, the stochastic approach models these hydraulic properties as spatial random processes. Typically, the hydraulic conductivity (K) is modeled as a spatially random process or field while other properties are treated as uniformly distributed. The approach utilized here is different in that it directly models the subsurface velocities as spatial random processes. This approach was discussed in detail in Chapter 2. Again, this technique has been found to require less computational effort than previous methods without loss of accuracy.

In addition to encountering large scale heterogeneities in hydraulic properties, reactive solutes are also subject to subsurface chemical and physical processes. For a nonpolar organic solute, sorption is the primary controlling mechanism which retards its migration. Sorption, as referred to here, includes partitioning into soil organic matter and/or physical adsorption. Since sorption sites are also present within regions of the soil where the fluid is immobile, such as intra-aggregate or dead-end pores, it has been recognized that the sorption process can be rate limited due to mass transfer resistances to and from these immobile regions within the soil. This phenomenon has been represented by various forms of the mobile-immobile domain model (van Genutchen and Wierenga, 1976; Brusseau and Rao, 1989)

The model presented here simulates the field-scale transport of dissolved nonpolar organic compounds in groundwater by coupling a stochastic approach for modeling advection with a mobile-immobile domain model to account for the sorption process. The first component accounts for the spatial variability of the physical subsurface properties on the movement of solutes.

The second reflects the additional effects due to the sorption of the solute and rate-limited mass transfer during transport. The model is presented through an analysis of the transport of tetrachloroethylene (PCE) at Borden and results are compared to those from the field experiment. The reaction coefficients are modeled as constant values and are selected independent of the field study by utilizing results from laboratory experiments reported in the literature. Model results are in the form of complete statistical description of the plume's spatial moments based on 2500 realizations of the 3-D subsurface flow field. These results are compared to the site data, analytical solutions, and previous studies.

The remainder of this chapter is divided into four sections. The first presents background information which lead to the development of the present approach. The next section discusses the methodology used to generate the subsurface flow fields and model the sorption process. The third section discusses the input model parameters used to simulate the transport of PCE at the Borden site. Finally, the last section presents the results of the simulation and comparisons with site data and other models.

3.2 Background

The following section discusses advancements in the fields of modeling flow through heterogeneous porous media and modeling the sorption of nonpolar organics compounds in soils. A more detailed discussion regarding the modeling of sorption on nonpolar organic compounds is provided in

Appendix C. The accomplishments and shortcomings of these previous efforts led to the development of the approach presented here.

3.2.1 *Stochastic Modeling of Subsurface Flow*

A number of stochastic approaches for predicting passive and reactive solute concentrations in heterogeneous geological formations have been reported in the literature (e.g., analytical methods by Dagan, 1982; Vomvoris and Gelhar, 1990; Rubin, 1991a; Rubin, 1991b; Kabala and Sposito, 1994; and numerical methods by Tompson and Gelhar, 1990; Burr et. al., 1994). In general, the previous analytical methods have focused on the determination of the first two moments (expected value and variance) of the solute concentration. For predictive purposes and the generation of confidence intervals, the use of only the first two moments is only valid when the distribution of the concentration is Gaussian. Recent work , though, has indicated that the concentration distribution is non-Gaussian and only approaches a Gaussian form at large sampling volumes (Bellin et. al., 1994). As such, the distribution is not fully characterized by its first two moments and it is necessary to develop full distributions of the concentrations. Utilizing the numerical methods cited previously, full concentration distributions could be computed by utilizing a Monte Carlo approach and performing several hundred to several thousand simulations. The computational requirements for 3-D analysis, though, would be exorbitant. For example, in their 3-D numerical analysis of reactive transport at the Borden site, Burr et. al. (1994) limited their results to only five realizations due to the excessive computational requirements. This indicates the limitations of previous efforts which

utilized numerical stochastic techniques to simulate field-scale transport. To overcome this limitations it is necessary to utilize a more rapid means of generating subsurface flow fields. The methodology outlined in Chapter 2 and utilized here is such a technique.

3.2.2 *Modeling of Sorption Processes*

In general, the modeling of sorption processes in large scale contaminant transport models has been mostly limited to the simplifying assumptions of instantaneous equilibrium, isotherm linearity, and adsorption-desorption isotherm reversibility (singularity). Behavior which deviates from these simplifying assumptions has been termed nonideal and can result from noninstantaneous surface reactions, diffusive mass transfer resistances, isotherm nonlinearity, and irreversibility of the adsorption-desorption process (Brusseau and Rao, 1989). The applicability of each of these phenomena depends on the characteristics of the sorbing compound and medium. For dilute concentrations of nonionic, nonpolar organic compounds in natural systems, hydrophobic sorption is the predominant mechanism and, therefore, surface kinetics, nonlinearity, and nonsingularity are not expected to play a major role (Brusseau and Rao, 1989). The observed nonideal behavior then must be attributed to physical mass transfer resistances. The sorption process is controlled by the rate at which the solute is transported to and from the water-sorbent interface since the reaction rate at this interface is effectively instantaneous.

Van Genutchen and Wierenga (1976) were one of the first to develop a conceptual and mathematical model for this phenomenon. Consider the movement of a contaminant through an aggregated porous medium as illustrated in Figure 3-1. Flow occurs only in the mobile water regions where the contaminant is transported by advection. The contaminant can only enter or exit the immobile water regions only by diffusion. These immobile regions are located within soil aggregates or dead-end pores. In both the mobile and immobile regions, the contaminant will undergo adsorption and desorption into the soil matrix. Assuming that the adsorption-desorption process is instantaneous, the rate of sorption will be controlled by the transfer of solute into and out of the immobile regions. This model of the sorption process has been typically referred to as the mobile-immobile domain model.

Assuming linear adsorption at the soil-water interface, the three-dimensional mathematical representation of this model, excluding pore scale dispersion, is (van Genutchen and Wierenga, 1976):

$$\left(\theta_m + f\rho_b K_d\right)\frac{\partial C_m}{\partial t} + \left[\theta_{im} + (1-f)\rho_b K_d\right]\frac{\partial C_{im}}{\partial t} = -\theta_m \mathbf{v}_m \nabla_x C_m \qquad (3\text{-}1a)$$

$$\left[\theta_{im} + (1-f)\rho_b K_d\right]\frac{\partial C_{im}}{\partial t} = \alpha(C_m - C_{im}) \qquad (3\text{-}1b)$$

where boldface letters indicates vectors; the subscripts m and im refer to the mobile and immobile regions, respectively; C is the aqueous concentration $[M/L^3]$; $\mathbf{v}$ is the linear or pore water velocity vector $[L/t]$; $\nabla_x C_m$ is the concentration gradient vector with respect to $\mathbf{x}$; θ is the porosity; f is the

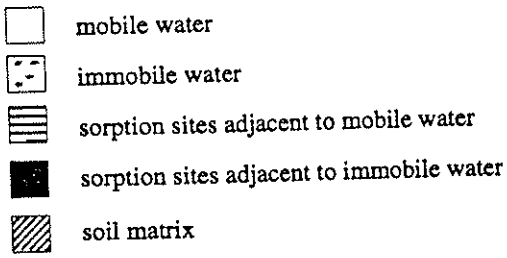

Figure 3–1: Schematic of Mobile–Immobile Domain Model

fraction of sorption sites in direct contact with the mobile phase; ρ_b is the soil bulk density [M/L^3]; K_d is the equilibrium distribution coefficient between the aqueous and sorbed phases [L^3/M]; and α is the first-order mass transfer coefficient which approximates the physical diffusion process [1/t]. This coefficient represents a lumped parameter which includes the contributions of diffusivity and tortuosity .

Equations 3-1(a) and (b) can be simplified by introducing retardation factors (R) and the parameter ϕ which is the fraction of water present in the mobile regions ($\phi = \theta_m/\theta$)

$$R_m \frac{\partial C_m}{\partial t} + \frac{1-\phi}{\phi} R_{im} \frac{\partial C_{im}}{\partial t} = -\mathbf{v}_m \nabla_x C_m \qquad (3\text{-}2a)$$

$$\theta(1-\phi) R_{im} \frac{\partial C_{im}}{\partial t} = \alpha(C_m - C_{im}) \qquad (3\text{-}2b)$$

where,

$$R_m = 1 + \frac{\rho_b f K_d}{\theta_m} = 1 + \frac{\rho_b f K_d}{\phi\theta}$$

$$R_{im} = 1 + \frac{(1-f)\rho_b K_d}{\theta_{im}} = 1 + \frac{(1-f)\rho_b K_d}{(1-\phi)\theta}$$

For modeling purposes, the required parameters are v, θ, ϕ, ρ_b, K_d, α, and f. A more general discussion of sorption modeling is provided in Appendix C.

3.3 Methodology

A methodology was developed to determine the complete statistical description of the transport of reactive solutes in 3-D heterogeneous formations. For nonpolar organic solutes, the methodology entails the coupling of a stochastic technique for generating a flow field with an immobile-mobile domain model for representing the sorption process. A Monte Carlo approach is utilized and several hundred to several thousand realizations of the flow field and plume migration are generated from which the full statistical distribution of the solute resident concentration, spatial moments, and other variables of interest can be determined.

3.3.1 *Generating 3-D Flow Field*

The technique utilized to generate the 3-D flow fields was discussed in Chapter 2 and is briefly summarized here. The premise of this technique is to achieve computational efficiency by relying on stochastic and geostatistical principles. The fluid velocity is computed directly at each node using Gaussian conditioning. The spatial mean and variance-covariance tensor of the velocity $\mathbf{v}$ (where $\mathbf{v}$ is a vector representing velocities in three directions) at a given node $\mathbf{x}_N$ (where $\mathbf{x}$ is a vector representing a location in 3-D space) are conditioned on a subset of the velocities previously generated, $\mathbf{v}(\mathbf{x}_1)$ to $\mathbf{v}(\mathbf{x}_{N-1})$, in order to maintain the spatial correlation structure of the velocity field and preserve mass continuity. The conditioning coefficients utilized are based on algorithms for the spatial covariance of the velocities derived from Darcy's Law and the flow equation. Given the conditional mean and

variance at the given node, random deviates are generated to compute the components of the vector **v** at that node for that particular realization. Moving systematically over the 3-D field, velocities are computed at each node to generate a single realization of the field. For each realization, the entire process is repeated.

The flow fields generated to simulate the Borden site are based on the velocity covariance algorithms presented by Rubin and Dagan (1992b). The characteristics of the site met the assumptions utilized to derive these algorithms. These include an exponential spatial correlation of the logconductivity, large flow domain, variance of the logconductivity less than unity, steady state conditions, and uniform average flow. The statistical anisotropy of the formation is represented by utilizing separate integral scales for the logconductivity in the vertical and horizontal direction ($I_{Y,V}$ and $I_{Y,H}$). The integral scale represents the length over which the values are spatially correlated.

3.3.2 *Simulation of Advection and Sorption*

The approach used to simulate the displacement of solutes in the aquifer is the Lagrangian one (Dagan, 1982). Consider the displacement of a single solute particle which is larger than the pore scale, to ensure the applicability of Darcy's law, but much smaller than $I_{Y,V}$ and $I_{Y,H}$ which enables it to accurately capture the media heterogeneity. The displacement of a tracer

particle is given by:

$$\frac{d\mathbf{X}(t,\mathbf{x}_0,t_0)}{dt} = \mathbf{V}(t) \tag{3-3}$$

where **X** denotes the trajectory of the particle whose origin is x_0 at t_0, and **V**(t) is the particle Lagrangian velocity. The resident concentration field ensuing from the displacement of the single particle is given by:

$$\mathbf{C}(\mathbf{x},t) = \frac{m}{\theta}\delta(\mathbf{x} - \mathbf{X}(t)) \tag{3-4}$$

where m is the mass of a solute particle; δ is the Dirac delta; and it is assumed that the effects of pore scale dispersion are negligible. The approach used here consists of simulating a large number of solute particles which together constitute the solute body. Hence, the displacement of a plume is performed by solving eqn 3-3 for a large number of initial coordinates x_0, according to the definition of the problem. The solution of eqn 3-3 is accomplished by moving the particle through a 3-D grid of velocities computed a priori according to the methodology described in the previous section. The particle is displaced using a relatively small time step ($\Delta\tau = 0.125$ where τ is the non-dimensional time defined as $\tau = Ut/I_Y$, and U is the mean velocity). The particle velocity at each location is determined using a linear interpolation scheme to conserve mass locally (Anderson and Woessner, 1992; Schafer-Perini and Wilson, 1991). To minimize the error incurred from transforming the Eulerian velocities into Lagrangian ones, a fourth-order Runge-Kutta integration

method is used (Anderson and Woessner, 1992). The particle tracking technique utilized is discussed further in Appendix B.

From the displacement of the cluster of particles, statistics such as the plume's mean displacement, its spatial moments, and the probability distribution function (PDF) of the travel times between the source and a plane of compliance downstream (Rubin and Dagan, 1992a), as well as solute fluxes (Dagan and Cvetkovic, 1993; Selroos and Cvetkovic, 1992) can be determined. By repeating these numerical experiments a large number of times, the complete statistical distribution of these variables can be obtained.

The use of particle tracking has gained wide acceptance, and while it is quite straightforward in the case of tracers, it is more complex in the case of reactive solutes since part of the solute is sorbed and immobilized. This difficulty can be resolved by reformulating eqn 3-2 in a Lagrangian framework. Defining a curvilinear coordinate system **s** along a streamline, the velocity vector is given by **v**(**s**). Eqn 3-2 now becomes:

$$R_m \frac{\partial C_m}{\partial t} + \frac{1-\phi}{\phi} R_{im} \frac{\partial C_{im}}{\partial t} = -\mathbf{v}_m \nabla_s C_m \tag{3-5}$$

where ∇_s refers to the gradient with respect to **s**. Using the auxiliary relationship , $\frac{\partial}{\partial \tau'} = v_{m,i} \frac{\partial}{\partial s_i}$, eqn 3-5 reduces to:

$$R_m \frac{\partial C_m}{\partial t} + \frac{1-\phi}{\phi} R_{im} \frac{\partial C_{im}}{\partial t} = -\frac{\partial C_m}{\partial \tau'} \tag{3-6}$$

Defining the following non-dimensional variables, the Lagrangian system is obtained:

$$\beta\frac{\partial C_2}{\partial T}+\frac{\partial C_1}{\partial T}=-\frac{\partial C_1}{\partial \tau} \tag{3-7a}$$

$$\frac{\partial C_2}{\partial T}=\omega(C_1-C_2) \tag{3-7b}$$

where,

$$C_1=\frac{C_m}{C_o} \qquad C_2=\frac{C_{im}}{C_o}$$

$$\omega=\frac{\alpha}{\theta(1-\phi)R_{im}}\frac{R_m I_{Y,h}}{U}$$

$$\beta=\frac{1-\phi}{\phi}\frac{R_{im}}{R_m}$$

$$\tau=\frac{U\tau'}{I_{Y,h}} \qquad T=\frac{Ut}{R_m I_{Y,h}}$$

Note that t denotes the elapsed travel time while τ' denotes advection time, i.e., the travel time of the tracer particle in the mobile zone. The variable τ is the dimensionless form of τ'; T is the dimensionless time relative to the retarded velocity in the mobile zone; $I_{Y,H}$ is the integral scale of the logconductivity in the horizontal direction; U is the mean fluid velocity; and C_o is the initial solute concentration.

Similar equations were obtained by Cvetkovic and Dagan (1994), Chen and Wagenet (1995), and Simmons (1982). Equations 3-7(a) and (b) can be most conveniently solved using Laplace transforms. Similar coupled equations

were solved by Hubert et. al. (1971) and later adapted by Lassey (1988) for instantaneous injection and a two-site kinetic model. Their solutions were developed for a uniform flow domain. Cvetkovic and Dagan (1994), following these solutions, developed an expression for instantaneous injection with negligible pore scale dispersion for the two-site kinetic model. Their solution was coupled with analytical expressions for the spatial moments of a tracer plume to derive the expected values for a reactive solute plume's centroid displacement and higher order spatial moments. The formulation of these analytical expressions required the assumption of ergodicity. This implies that a unique realization will behave with the same probabilities as an ensemble of possible realizations. In practical terms, ergodicity translates into the requirement that the extent of the plume normal to the mean flow direction must be much larger than the integral scale (Dagan, 1991).

In the first steps, the solution presented here is quite similar to the one by Cvetkovic and Dagan (1994) since the mobile-immobile domain model and the two-site kinetic model are mathematically analogous (Nkedi-Kizza et. al., 1984). This approach proceeds further than these previous efforts by coupling the solution with a numerical particle tracking approach to derive a more complete statistical description of the spatial moments of the plume and avoid the limitations of assuming ergodic conditions. The solution for eqn 3-7(a) and (b) is expressed for a single particle as:

$$C_1(\tau,T) = \frac{m}{\theta_m v_{1,m}} \gamma(\tau,T)\delta(s_2)\delta(s_3) \qquad (3\text{-}8)$$

Using Laplace transforms and solving for instantaneous injection, the expression for γ is:

$$\gamma(\tau,T) = e^{-\omega\beta T}\delta(T-\tau) + \left(\omega^2\beta\tau\right)e^{-\omega(T-\tau+\beta\tau)}\tilde{I}_1\left[\omega^2\beta\tau(T-\tau)\right]H(T-\tau) \qquad (3\text{-}9)$$

where,

$$\tilde{I}_1(z) = \frac{I_1\left(2\sqrt{z}\right)}{\sqrt{z}}$$

I_1 is a modified Bessel function of the first kind of order one; and H and δ are the Heaviside and Dirac functions, respectively. The derivation of eqn 3-9 from eqn 3-7 is shown in detail in Appendix B.2. The overall approach consists of simulating a large number of solute particles which together constitute the solute body. For each solute particle, eqns 3-8 and 3-9 are solved at each time step $\Delta\tau$ for all values of $T' > \tau$, where T' are pre-selected times of interest. The contribution of the solute particle to the total displacement and spreading of the plume is accounted for by utilizing eqn 3-8 in the expressions for the first and second spatial moments (which are transformed to the curvilinear coordinate system **s**). This process is repeated for a large number of initial coordinates $\mathbf{x}_0$ to determine the spatial moments for the plume for that particular realization. By using multiple realizations of the flow field, a complete statistical description of the spatial moments can be determined. In addition, the assumption of ergodicity is not necessary and the migration of non-ergodic plumes can be evaluated.

The impact of incorporating a mobile-immobile domain model can be illustrated by a further examination of eqn 3-9. This equation represents the sorption and intraparticle diffusion of portions of the solute parcel as it moves and is essentially stretched along a streamline as a function of its travel time. The parameter ω represents the effective rate of mass transfer into the immobile zones relative to the rate of advective transport. The parameter β represents the distribution of mass between the mobile and immobile zones. Figures 3-2(a) and (b) illustrate the effect of these two parameters and the rate-limited mass transfer process, in general, on the arrival of the solute parcel and its contribution to the total solute concentration relative to a parcel sorbed only in the mobile zone. The expression γ is shown with respect to time relative to the arrival of a solute particle transported and sorbed only in the mobile zone. As ω approaches zero, there is essentially no diffusion of solute into the immobile zone and the maximum contribution and arrival time are unaffected. As ω increases, a slow exchange of solute between the mobile and immobile zone occurs causing a decrease in its maximum contribution and a significant amount of tailing causing a shift in the mean arrival time. As ω approaches infinity, the rate of mass transfer is much more rapid than the rate of advective transport and the solute is essentially at equilibrium instantaneously. A new equilibrium proportioning and mean arrival time is approached which reflects the inclusion of the additional sorption sites within the immobile zone. The parameter β also affects the maximum value and the extent of tailing. This is illustrated in a comparison of Figure 3-2(a) where $\beta = 1$ with Figure 3-2(b) where $\beta = 3$. As β increases, more of the solute is detained in the

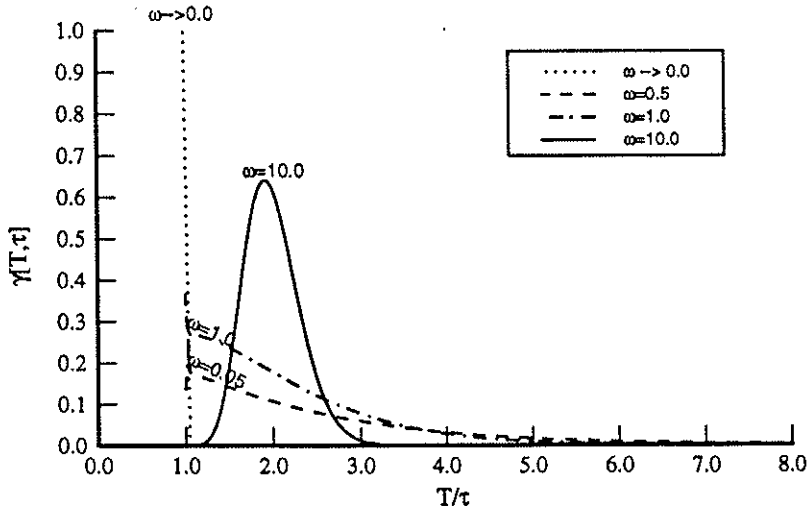

(a) $\beta = 1$

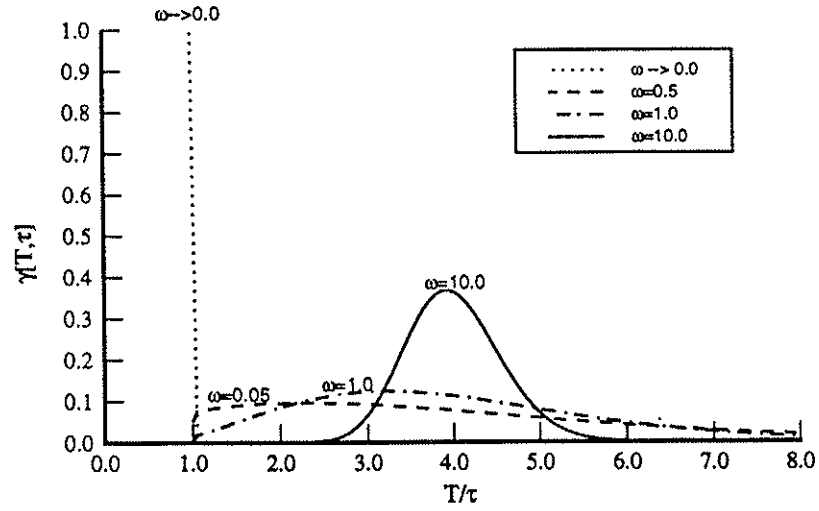

(b) $\beta = 3$

Figure 3-2: Effect of Parameters ω and β on γ for the case of τ=2

immobile zone resulting in a more pronounced tailing, a reduced peak contribution, and a later mean arrival time.

3.4 The Borden Site and Model Input Parameters

The application of the model is presented through an analysis of transport of PCE at the Borden site. This section provides a brief description of the Borden study and discusses the selection of input parameters for the model simulations. The Borden study was selected because of the availability of detailed and reliable field data for comparison purposes. PCE, in particular, was selected because, unlike other organic compounds injected at the site, it maintained a constant mass in solution after an initial period indicating that biodegradation and chemical transformation played a minor role in its transport and that sorption should be the primary controlling mechanism.

3.4.1 *Description of the Borden Study*

A natural gradient experiment was conducted at this site in an unconfined sand aquifer underlying an inactive sand quarry (Mackay et. al., 1986). The soil is a fine to medium-grained sand and has a low organic carbon content ranging from 0.01 % to 0.09% (average of 0.02%) (Mackay et. al., 1986). A 12 m^3 solution containing PCE and other solutes was injected over an interval 2.0 to 3.6 m below the ground surface. The water table was at a depth approximately 1 m below the ground surface during the study. The mass of PCE was 0.36 g with a resulting initial concentration of PCE was 30 ug/L. A dense multilevel array of 5,000 samplers was installed and monitored periodically over a 3 year period. The area covered by these samplers was approximately 120 m x 80 m.

The vertical extent of the aquifer was approximately 9 m to a confining layer of thick, silty clay deposit.

The utilization of the mobile-immobile model with linear adsorption is appropriate for simulating the transport of PCE at the Borden site. PCE was at dilute concentrations (30 ug/L which is less than 0.1 % of its solubility); batch sorption tests indicated that the isotherms were linear for the range of interest (< 50 ug/L) (Ball and Roberts, 1991a); and the isotherms were found to be reversible (Curtis et. al., 1986). As such, the sorption of PCE onto Borden soils is not expected to be nonlinear or nonsingular and linear adsorption can be assumed once the constituent reaches the sorption sites.

3.4.2 *Subsurface Hydraulic Properties*

Table 3-1 lists the subsurface hydraulic parameters used in the model simulation of the Borden site. These parameters are based on the analysis of field measurements from the original study (Freyberg et. al., 1986) and a follow-up analysis performed by Woodbury and Sudicky (1991).

Table 3-1: Subsurface Hydraulic Properties for Borden

Parameter	Value	Source
average linear velocity (U)	9.1 cm/d	Mackay et. al. (1986)
porosity (θ)	0.33	Mackay et. al. (1986)
soil bulk density (ρ_b)	1.81 g/cm^3	Mackay et. al. (1986)
variance of logconductivity (σ_Y^2)	0.24	Woodbury and Sudicky (1991)
horizontal integral scale of Y ($I_{Y,H}$)	5.1 m	Woodbury and Sudicky (1991)
vertical integral scale of Y ($I_{Y,V}$)	0.21 m	Woodbury and Sudicky (1991)
fraction of water in the mobile zone (ϕ)	0.87	Goltz and Roberts (1988)

The value listed for the ratio of mobile water content to the total water content (ϕ) is based on the tracer results from the natural gradient experiment. The observed mean pore velocity was 0.091 m/d (Freyberg et. al., 1986) which was higher than the expected pore velocity of 0.079 m/d based on the hydraulic conductivity, total porosity, and hydraulic gradient (Mackay et. al., 1986). Since the observed velocity represents flow through only the mobile region, the parameter ϕ can be estimated based on this ratio (Goltz and Roberts, 1988):

$$\phi = \frac{\theta_m}{\theta} = \frac{\theta_m}{\theta}\frac{K\Delta h}{K\Delta h} = \frac{K\Delta h/\theta}{K\Delta h/\theta_m} = \frac{v}{v_m} = \frac{0.079\,m/d}{0.091\,m/d} = 0.87 \qquad (3\text{-}10)$$

It should be noted that no laboratory measurements of ϕ for the Borden site have been reported. Laboratory techniques to measure ϕ have been reported in the literature but its direct measurement is often difficult (Nkedi-Kizza et. al., 1984).

3.4.3 *Sorption Parameters*

Table 3-2 lists the input parameters (K_d, α , and f) selected for modeling the sorption process. These parameters are primarily based on the laboratory results from column tests performed by Ptacek and Gilham (1992) and batch equilibrium tests performed by Ball and Roberts (1991a; 1991b). Since these tests represent two different approaches to quantifying mass transfer coefficients, two scenarios are presented and primarily represent input parameters based on these two sets of laboratory experiments, respectively. A

third scenario was also included for comparison purposes and assumes linear equilibrium with no immobile regions (f = 1). Each of the input sorption parameters is discussed below.

Table 3-2: Sorption Parameters for PCE and Borden Soil

Parameter	Value	Source
SCENARIO 1:		
mass transfer coefficient (α)	0.0046 / day	estimated using data from Ptacek and Gilham (1992)
distribution coefficient (K_d)	0.76 mL/g	Ball and Roberts (1991a)
fraction of sorption sites in the mobile zone (f)	0.32	estimated using data from Curtis et. al. (1986)
SCENARIO 2:		
mass transfer coefficient (α)	0.0076 / day	estimated using data from Ball and Roberts (1991b)
distribution coefficient (K_d)	0.76 mL/g	Ball and Roberts (1991a)
fraction of sorption sites in the mobile zone (f)	0.25	calculated using data from Ball and Roberts (1991a)
SCENARIO 3:		
distribution coefficient (K_d)	0.76 mL/g	Ball and Roberts (1991a)
fraction of sorption sites in the mobile zone (f)	1.0	

Ball and Roberts (1991a) performed batch equilibrium sorption experiments for PCE and Borden soil. These studies indicated that equilibrium was closely approached in 20 days. Using concentrations within the range of the field concentrations (< 50 ug/L), Ball and Roberts (1991a) estimated that the distribution coefficient (K_d) was 0.76 mL/g. This is approximately 60% higher than the original estimate reported by Curtis et. al. (1986) based on a 3 day

equilibrium test. This observed difference was attributed to the additional equilibrium time allowed and, therefore, the estimate by Ball and Roberts (1991a) was deemed more appropriate and used for all scenarios.

The mass transfer coefficients (α) selected for the first two scenarios are based on two different types of laboratory studies using PCE and Borden soil. The mass transfer coefficient for the first scenario was selected using the results from the two low flow column tests performed by Ptacek and Gilham (1992). The column flow rate and length were 18 cm/d and 10 cm, respectively. Their results were reported as fitted parameters to a two-site kinetic model but these can be adapted to a mobile-immobile model due to the mathematical similarities between the models (Nkedi-Kizza et. al., 1984). Using the average of the results from these two experiments, the parameter ω in eqn 3-7(b) and 3-9 is 0.661. The resulting mass transfer coefficient α in eqn 3-2(b) is 0.0046/day. The computations of these values is shown in Appendix D.

For the second scenario, the selection of the α is more direct. Ball and Roberts (1991b) estimated a form of mass transfer coefficient from their series of batch equilibrium experiments. Their estimated coefficient of 1.8×10^{-7}/s was a lumped parameter accounting for intraparticle diffusivity, tortuosity, constrictivity, and interior grain retardation. It is directly equivalent to a dimensional form of the parameter ω in eqn 3-7(b) and 3-9. The resulting non-dimensional value for ω is 0.872 and the mass transfer coefficient α, as defined here, is 0.0076/day. The computations of these values is shown in Appendix D.

In most of the previous studies, the fraction of sorption sites in the mobile zone (f) has been assumed to be equal to the fraction of water in the mobile zone (ϕ) (Burr et. al., 1994; Goltz and Roberts, 1988; Ptacek and Gilham, 1992; Brusseau, 1992). This assumption was first proposed by Nkedi-Kizza et. al. (1984) as a working hypothesis due to the difficulties in measuring f in laboratory experiments. The validity of this assumption though has been recently questioned (Thorbjarnarson and Mackay, 1994; Brusseau, 1994). Its basis is questionable since it is likely that the amount of organic carbon or the available surface area within the interior aggregates would be greater than that present in the larger pores of the mobile zones. This was demonstrated for other compounds and soils by Wood et. al. (1990) who found that more than 80% of the sorption sites were within the interior grains. Furthermore, the equality assumption ($f = \phi$) severely alters the form of the mobile-immobile model. The retardation factor for the mobile zone is reduced to the overall retardation factor:

$$R_m = 1 + \frac{f\rho_b K_d}{\theta_m} = 1 + \frac{f}{\phi}\frac{\rho_b K_d}{\theta} \xrightarrow{f=\phi} 1 + \frac{\rho_b K_d}{\theta} = R \qquad (3\text{-}11)$$

As a result, the sorption attributable to the mobile zone is overestimated. With this in mind, an alternative method for estimating f was pursued here. Since no laboratory experiments have been reported to directly measure f, other laboratory results were used to estimate its value. For the first scenario, f was estimated based on the ratio between the sorption which occurs almost instantaneously during batch equilibrium tests and the asymptotic values.

The assumption is that only sorption sites within the mobile zones of the soil would be immediately available. The results from Curtis et. al. (1986) indicate that the K_d would be approximately 0.24 mL/g after the initial contact period (less than 2 hours of equilibration time). Given that the true K_d is 0.76 mL/g, f was estimated to be 0.32.

For the second scenario, surface area measurements from Ball and Roberts (1991a) were used to estimate f. The measured surface area for the bulk sample was 0.42 m^2/g and for the pulverized soil was 1.7 m^2/g. The pulverization technique was believed to only expose the internal sites and not create new surfaces (Ball and Roberts, 1991a). As such, the ratio of the surface area of the bulk sample to that of the pulverized sample should give a fair estimation of the fraction of sorption sites within the mobile zone (f). The resulting estimation for f is 0.25 for the second scenario.

As noted above, all of the selected model input sorption parameters are based on laboratory experiments and none have been fitted to field observations. This approach to selecting input parameters is necessary since many of the rate-limited sorption processes can be modeled in a mathematically analogous manner (Nkedi-Kizza et. al., 1984).

3.5 Model Results and Comparisons with Data from the Borden Study

The transport of PCE at the Borden site was simulated utilizing the input parameters discussed in the previous section. The simulated field was 28 $I_{Y,H}$ by 16 $I_{Y,H}$ by 24 $I_{Y,V}$ to ensure that no artificial boundary conditions affected the

results (Rubin and Dagan, 1988). The discretization was 0.25 $I_{Y,H}$ horizontally and 0.25 $I_{Y,V}$ vertically (approximately 712,000 nodes). The initial plume was 0.6 $I_{Y,H}$ by 1.2 $I_{Y,H}$ by 7.6 $I_{Y,V}$ and represented by 5500 particles. The plume migration was modeled over a period equivalent to 720 days using the methodology discussed previously.

A sample of the resulting aqueous concentrations (C_1) for PCE after being transported an equivalent of 710 days through a single realization of the flow field is illustrated in Figures 3-3(a) and (b). The concentrations shown are based on the input parameters for the first scenario. Figure 3-3(a) illustrates the dimensions and shape of the injected plume. Figure 3-3(b) is an isosurface indicating areas where $C_1 > 0.01$. The density of the shading corresponds with the magnitude of the concentration with the lightest shading indicating concentrations near zero. The outer surface of the plume is irregular and the shape is distorted relative to the initial well-defined injection geometry. These are due to the shear by the variable velocity field. Areas of the highest concentration are not located in the center of the plume and are non-continuous.

To compare model results with the Borden field data and other studies, 2500 realizations of the flow field and subsequent tracking of the plume were completed. As noted previously, three scenarios are considered -- two utilizing the mobile-immobile domain model and one assuming equilibrium sorption for comparison purposes. From this analysis, the mean values and the 95% confidence intervals of the plume's spatial moments were

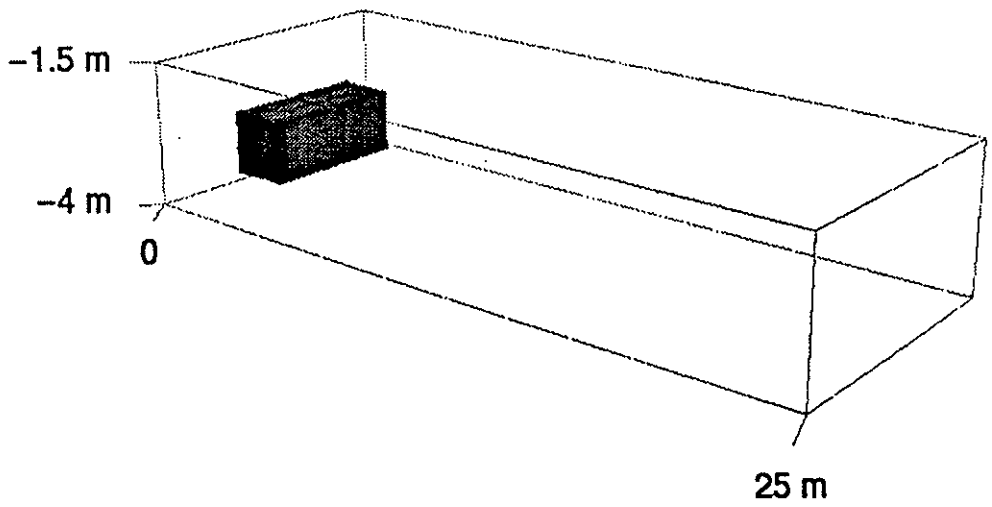

(a) t = 0 days

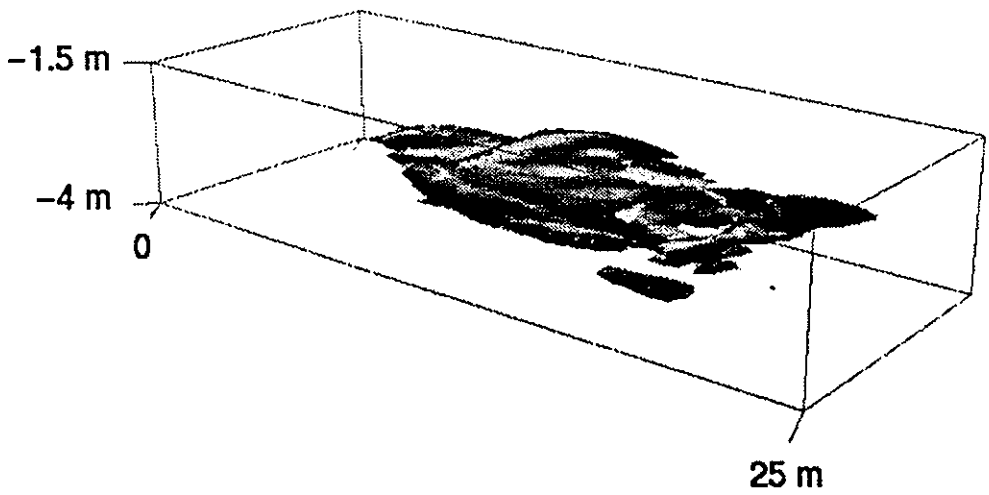

(b) t = 710 days

Figure 3-3: Sample Isosurface of Solute Concentrations for a Single Realization [$C_1 > 0.1\ C_o$]

determined. These are compared to field data from the Borden site, analytical solutions, and previous studies in the following sections.

3.5.1 *Spatial Moments of the Plume*

The results from the Borden field experiment were reported in the form of the zero, first, and second spatial moments of the plume (Roberts and Mackay, 1986; Roberts et. al., 1986). These correspond to the mass of PCE in solution, the displacement of the centroid of the plume, and the spreading of the plume, respectively. Each of these is compared with the model results below.

Figure 3-4 compares the mass of PCE in solution with time from the Borden site (Roberts and Mackay, 1986; Roberts et. al., 1986) with the model results from single realizations for each of the three scenarios. Since the reaction coefficients are constant and uniform, the total mass of solute in solution at a given time does not vary between realizations. The distribution and location of this mass throughout the aquifer, though, will of course vary between realizations. As shown in Figure 3-4, the total mass in solution decreases with time somewhat rapidly and then maintains a constant value. The initial decrease reflects the rate of the mass transfer into immobile regions relative to advective transport whereas the final mass in solution reflects the distribution of solute between sorbed and aqueous phases as indicated by the coefficient K_d. The model results for the first two scenarios follow the trends observed in the field indicating that the selected coefficients α and K_d are appropriate. The equilibrium scenario which excludes immobile zones

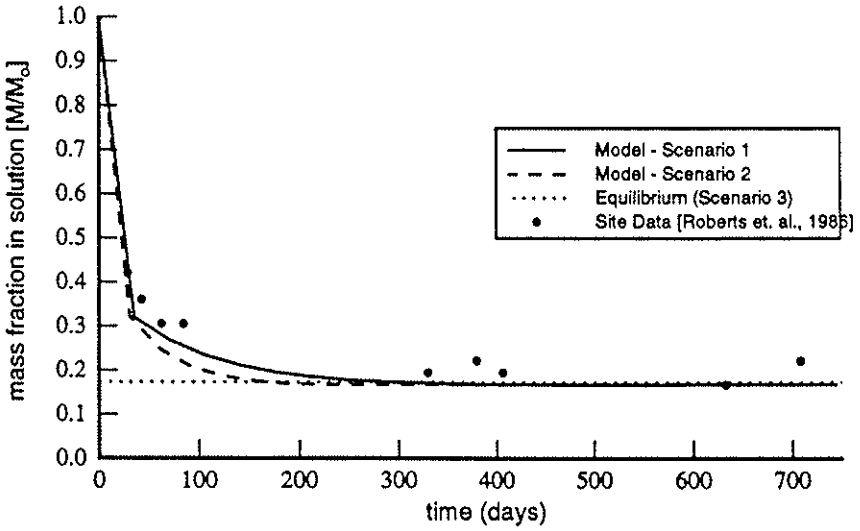

Figure 3-4: Mass of PCE in Solution

results in lower solute concentrations at early times than those observed in the field.

Figures 3-5(a-c) compare the displacement of the centroid of the plume (first spatial moment) with the mean and 95% confidence intervals based on the 2500 realizations generated for the three model scenarios. The mean displacement for scenarios 1 and 2 clearly follows the field observations. The consequence of the presence of sorption sites within the immobile regions of the soil and the limitations of diffusive mass transfer is that initially the plume is less retarded and migrates more rapidly. As adequate time is allowed for the solute material to diffuse into the immobile regions and sorb to these interior sites, the rate of displacement decreases. The mean values determined by the model for the first scenario correspond almost exactly with the field values. This indicates that results from the laboratory experiment can be used to determine the mean displacement of a plume in the field. The results for the second scenario, which are based on a much different set of laboratory experiments, also closely follow the field trends. On the other hand, the equilibrium model (scenario 3) results in an under prediction of the displacement of the plume as has been found by others (Curtis et,. al., 1986). If all the sorption sites were readily accessible and adjacent to mobile regions then the plume would have moved much slower and its rate of movement would have been constant.

Figure 3-5 also illustrates the 95% confidence intervals for the first spatial moments based directly on the analysis of the 2500 realizations performed for each scenario. The observed data is well within these 95% confidence

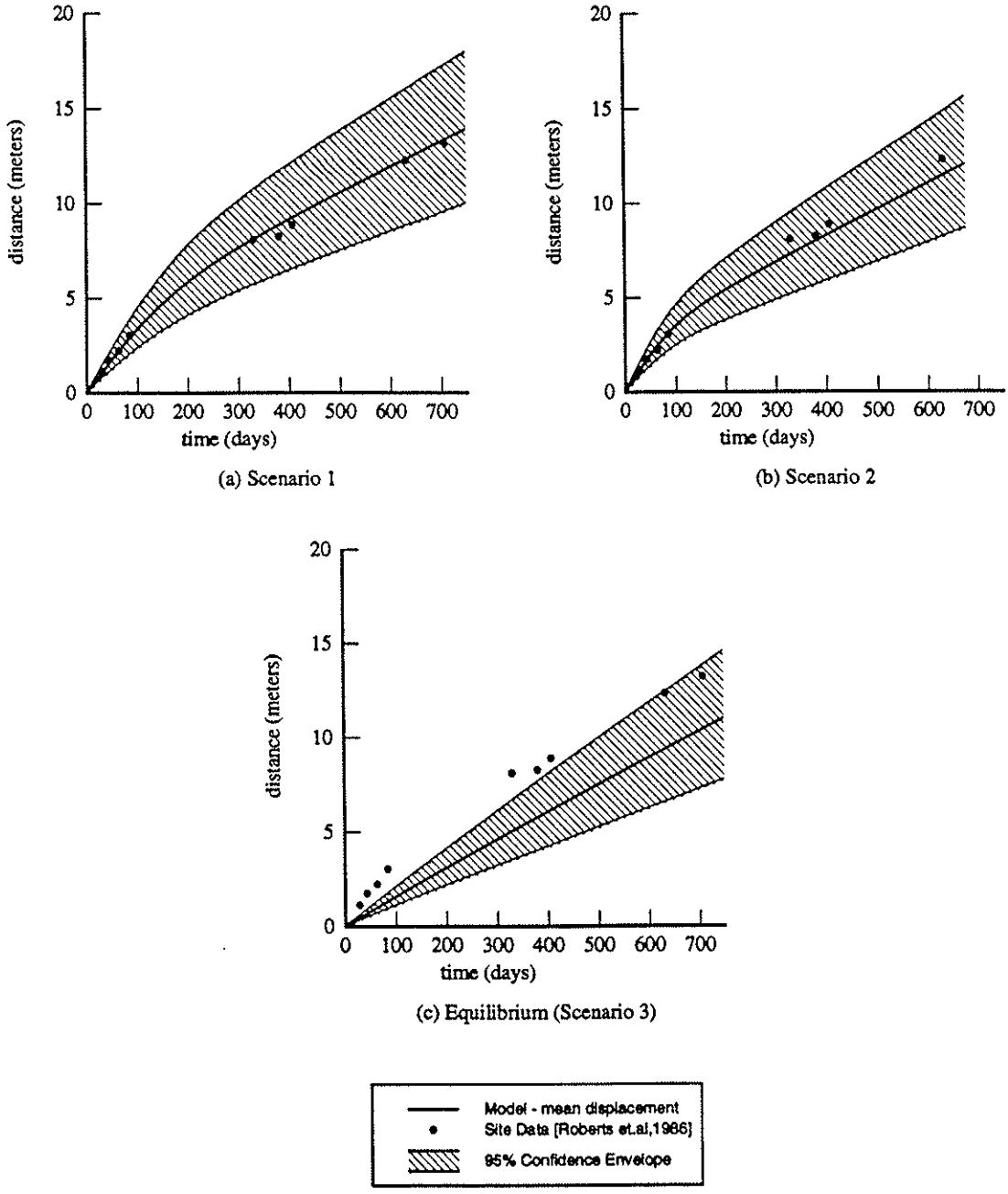

Figure 3-5: Displacement of the Centroid of the PCE Plume

intervals for both scenarios 1 and 2. Despite the relative low variance of the logconductivity (σ_Y^2 =0.24), the confidence intervals are still large and represent a range of +/- 30% about the mean. These intervals, in part, reflect the effects of the unsampled heterogeneity of the hydraulic conductivity on the transport process. This unsampled heterogeneity is quantified here by generating multiple realizations of the flow field. In addition, the non-ergodic nature of the plume further contributes to the uncertainty in its mean displacement. Given the dimensions of the injected plume at the Borden site, it is not expected that the flow paths encountered in an unique realization of the plume's migration would include the ensemble of all feasible possibilities. For the ergodic hypothesis to hold requires that the initial extent of the solute plume lateral to the direction of flow be one to two orders of magnitude larger than the logconductivity integral scale, I_Y (Dagan, 1991). For the Borden experiment, the injected plume was much smaller along the lateral (1.6 I_Y) and the assumption of ergodicity does not apply. The large confidence intervals generated here suggest that for analysis of plume migration in similar formations, the uncertainty in the mean displacement of the plume can be substantial.

The impact of intraparticle diffusion into the immobile regions of the soil matrix on field-scale transport can be illustrated by comparing the retardation factors from the simulations with those measured at the site. The retardation factors R are defined here as:

$$R = \frac{v_{tracer}}{v_{PCE}} \tag{3-12}$$

Using the technique followed by Roberts et. al. (1986), retardation factors were calculated using the mean displacement results from the model. Figure 3-6 compares the observed R with the model simulations. The retardation factor increases with time and the model results follow this trend. The rate of increase is rapid at early times and then slows toward the end of the study. Scenario 1, in particular, follows this trend throughout the simulation whereas scenario 2 overestimates the rate of increase at later times. The equilibrium scenario overestimates R at early times and underestimates it at later times. The overestimation of R at early times results from the exclusion of the time required to establish equilibrium within the interior sorption sites of the soil. In general, the field data and modeling results indicate that the retardation factor R is nonstationary and therefore can not be represented by an average, uniform value for modeling purposes.

The second spatial moments of the PCE plume based on site data were computed by Roberts and Mackay (1986). No previous efforts to explain these spatial moments using theoretical models with laboratory data have been reported in the literature. Models, though, have been directly fitted to these observed values (Quinodoz and Valocchi, 1993) Figure 3-7 compares the longitudinal second spatial moment of the plume with model simulations for the three scenarios. For the first two scenarios, the observed site values are less than the expected values of the second spatial moment, based on 2500 realizations. This reflects the non-ergodic nature of the plume. The observed values do fall within the 95% confidence intervals. These intervals represent a range of almost +/- 50 % about the mean. This uncertainty is again

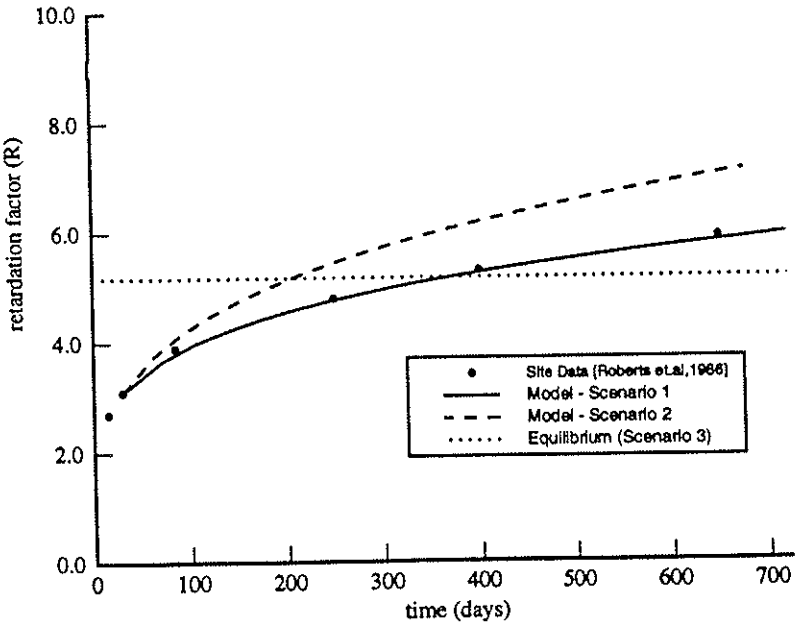

Figure 3-6: Comparison of Retardation Factors

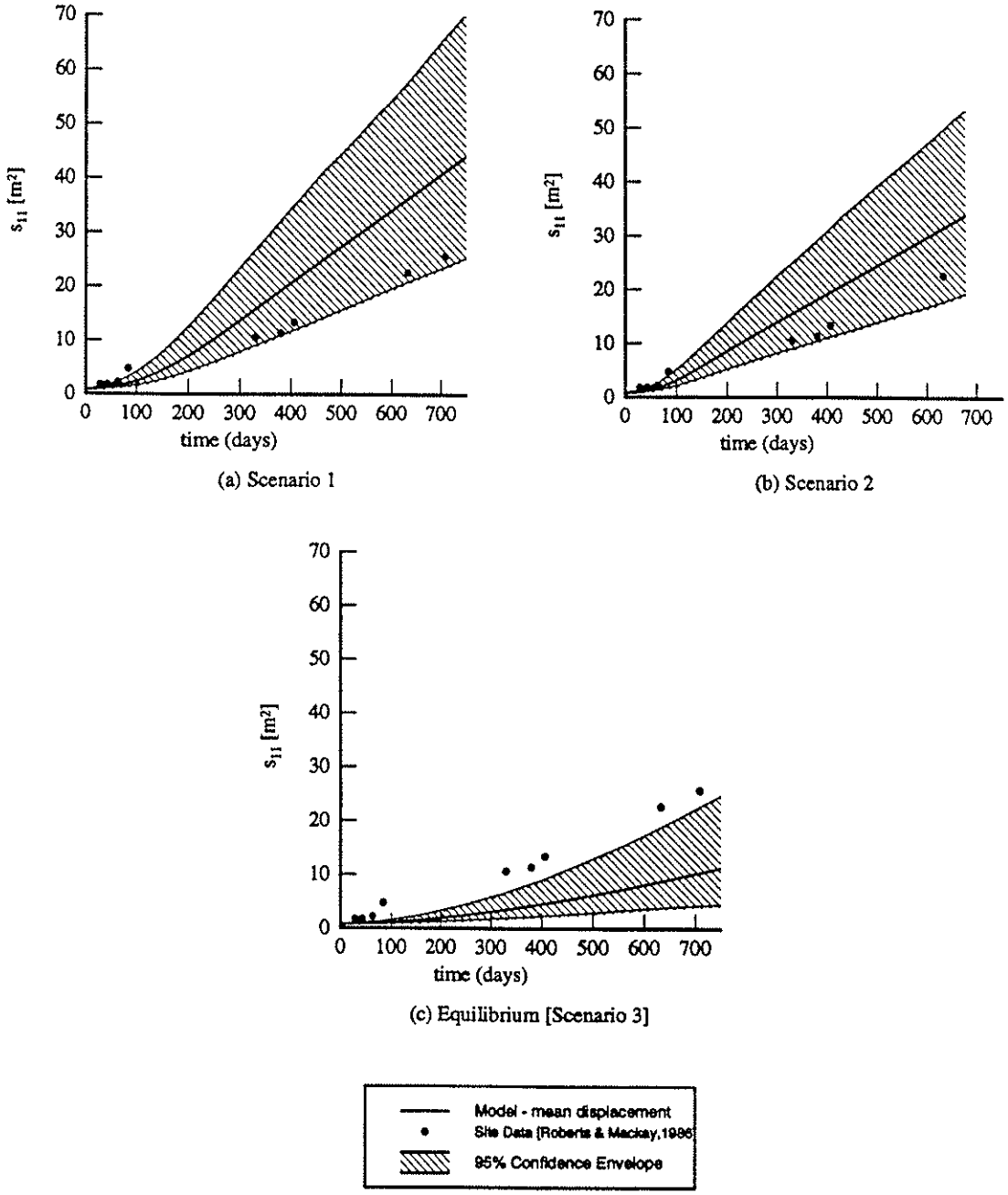

Figure 3-7: Second Spatial Moment of the PCE Plume along the Longitudinal Direction [s_{11}]

attributable to the heterogeneity of the subsurface and the non-ergodic nature of the plume. For the given subsurface properties at the site, the realm of possible formations and subsequent plume spreading generated by the model are inclusive of those observed at the site. Figure 3-8 illustrates the results from selected single realizations (from the 2500 realizations) of the flow field and plume migration. The second spatial moments correspond well the observed site values. This particular realization could not be identified a priori. It is shown here to indicate that observed site values correspond with the possibilities generated by the model. Lastly, for the equilibrium scenario (Figure 3-7c), the second spatial moments are underestimated and the observed data falls outside of the generated confidence intervals.

3.5.2 *Comparison with the Analytical Form of the Solution*

As discussed previously, Dagan and Cvetkovic (1994) coupled their expression for the 2-site kinetic model with analytical expressions for the zero, first, and second spatial moments of a tracer plume. Utilizing a similar approach analytical solutions can be derived for the mobile-immobile model for comparison with the numerical results reported above. Figures 3-9(a) and (b) compare the numerical results for the first scenario with analytical solutions. For the first spatial moments, the solutions are virtually the same. For the second spatial moments, though, the model and analytical solutions are markedly different. The analytical solution result in estimates approximately 40% higher than those from the numerical simulations. This difference is the result of the assumption of ergodicity in the analytical approach. This assumption leads to an overprediction of the second spatial moment since it

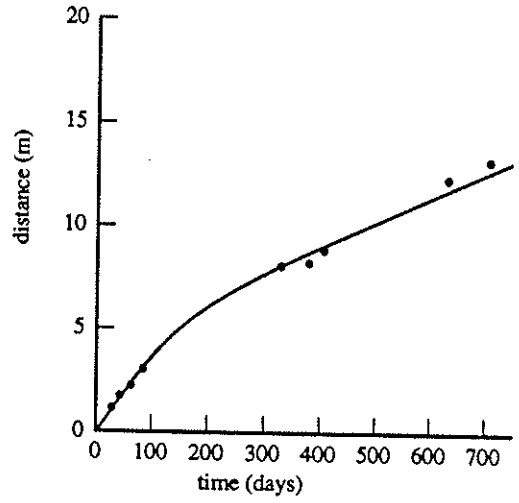

(a) Displacement of Plume Centroid

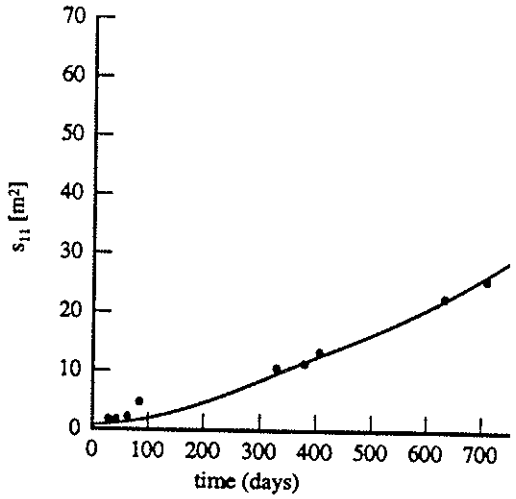

(b) Longitudinal Second Spatial Moment

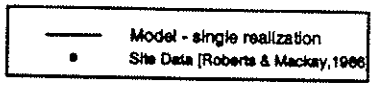

Figure 3-8: Results for a Selected Single Realization

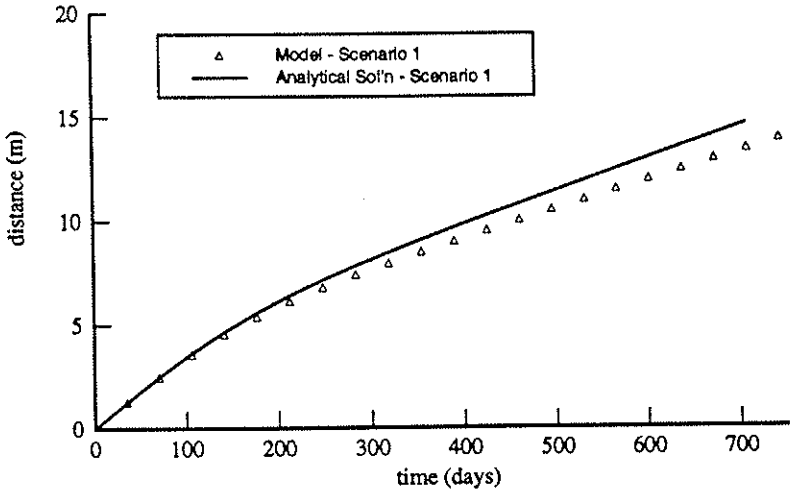

(a) Mean Displacement of the Plume Centroid

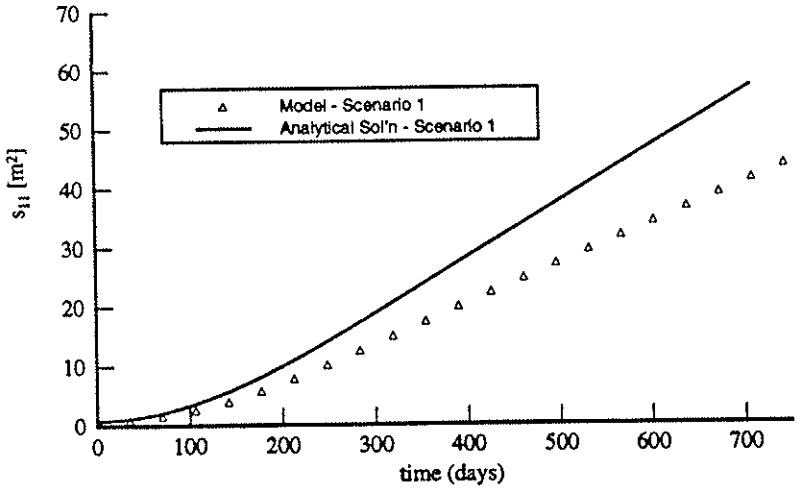

(b) Longitudinal Second Spatial Moment [s_{11}]

Figure 3-9: Comparison of Model Results with Analytical Solutions

includes variations in the mean displacement of the plume as well as the variations about the mean (Dagan, 1991). The assumption of ergodicity does not appear to apply to the Borden field experiment.

3.5.3 *Comparison with Other Modeling Studies*

Several other researchers have compared their models with the field data for PCE transport at the Borden site. These comparisons have been limited to the first spatial moment. Figure 3-10 compares the model results presented here with those from Goltz and Roberts (1988) and Burr et. al. (1994). The model results presented here follow the site data more closely than these previous studies and capture the general observed trends. Both of these other studies utilized a form of the mobile-immobile domain model as part of their analysis and those results are shown here. The differences are in the selection of input parameters and in the method of accounting for solute spreading due to physical heterogeneities. Table 3-3 compares the input parameters used for these other studies with those used with the present model.

Table 3-3: Comparison of Modeling Parameters from Previous Studies

Study	K_d	α (day^{-1})	ϕ	f
Goltz and Roberts (1988)	0.48	0.0006-0.046	0.86	0.86 and 0.4
Burr et. al. (1994)	0.526*	67.2	0.87	0.87
Present study: Scenario 1:	0.76	0.0046	0.87	0.32

*Geometric mean used for generating K_d fields

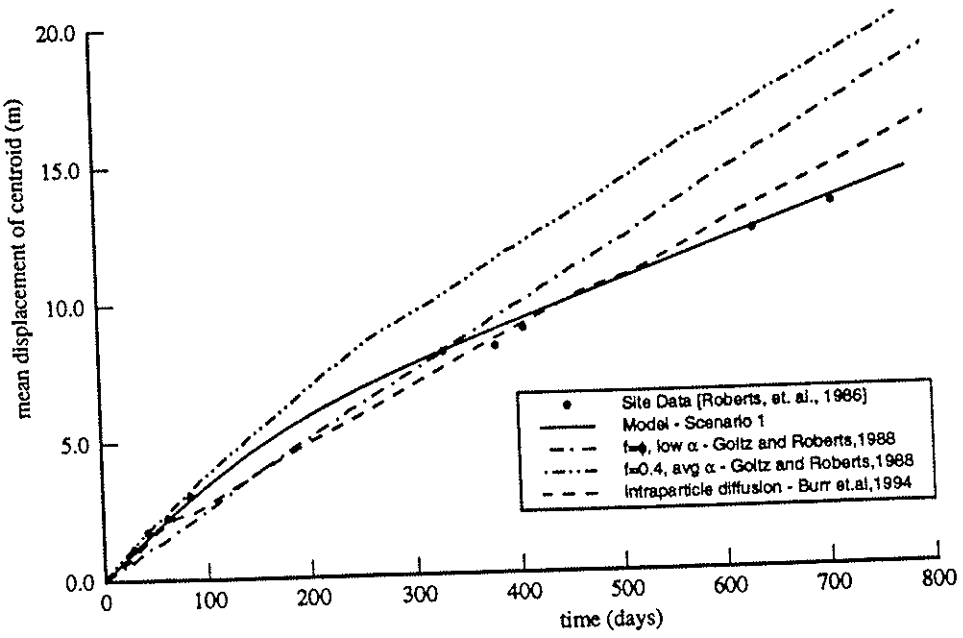

Figure 3-10: Comparison with Previous Studies

The selection of K_d for the other studies is based on the original laboratory experiments by Curtis et. al. (1986). As mentioned previously, Ball and Roberts (1991a) found that additional equilibrium time was required and therefore these values were deemed more appropriate for this study. The selection of α was also different. Burr et. al. (1994) used an empirical expression relating K_d and α to determine its value. The value used by Burr et. al. (1994) is orders of magnitude larger than those used here. Their rate of mass transfer between the immobile and mobile zones is rapid and nearly instantaneous resulting in a virtually linear behavior for the displacement of the centroid with respect to time. Goltz and Roberts (1988) attempted to directly determine α by calculating it based on molecular diffusion. Quantifying inner pore diffusion lengths is difficult and their resulting estimates ranged over two orders of magnitude. It should be noted that the Goltz and Roberts study was completed prior to the work of Ball and Roberts and, therefore, some of the experimental results used here were not available.

The selection of f in the present study is different from those in previous studies. The other studies assumed that $f = \phi$ which may not be appropriate, as discussed previously. Goltz and Roberts (1988) originally used this assumption and then reduced the value of f in an attempt to better fit the field data at early times. These modified estimates are also included in Figure 3-10. The f values used here were based on two different methods -- the portion of sorption occurring rapidly in batch equilibrium tests and the ratio of surface area for bulk and pulverized samples of the Borden soil.

The results presented here indicate that laboratory values for sorption parameters can be used to model field-scale transport, and that the proper selection of these model input parameters is vital. Distribution coefficients must be based on experiments were sufficient time was allowed for equilibrium. The assumption of $f=\phi$ for modeling purposes does not appear to be valid. An alternative is to estimate f based on batch equilibrium experiments or surface area measurements. The importance of using only laboratory data for the input parameters can not be overstated. Many of the mechanisms which can influence the transport of reactive contaminants can be modeled in similar mathematical forms. Fitting parameters to these models based on observed field data does not confirm that the controlling mechanisms have been identified but merely that the true controlling mechanisms can be represented by a similar mathematical form. By limiting input parameters to independent laboratory results, additional credibility can be given to the recognition of a certain process as controlling and leads to a better understanding of the transport of reactive contaminants on the field-scale.

3.6 Conclusions

The model results presented here account for the primary phenomena which control transport and captured the major trends observed in the field-scale experiment performed at Borden. The model couples a stochastic technique for generating 3-D flow fields with a mobile-immobile model for simulating sorption processes. The form of the model allows for the generation of 95% confidence intervals for predictive purposes. The model simulations are

based on basic site information and independent laboratory data for the sorption parameters. No parameters are fitted to field results for the plume migration. A number of conclusions can be drawn from the utilization of the model to simulate the transport of PCE at the Borden site:

- The coupling of the stochastic approach for modeling advective transport with a mobile-immobile model for simulating sorption processes captured the major trends observed in the field data for PCE at the Borden site. This included nearly identical values for the zero and first spatial moments of the plume. The observed second spatial moments were within the predicted 95% confidence intervals. The model results more closely resembled the field data than previous studies reported in the literature.
- One of the primary mechanism controlling the sorption of PCE in the Borden soil appears to be intraparticle mass diffusion which can be adequately modeled using a mobile-immobile domain approach.
- An analytical solution is available which can account for the general trends observed for the first spatial moment. These solutions, though, dramatically overestimate the second spatial moment and do not allow for direct determination of confidence intervals. This overestimation is due to the assumption of ergodicity utilized in the derivation of the solution.
- The results presented here also indicate that proper selection of model input parameters is vital. Equilibrium distribution coefficients must be based on experiments were sufficient time was allowed for equilibrium. The assumption of $f=\phi$ for modeling

purposes does not appear to be valid. An alternative is to estimate f based on batch equilibrium experiments or surface area measurements.

- The method for generating 3D flow fields is rapid and allowed for generating 2500 realizations of the field for statistical analysis. Previous studies had only reported results from several realizations.

The importance of using only laboratory data for the input parameters can not be overstated. Many of the mechanisms which can influence the transport of reactive contaminants can be modeled in similar mathematical forms. Fitting parameters to these models based on observed data does not confirm that the controlling mechanisms have been identified but merely that the true controlling mechanisms can be represented by a similar mathematical form. In addition, a major constraint in developing sorption models has been the inability to observe sorption processes on the microscopic scale. As such, a macroscopic analysis, as presented here, can only indicate that mass transfer resistances in the aqueous phase may be the controlling mechanism.

Recently, Turcke and Kueper (1996) completed additional sampling and analysis of the subsurface hydraulic properties at the Borden site. Their sampling location was approximately 60 m from the sampling area used in the original study. The correlation structure and correlation scales determined for their samples are similar to those reported by Woodbury and Sudicky (1991). The mean and variance (of the log-permeability), though,

could not be shown to be statistically similar to those reported in previous studies. In general, the parameters listed in Table 3-1, as well as the sorption parameters, are subject to variations and uncertainties due to experimental imprecision. Accounting for these uncertainties might result in larger confidence intervals than those shown in Figures 3-5 and 3-7.

The model, in the form presented here, is for the simulation of the transport of dissolved nonpolar organic solutes. It should be noted that for other types of dissolved contaminants such as ionic and/or polar organic compounds and metals, the sorption process may be limited by other mechanisms such as surface reaction kinetics. This process has been modeled by utilizing two-site kinetic models (Cameron and Klute, 1977; Selim et. al., 1976), multiple site models (Pedit and Miller, 1994), or a distribution of sorption sites (Chen and Wagenet, 1995). The two-site model allows for a certain portion of the sites to be treated as kinetically limited while the remainder are assume to achieve equilibrium instantaneously. The two-site model is mathematically analogous to the mobile-immobile domain model and both models can be represented by a generalized form where only the definition of the dimensionless parameters differs (Nkedi-Kizza et. al., 1984; Haggerty and Gorelick, 1995). The approach shown here can, therefore, be applied to these other types of dissolved contaminants by replacing the parameters in eqn 3-2 with those for the 2-site model. For incorporating other types of kinetic models, accounting for the presence of nonaqueous phase liquids (NAPL), or including continuous sources, eqn 3-1 would have to be modified and new expressions derived for eqns 3-5 through 3-9 using different boundary conditions, if applicable. The technique though would remain the same

Also, for modeling field sites other than Borden, other algorithms for the velocity covariance may be more appropriate and can be utilized by the model for determining the conditioning coefficients for the flow fields. For example, algorithms have been derived to represent a uniformly-recharged field (Rubin and Bellin, 1994) and a nonstationary logconductivity field (Rubin and Seong, 1994).

In conclusion, the relative importance of the potential controlling mechanisms will depend on the type of solute, the properties of the aquifer material, and the scale of the analysis. For field-scale applications, the utilization of a mobile-immobile domain model within the framework of 3-D stochastic groundwater model appears to adequately simulate the transport of dissolved nonpolar organic compounds. Proper selection and interpretation of laboratory experiments is necessary for determining the input sorption parameters. As demonstrated here, the unmapped heterogeneities of the subsurface hydraulic properties and the non-ergodic nature of a plume can be important factors in assessing the field-scale transport of reactive solutes.

CHAPTER 4

The Coupled Effects of Subsurface Heterogeneities and Nonequilibrium Processes on Reactive Solute Transport

The inter-relationship between heterogeneities in subsurface hydraulic properties and the nonequilibrium processes associated with the sorption of solutes are analyzed for field-scale transport in three-dimensional porous media. Formations are considered in which the hydraulic properties are statistically anisotropic and the spatial variability of the groundwater velocity is represented as a spatially random process. The analysis is completed using a model which couples a stochastic technique for generating 3-D flow fields with a mobile-immobile domain or 2-site kinetic model to account for sorption and intraparticle mass diffusion or surface reaction kinetics. Rate coefficients are assumed to be spatially uniform. The inter-relationships between subsurface heterogeneities and nonequilibrium processes are analyzed in terms of local solute concentrations and their cumulative distribution functions (CDF). The transport mechanisms are found to be non-additive due to the rate dependency of the nonequilibrium processes. For statistically isotropic formations, the CDF is found to be similar to a truncated normal distribution for instances when the characteristic time of the nonequilibrium process is on the order of advective transport. For statistically anisotropic formations, the CDF for reactive solute concentrations closely resembles a log-normal distribution. For tracer concentrations, the distributions are found to be non-Gaussian in 3-D statistically isotropic and anisotropic formations. The coefficient of variation for tracers in these 3-D formations is also found to follow the expression given by Dagan (1989).

4.1 Introduction

Most research in the field of modeling of contaminant and tracer transport processes has focused on determining the ensemble mean concentration of solutes in natural porous formations. Less effort has been devoted to the

areas of concentration uncertainty and probability distribution functions (PDF) of concentrations. As a result, estimates are usually limited to the mean and variance of solute concentrations at points of interest. Unless its distribution is known (e.g., Gaussian), solute concentrations are not fully characterized by their first two moments. Previous efforts in this area indicate that the distributions are non-Gaussian. In a two-dimensional analysis, Bellin et. al. (1994) found that the PDF of tracer concentrations were non-Gaussian except when averaged over large areas. Kabala and Sposito (1994) expanded on this work to consider instantly adsorbing reactive solutes. They demonstrated that point concentrations are highly uncertain except at their mean arrival times. They also proved that instantly adsorbing reactive solutes also have a non-Gaussian concentration PDF. The distribution was found to be bi-modal with a sharp peak at zero concentration. This corresponds with the theory for tracer transport put forth by Dagan (1982).

The analysis in this chapter expands on these previous efforts and considers reactive solutes which are subject to physical or chemical nonequilibrium processes. These processes can include intraparticle diffusion, diffusion within the solid matrix, or surface reaction kinetics. These have been previously represented by first-order rate models. The transport of these solutes through 3-D geological formations is analyzed. Except as noted above, little work has been done to investigate the form of solute concentration distributions undergoing field-scale transport.

The uncertainties and statistical distribution of local solute concentrations are also important for regulatory considerations. The current regulatory

environment requires or implies the estimation of solute concentrations in a probabilistic manner. A number of these regulations are discussed in Chapter 1 and indicate the need to determine full statistical distributions of solute concentrations to meet regulatory requirements.

This chapter focuses on analyses of local solute concentrations during transport whereas Chapter 3 considered the spatial moments of the plume. Generic solutes and aquifers are considered, and their properties are defined by the model parameters ω, β, R_m, e, and σ_Y^2. The remainder of this chapter is divided into three sections. First, the methodology utilized to simulate the transport of contaminants is summarized. Next, results for local solute concentrations are presented and the combined effects of the physical subsurface properties and nonequilibrium sorption processes are analyzed. This includes analysis of the form and general characteristics of the CDFs of local solute concentrations at specified points in the field. These CDFs are generated utilizing a monte carlo approach and are based on 350 to 500 realizations of the field under different conditions. The last section presents the conclusions which can be drawn from this analysis.

4.2 Methodology

The methodology presented and discussed previously in Chapters 2 and 3 is used to generate several hundred realizations of the flow field and simulate subsequent plume migration from which the full statistical distribution of the solute resident concentrations can be determined. The approach entails the coupling of a stochastic technique for generating a flow field with an

immobile-mobile domain or two-site model for representing the sorption process. The methodology utilized for simulating the flow fields and solute transport processes are discussed separately below.

4.2.1 *Generating 3-D Flow Field*

The technique utilized to generate the 3-D flow fields is discussed in detail in Chapter 2 and is briefly summarized here. Using sequential Gaussian conditioning, the components of the fluid velocity vector are computed directly at each node. The spatial mean and variance-covariance tensor of the velocity $\mathbf{v}$ (where $\mathbf{v}$ is a vector representing velocities in three directions) at a given node $\mathbf{x}_N$ (where $\mathbf{x}$ is a vector representing a location in 3-D space) are conditioned on a subset of the velocities previously generated, $\mathbf{v}(\mathbf{x}_1)$ to $\mathbf{v}(\mathbf{x}_{N-1})$, in order to maintain the spatial correlation structure of the velocity field and preserve mass continuity. The conditioning coefficients utilized are based on algorithms for the spatial covariance of the velocities derived from Darcy's Law and the flow equation. Various solutions have been derived for the velocity covariance for a number of field conditions (Rubin and Dagan, 1992b; Rubin, 1990; and Zhang and Neuman, 1992; Rubin and Bellin, 1994; Rubin and Seong, 1994; Indelman and Rubin, 1995). These include algorithms which allow for statistical anisotropy of the integral scale of the logconductivity. Given the conditional mean and variance at the given node, random deviates are generated to compute the components of the vector $\mathbf{v}$ at that node for that particular realization. Moving systematically over the 3-D field, velocities are computed at each node to generate a single realization of the field. For each realization, the entire process is repeated. This technique

generates large 3-D fields more rapidly than previous numerical approaches (see Chapter 2 and Cushey et. al., 1995). The generated flow fields have also been shown to maintain the desired statistics of the fluid velocity, exhibit the specified spatial correlation structure, and maintain mass continuity on an individual block basis (see Chapter 2 and Bellin et. al., 1994; Cushey et. al., 1995).

The flow fields generated for the analysis in this chapter are based on the velocity covariance algorithms presented by Rubin and Dagan (1992b). The assumptions utilized to derive these algorithms include an exponential spatial correlation structure for the logconductivity, a large flow domain, variance of the logconductivity less than unity, steady state conditions, and uniform average flow. The statistical anisotropy of the formation is represented by utilizing separate integral scales for the logconductivity in the vertical and horizontal direction ($I_{Y,V}$ and $I_{Y,H}$, respectively). The integral scale represents the length over which the values are spatially correlated. The parameter e is used to represent the ratio of the integral scales ($e = I_{Y,V} / I_{Y,H}$)

4.2.2 *Simulation of Advection and Sorption*

A Lagrangian approach is used to simulate the displacement of sorbing solutes in heterogeneous porous media. This approach is discussed in detail in Chapter 3 and consists of simulating a large number of solute particles which together constitute the solute body. Single solute particles are larger than the pore scale, to ensure the applicability of Darcy's law, but are much smaller than $I_{Y,V}$ and $I_{Y,H}$ which enable the accurate capture of the media

heterogeneity. As discussed in Chapter 3, the equations for sorption modeling are reformulated in a Lagrangian framework by defining a curvilinear coordinate system s along a streamline. The rate coefficients are assumed to be spatially uniform. The final set of equations and the definition of parameters for the mobile-immobile domain model are reiterated below for comparison with the two-site kinetic model. The mathematical analogy between the mobile-immobile and two-site kinetic models is also discussed.

The following Lagrangian system for the mobile-immobile domain model, assuming negligible pore scale dispersion, was derived in the last chapter (equations 3-7a,b):

$$\beta \frac{\partial C_2}{\partial T} + \frac{\partial C_1}{\partial T} = -\frac{\partial C_1}{\partial \tau} \tag{4-1a}$$

$$\frac{\partial C_2}{\partial T} = \omega (C_1 - C_2) \tag{4-1b}$$

where,

$$\omega = \frac{\alpha}{\theta(1-\phi)R_{im}} \frac{R_m I_{Y,h}}{U} \tag{4-1c}$$

$$\beta = \frac{1-\phi}{\phi} \frac{R_{im}}{R_m} \tag{4-1d}$$

$$R_m = 1 + \frac{\rho_b f K_d}{\phi \theta} \tag{4-1e}$$

$$R_{im} = 1 + \frac{(1-f)\rho_b K_d}{(1-\phi)\theta} \tag{4-1f}$$

$$C_1 = \frac{C_m}{C_o} \qquad C_2 = \frac{C_{im}}{C_o} \tag{4-1g}$$

$$\tau = \frac{U\tau'}{I_{Y,h}} \qquad T = \frac{Ut}{R_m I_{Y,h}} \tag{4-1h}$$

The subscripts m and im refer to the mobile and immobile regions, respectively. In the primary expressions, C is the aqueous concentration [M/L^3]; C_o is the initial solute concentration [M/L^3];T is the dimensionless time relative to the retarded velocity in the mobile zone; and τ is the dimensionless travel time of the tracer particle in the mobile zone. The parameter ω represents the ratio of the characteristic time for advective transport with equilibrium sorption in the mobile zones [$I_{Y,H}/(U/R_m)$] to the characteristic time for mass transfer into the immobile zones. The parameter β represents the distribution of mass between the mobile and immobile zones. The expressions for the retardation factors (R) include the following parameter definitions: ϕ is the fraction of water present in the mobile regions ($\phi = \theta_m/\theta$); θ is the porosity; f is the fraction of sorption sites in direct contact with the mobile phase; ρ_b is the soil bulk density [M/L^3]; and K_d is the equilibrium distribution coefficient between the aqueous and sorbed phases [L^3/M]. The parameter α is the first-order mass transfer coefficient which approximates the physical diffusion process between the mobile and immobile zones and has units [1/t]. This coefficient represents a lumped parameter which includes the contributions of diffusivity and tortuosity. These parameters are discussed in more detail in Chapter 3. Lastly, length scales and time scales are represented in terms of $I_{Y,H}$, the integral scale of the logconductivity in the horizontal direction and U , the mean fluid velocity. Note that t denotes the elapsed travel time while τ' denotes advection time, i.e., the travel time of the tracer particle in the mobile zone.

As discussed in Chapter 3 and Appendix C, nonideal behavior of sorbing solutes can result from noninstantaneous surface reactions, diffusive mass transfer resistances, isotherm nonlinearity, and irreversibility of the adsorption-desorption process (Brusseau and Rao, 1989). The applicability of each of these phenomena depends on the characteristics of the sorbing compound and medium. Observed nonideal behavior is most commonly attributed to physical mass transfer resistances and the kinetics of surface reactions. These are also designated as physical and chemical nonequilibrium processes, respectively. Models which couple these processes with instantaneous equilibrium sorption are referred to as mobile-immobile domain models and two-site kinetic models, respectively. The basis and development of the mobile-immobile domain model is discussed in Chapter 3. The two-site model was first proposed by Cameron and Klute (1977) and Selim et. al. (1976). The premise is that sorption to a certain fraction of sites can be represented by instantaneous equilibrium and the remainder can be represented by a first-order kinetic expression. The two-site model is mathematically analogous to the mobile-immobile model (Nkedi-Kizza, et. al., 1984). For this reason, eqns 4-1(a,b) can also be used to represent the two-site model by redefining the parameters ω and β as well as the other non-dimensional parameters:

$$\omega = k\frac{R_{eq}I_{Y,h}}{U} \tag{4-2a}$$

$$\beta = \left(\frac{R}{R_{eq}} - 1\right) \tag{4-2b}$$

$$R = 1 + \frac{\rho_b K_d}{\theta} \tag{4-2c}$$

$$R_{eq} = 1 + \frac{F\rho_b K_d}{\theta} \tag{4-2d}$$

$$C_1 = \frac{C}{C_o} \qquad C_2 = \frac{S}{K_d C_o} \tag{4-2e}$$

$$\tau = \frac{U\tau'}{I_{Y,h}} \qquad T = \frac{\mathrm{U}t}{R_{eq} I_{Y,h}} \tag{4-2f}$$

where the subscript *eq* refers to instantaneous equilibrium sites; k is the first-order kinetic rate coefficient [1/t]; S is the sorbed concentration [M/M]; and F is the fraction of sites that are assumed to be at equilibrium instantaneously. For the two-site model, ω represents the ratio of the characteristic time of advective transport with sorption to instantaneous equilibrium sites to the characteristic time for the reaction rate for kinetic sites ($1/k$).

This overall approach surpasses previous efforts reported in the literature by coupling the solution of eqn 4-1 with a numerical particle tracking approach to allow for the determination of local solute concentrations and subsequent statistical distribution of these concentrations. The solution for eqn 4-1(a) and (b) is expressed for a single particle as (eqn 3-8):

$$C_1(\tau, T) = \frac{m}{\theta_m v_{1,m}(\mathbf{s})} \gamma(\tau, T)\delta(s_2)\delta(s_3) \tag{4-3}$$

where m is the mass of a solute particle, v is the linear or pore water velocity [L/t], and δ is the Dirac function. The local linear velocity $v_{1,m}(\mathbf{s})$ is directly

available from the generated flow field. Using Laplace transforms and solving for instantaneous injection, the expression for γ is (eqn 3-9):

$$\gamma(\tau,T) = e^{-\omega\beta T}\delta(T-\tau) + \left(\omega^2\beta\tau\right)e^{-\omega(T-\tau+\beta\tau)}\tilde{I}_1\left[\omega^2\beta\tau(T-\tau)\right]H(T-\tau) \qquad (4\text{-}4)$$

where,

$$\tilde{I}_1(z) = \frac{I_1\left(2\sqrt{z}\right)}{\sqrt{z}}$$

I_1 is a modified Bessel function of the first kind of order one and H is the Heaviside function. This derivation is discussed in Chapter 3 and Appendix B.2. In general, the sorption process is described by the parameters ω, β, and R_m for the mobile-immobile model and ω, β, and R_{eq} for the two-site kinetic model.

4.3 Analysis of Local Solute Concentrations

The methodology presented above was used to generate a series of simulations to analyze the impact of the subsurface heterogeneities and sorption parameters on solute concentrations and their statistical distributions. Figure 4-1 is a schematic of the relative positions of the solute plume injection point and the detection blocks in the flow domains generated. The source is instantaneously injected and the transport of the plume is modeled over the generated flow field. For the results presented here, the source has dimensions of L_X=0.1 $I_{Y,H}$, L_y=0.5 $I_{Y,H}$, and L_z = 0.5 $I_{Y,H}$ or $\frac{0.5}{e} I_{Y,V}$. The detection blocks are cubes with the dimension of Δ_X=0.05 $I_{Y,H}$, Δ_y=0.05 $I_{Y,H}$, and Δ_Z=0.05 $I_{Y,H}$ or $\frac{0.05}{e} I_{Y,V}$. The parameters $I_{Y,H}$ and $I_{Y,V}$ refer to

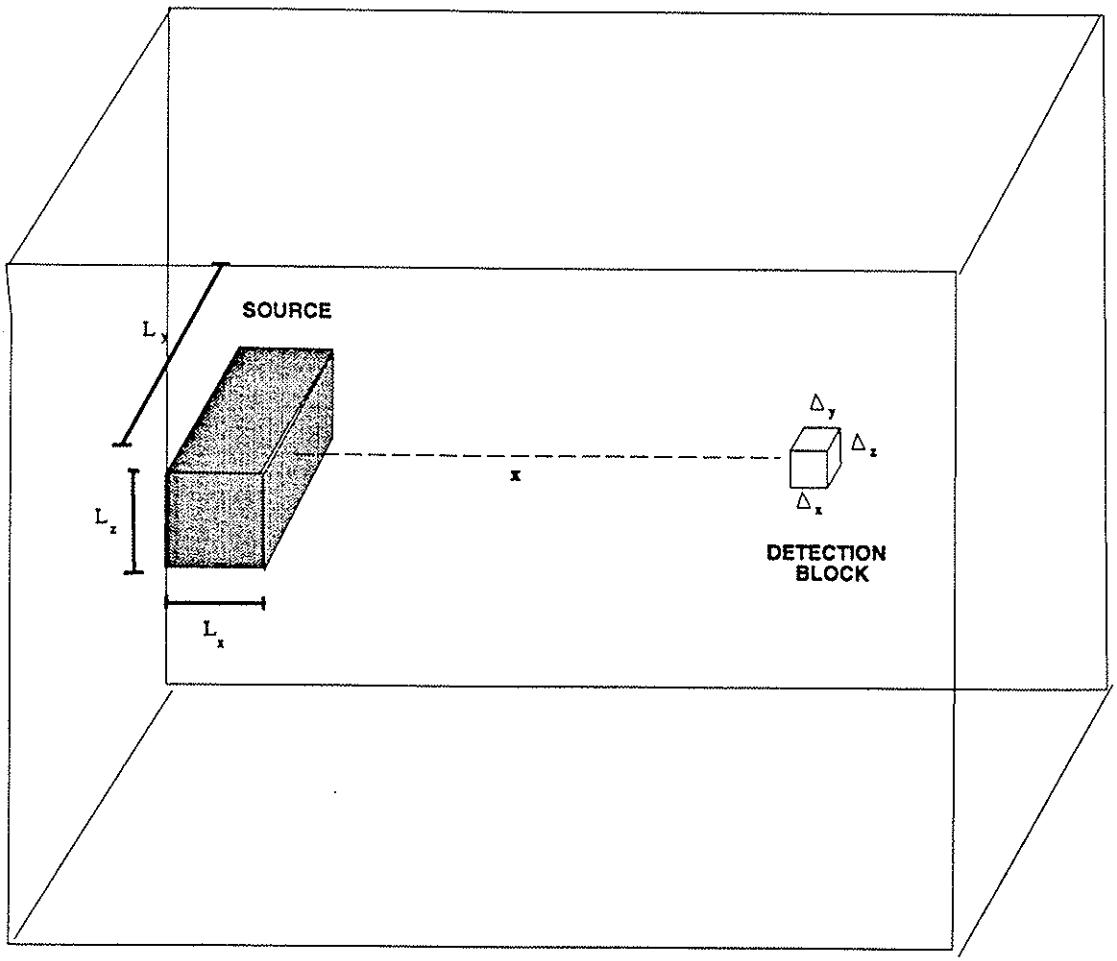

Figure 4–1: Schematic of Contaminant Source and Detection Block

the integral scales of the hydraulic conductivity along the horizontal direction (x and y) and vertical direction (z), respectively. The ratio e was included in the setting of these dimensions so that flow field domains with different representations of statistical anisotropy would have identical dimensional values for the source and detection blocks. The solute plume is modeled using 1,600 to 16,000 particles. The discretization for the velocity field is 0.25 $I_{Y,H}$ horizontally and 0.25 $I_{Y,V}$ vertically. The assumptions regarding the groundwater velocity field discussed at the end of section 4.2.1 apply here. These include an exponential spatial correlation structure for the logconductivity, a large flow domain, variance of the logconductivity less than unity, steady state conditions, and uniform average flow. A time step of $\Delta\tau = 0.01$ is used for all of the analyses presented in this chapter. The concentration referred to here is a resident concentration, and the detection block is equivalent to sampling with a constant volume technique. For the results shown, all lengths are non-dimensionalized by the integral scale of the logconductivity in the horizontal direction ($I_{Y,H}$) and all times are non-dimensionalized by the mean groundwater velocity (U) and $I_{Y,H}$.

The principal results presented here are for the statistics and statistical distributions of solute concentrations based on multiple realizations of the flow field (subsections 4.3.1-4). Before analyzing these results, from multiple realizations, some preliminary insights into the potential effects of the parameters ω, σ_Y^2, and e on plume movement can be formulated on the basis of single realizations. The effects of these individual parameters are analyzed for the transport of solute plume through a single realization of the flow field. For this preliminary analysis, the same set of uncorrelated normal

random deviates is used so that observed differences are attributable to varied parameters only (see Appendix A.2 for a discussion of the utilization of random deviates). The sorption parameters $\beta = 2$ and R_m (or R_{eq}) = 2 are used and other parameters are varied as discussed below.

First, the effect of the sorption parameter ω is considered. Figure 4-2 illustrates the results for three solute plumes transported through a homogeneous porous medium. The three scenarios are for ω = 0.1, 1, and 10 and represent cases where the characteristic time of the nonequilibrium process is greater than, equivalent to, and less than the characteristic time of equilibrium sorption and advective transport. The results shown are the local solute concentration at a distance of 4 $I_{Y,H}$ from the injection point. These can be analyzed both in terms of the mobile-immobile model and the two-site kinetic model. For the first case (ω=0.1), the characteristic time of the nonequilibrium process (mass transfer for the mobile-immobile model or reaction kinetics for the two-site model) is long relative to that of advective flow and equilibrium sorption (sorption adjacent to mobile fluid zones or instantaneous equilibrium sites). A majority of the contaminant remains in mobile zones where it undergoes sorption to a limited number of sites or, for the two-site kinetic model, only undergoes sorption on instantaneous equilibrium sites since the kinetics are slow for the nonequilibrium sites relative to the advective flow. The solute reaches the location at approximately the retarded velocity for the mobile zone or instantaneous equilibrium fraction. There is a long tailing because the material that does reach the immobile zones or undergoes kinetic reactions is released slowly. For the second case (ω=1), the characteristic time for the nonequilibrium

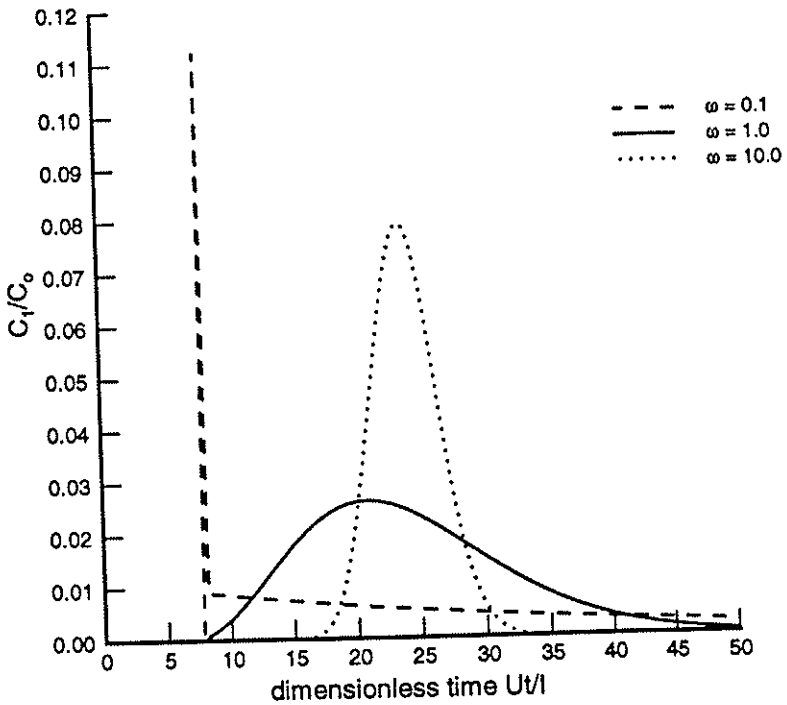

Figure 4-2: Effect of Sorption Parameter ω on Local Solute Concentration at $x = 4\ I_{Y,H}$ in a Single Realization of Homogeneous Porous Media

processes is on the same order of that for advection. Adequate time is allowed for the nonequilibrium processes to occur. The solute is present at this location for an extended period of time due to these nonequilibrium mechanisms. For the last case (ω=10), the characteristic time of the nonequilibrium processes is less than that for advection. For the mobile-immobile zone approach, mass transfer into immobile zones is rapid relative to advective transport and most of the sorption sites are immediately available. The slower arrival time is merely attributable to the exposure of additional sorption sites within the interior of the soil matrix. For the two-site model, the rate of the surface reactions for the nonequilibrium sites are fast relative to the advective flow and most sites are essentially instantaneous.

Figure 4-3 (a,b) illustrates the solute concentrations at a distance of 2 and 4 $I_{Y,H}$ from the source for increasingly more heterogeneous porous media. These results are for a sample single realization for a reactive solute with ω = 1.0. For the example shown here, the maximum concentration decreases and occurs at earlier times for the heterogeneous porous media cases. The earlier time for the peak concentration indicates the presence of regions of higher velocity in the flow field. For higher σ_Y^2, the time corresponding to the maximum concentrations approaches that of a solute sorbing only in the mobile phase or sorbing only on instantaneous equilibrium sites. This indicates that the spatial variability of the hydraulic conductivity becomes a more dominant factor and the effect of the nonequilibrium processes is diminished. At the second location, no concentrations are measured for the

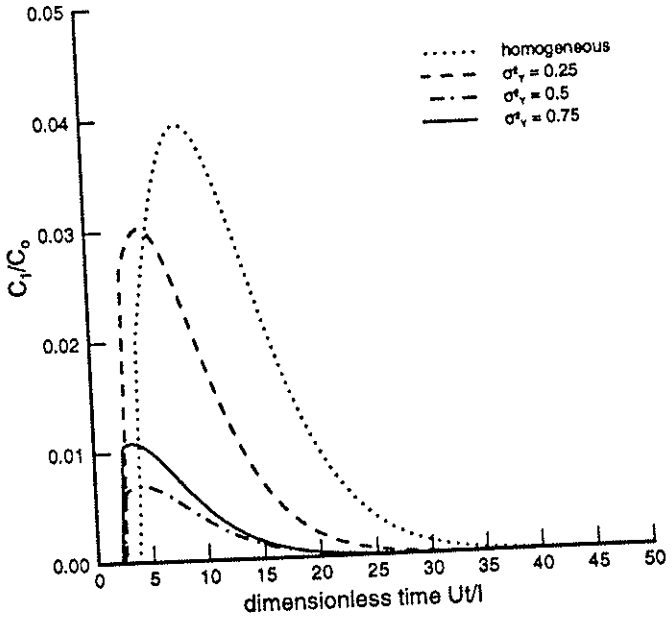

(a) $x = 2\ I_{Y,H}$

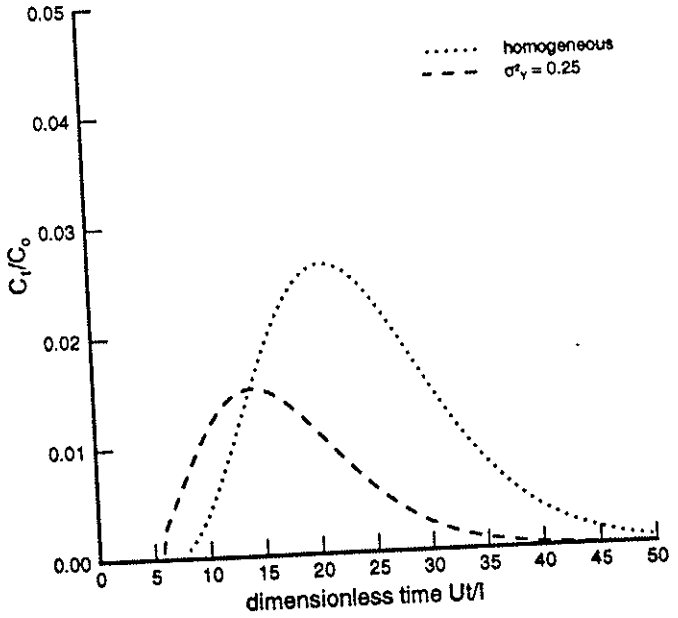

(b) $x = 4\ I_{Y,H}$

Figure 4-3: Effect of Increasing Heterogeneity on Local Solute Concentration [with ω=1] in a Sample Single Realization of a Statistically Isotropic Formation

two higher variabilities. The availability of alternate flowpaths results in the plume bypassing this detection point completely.

The ratio of the integral scales of the logconductivity can also affect the solute concentration. This is illustrated by considering two scenarios in which the integral scale in the vertical direction is one-tenth and one-twentieth of that in the horizontal direction (e = 0.1 and 0.05, respectively). Figure 4-4 shows these results for σ_Y^2=0.25, ω=1, β=2, R_m=2 and compares them with the statistically isotropic case (e=1) for a single realization. For this example, as e decreases ($e = I_{Y,V}/I_{Y,H}$) the magnitude and time of the peak concentration increase. For the e=0.05 case, the increases are more substantial. This can be attributed to the contaminant encountering less extensive regions of high and low flow (see Chapter 2, Figure 2-9). Again, the results shown in Figures 4-2 to 4-4 are for sample single realizations and are presented for preliminary analysis purposes. Results for multiple realizations are presented in subsections 4.3.1-4.

The following four subsections consider the impact of subsurface heterogeneities combined with nonequilibrium processes on local solute concentration statistics including full distributions. Two configurations of the flow domain are considered -- one statistically isotropic (e=1) and one statistically anisotropic (e=0.1). To generate the statistical distribution of the concentration, 350 to 500 realizations for each configuration of the flow field and subsequent tracking of the plume were completed. The results are analyzed to determine the form and general characteristics of the distribution. Additional realizations would be necessary to analyze low probability events.

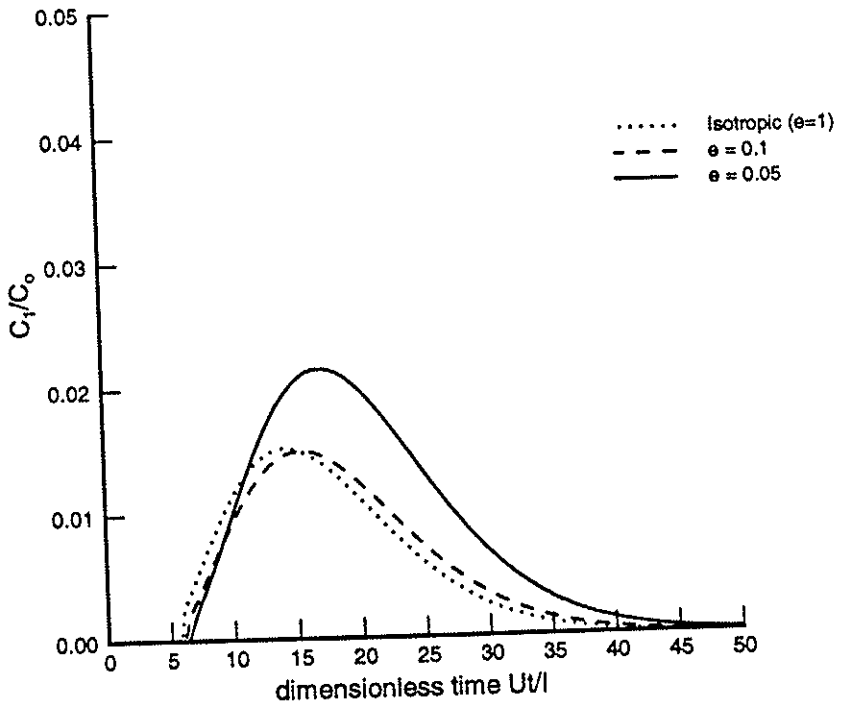

Figure 4-4: Effect of Statistical Anisotropy on Local Solute Concentration at $x = 4\ I_{Y,H}$ for Sample Single Realizations [with ω=1 and σ^2_Y=0.25]

For the results shown below, a variance of 0.25 is assumed for the logconductivity, β is set to 2.0, R_m is set to 2.0, and ω is varied as noted in the figures and discussion. These rate coefficients are all assumed to be spatially uniform.

4.3.1 *Statistically Isotropic Formations*

Five hundred realizations of the flow field in a statistically isotropic heterogeneous porous media (with σ_Y^2=0.25) were generated. The transport of a solute plume through the flow field was simulated for four scenarios (three reactive and a tracer) and local solute concentrations were determined for detection blocks at two locations over time for each realization (as shown in Figure 4-1). The mean and coefficient of variation of the concentrations and their statistical distribution are determined and discussed below.

Average Concentration and Coefficient of Variation

Figure 4-5(a-b) shows the average concentration and the coefficient of variation (CV) with time at the locations x = 2 and 4 $I_{Y,H}$, for a statistically isotropic formation (e=1) based on these realizations. The three scenarios considered (ω = 0.1, 1.0, and 10.0) represent cases were the characteristic time of the non-equilibrium process is greater than, equivalent to, and less than that for advective transport and equilibrium sorption. The maximum average concentrations occur earliest for the ω=0.1 scenario, but solute is present for an extended period of time with tailing continuing beyond the maximum time modeled. For this scenario (ω=0.1), the time of maximum average concentration corresponds with $R_m\tau$ and indicates that the

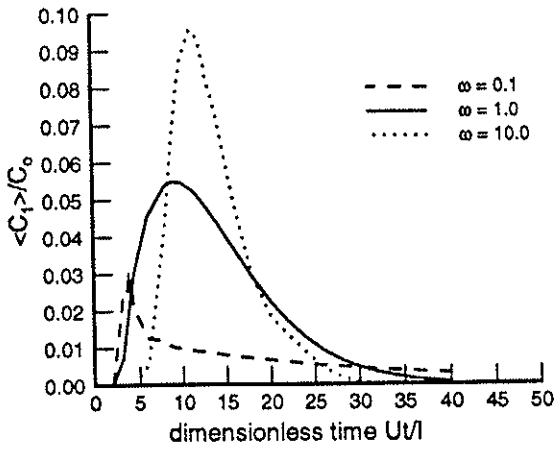

(a) average concentration at $x = 2\ I_{Y,H}$

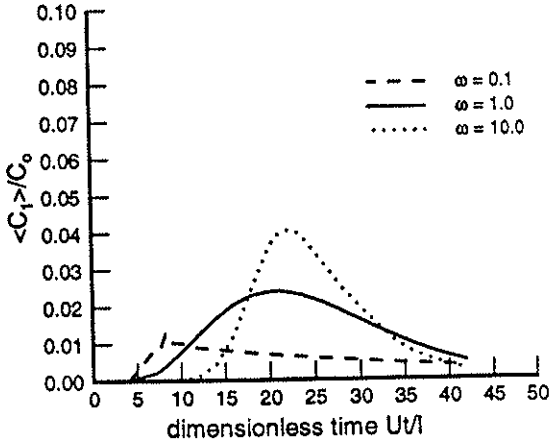

(b) average concentration at $x = 4\ I_{Y,H}$

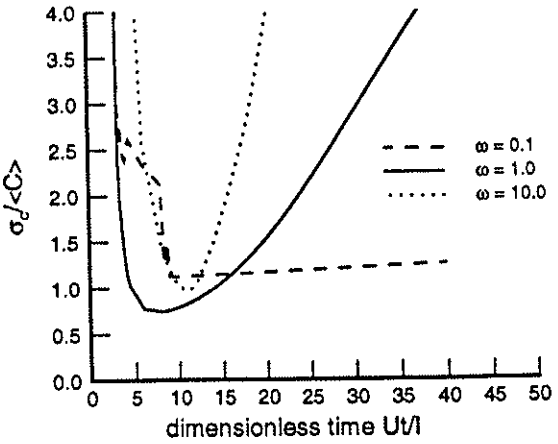

(c) coefficient of variation at $x = 2\ I_{Y,H}$

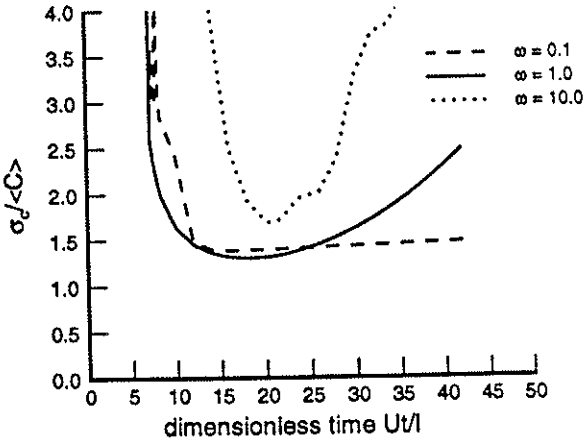

(d) coefficient of variation at $x = 4\ I_{Y,H}$

Figure 4-5: Average Concentration and Coefficient of Variation for Reactive Solutes in a Statistically Isotropic Formation

nonequilibrium processes have not affected the time of arrival but have resulted in excessive tailing. For the other scenarios, the time of maximum average concentration increases due to the presence of the nonequilibrium process. The average concentrations decrease with distance from the injection point for all scenarios.

The coefficient of variation (CV) is also shown in Figure 4-5. The minimum value corresponds with the occurrence of the maximum average concentration for the ω=1 and ω=10 scenarios. For ω=0.1, the minimum value corresponds with the time that the nonequilibrium processes affect the solute concentration as indicated by the kink in the average concentration curve. At the time of maximum average concentration, the CV for this scenario is equivalent to the minimum value for a tracer at that same location (as discussed below). For all three scenarios, the minimum CV was higher for a detection location at 4 $I_{Y,H}$ than at 2 $I_{Y,H}$.

Figure 4-6 illustrates these results for a non-reactive solute or tracer at these same locations. The observed average concentrations are much more irregular and indicate the bimodal nature of tracers. At a given time and location, a tracer is either present or not and remains in the sampling zone for only a brief period. For reactive solutes, though, if the solute arrived at an earlier time than the sampling time, some portion may still remain due to nonequilibrium considerations (e.g., the time required to diffuse out of interior grains or desorb from soil surfaces). For tracers, the minimum CV values was found to occur at the same time as the maximum average concentration. Similar results have been reported by Bellin et. al., (1994) for

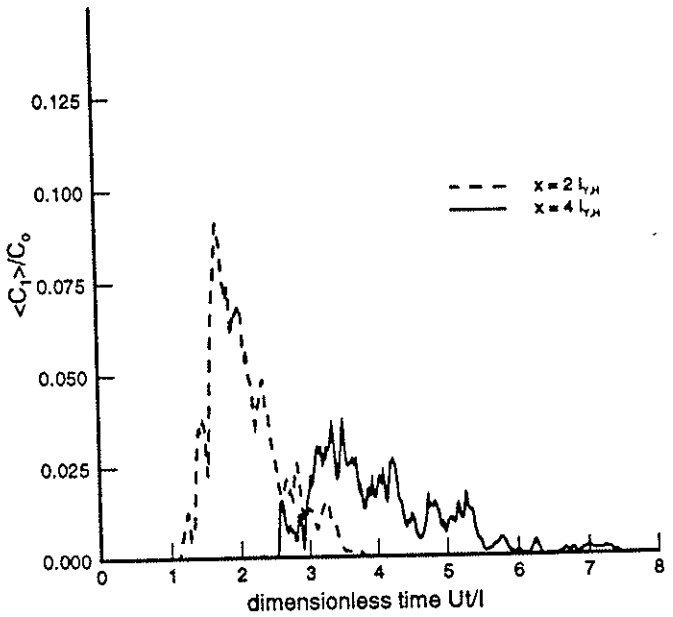

(a) average concentration

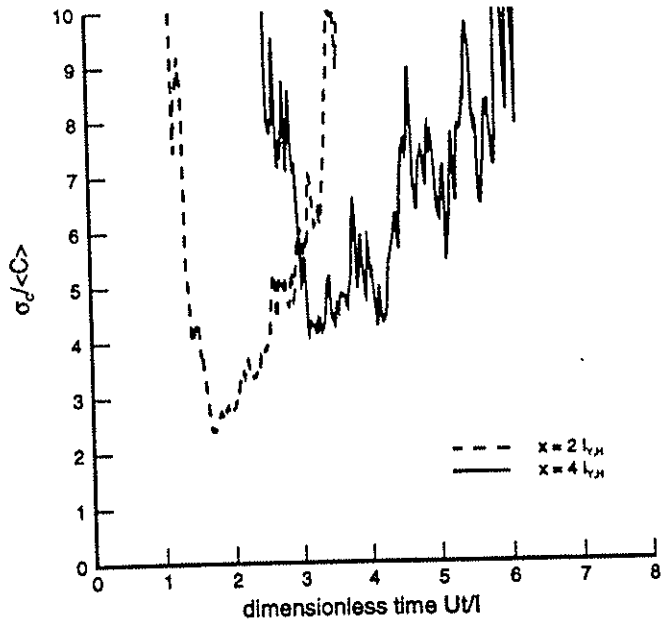

(b) coefficient of variation

Figure 4-6: Average Concentration and Coefficient of Variation for Tracer for Statistically Isotropic Formation

simulated tracer transport in 2-D statistically isotropic formations and by Kabala and Sposito (1994) for instantaneously adsorbing solutes.

Dagan (1982, 1989) derived an expression for the variance of the point concentration of a tracer for the case of negligible pore scale dispersion:

$$\sigma_c^2(\mathbf{x},t) = \langle C(\mathbf{x},t)\rangle\left(C_0 - \langle C(\mathbf{x},t)\rangle\right) \tag{4-5}$$

Because this expression is for a point concentration, it represents an upper bound solution. The resulting expression for CV is:

$$\frac{\sigma_c(\mathbf{x},t)}{\langle C(\mathbf{x},t)\rangle} = \sqrt{\frac{C_0}{\langle C(\mathbf{x},t)\rangle} - 1} \tag{4-6}$$

Figure 4-7 compares this expression with the results shown in Figure 4-6b. The <C(x,t)> is taken from the model results (Figure 4-6a). The CV from the model results are for volume-averaged concentrations and therefore are expected to be lower than those calculated using eqn 4-6 since it is for point concentrations. All of the model results are less than the analytical expression. Since the volumes are small ($O(10^{-4}\ I_{Y,H}^3)$), the results in many instances are found to be quite similar to those for point concentrations. This comparison indicates that eqn 4-6 holds for tracer transport in 3-D statistically isotropic heterogeneous formations. This equation would not apply to reactive solutes subject to nonequilibrium processes because it is based on the premise that the distribution is bimodal.

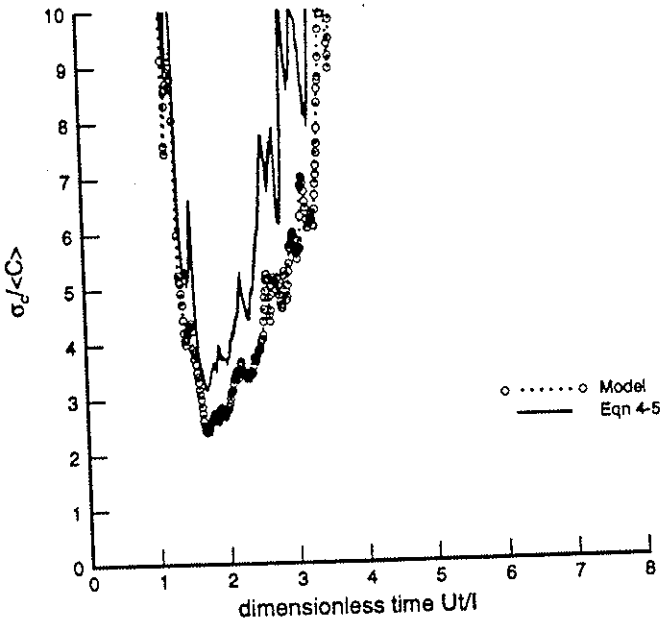

(a) $x = 2\ I_{Y,H}$

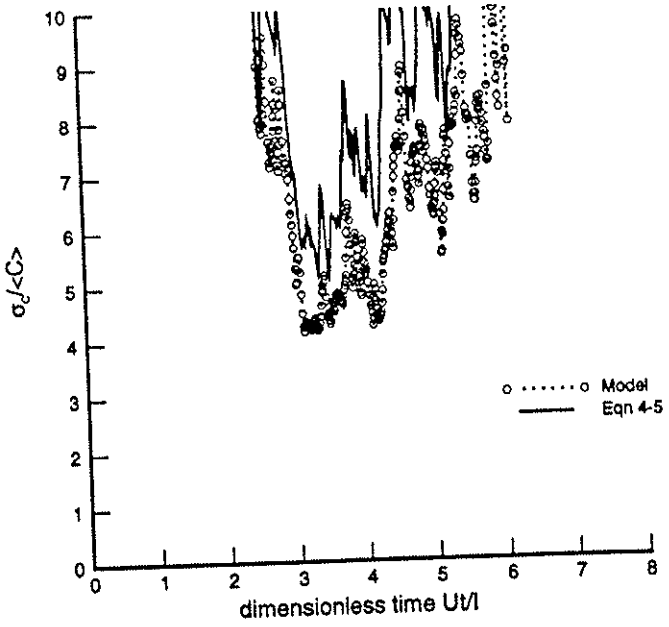

(b) $x = 4\ I_{Y,H}$

Figure 4-7: Comparison of Tracer Coefficient of Variation with Equation 4-6

For the results shown here, the minimum CV is higher at the further location ($x = 4\ I_{Y,H}$). Though only representing results for two locations, this comparison corresponds with the trend derived by Dagan (1989) that the CV of the center of mass of a tracer plume increases with time and eventually goes to infinity for the case of negligible pore scale dispersion (or infinite Peclet number, P_e). For the case of a finite P_e, Kapoor and Gelhar (1994) postulated that the CV for the center of mass of a plume will decrease with time and eventually approach zero. The recent analysis by Dagan (1996) and Fiori and Dagan (1996) contradicts these results and show that, for a large but finite P_e, the CV approaches a constant value rather than zero. Their solution, unlike that of Kapoor and Gelhar (1994a,b), includes a closure relationship which accounts for the covariance of concentration gradients across the plume boundaries as a function of P_e. The inclusion of this in the variance reduction term results in it being of the order $P_e^{-1/2}$. For the case of infinite P_e, this term vanishes and the concentration variance and CV go to infinity. Though the model results shown here for CV can not be used to further confirm these recent findings of Dagan (1996), they do further validate the upper bound expression for CV (eqn 4-6) for the case of negligible pore scale dispersion (infinite P_e).

Statistical Distribution of Concentrations

Figure 4-8(a-f) illustrates the PDF and CDF for reactive compounds at the same location ($x = 4\ I_{Y,H}$) for the three scenarios (ω=0.1, 1, 10) based on 500 realizations. The distributions shown are at the time of maximum average concentration at that location for that scenario. These non-dimensional times ($Ut/I_{Y,H}$) are 8, 20.8, and 22, respectively. These times can be estimated

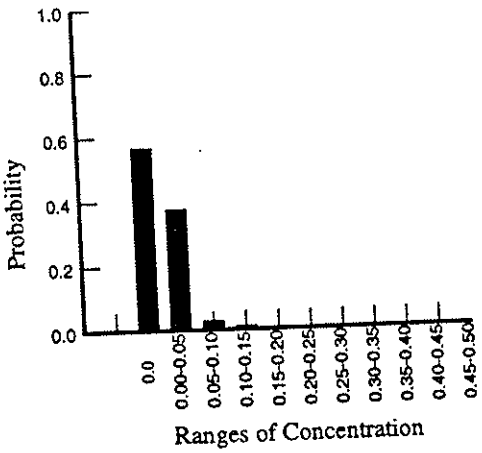

(a) PDF for ω=0.1

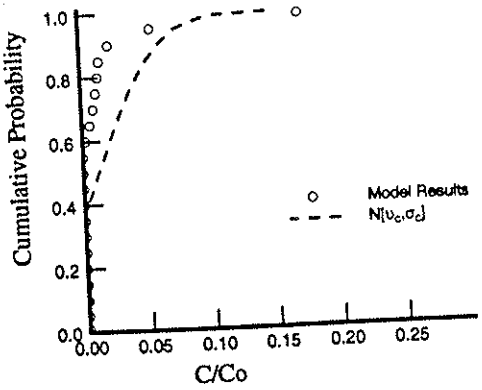

(d) CDF for ω=0.1

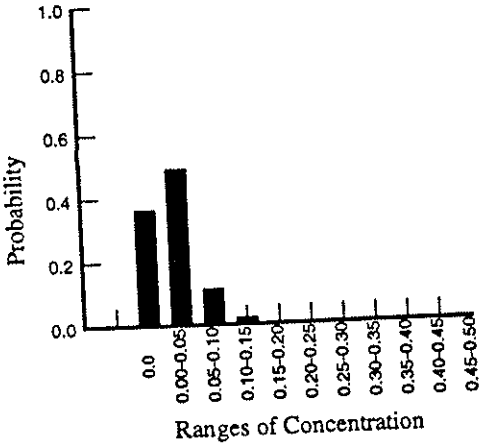

(b) PDF for ω=1

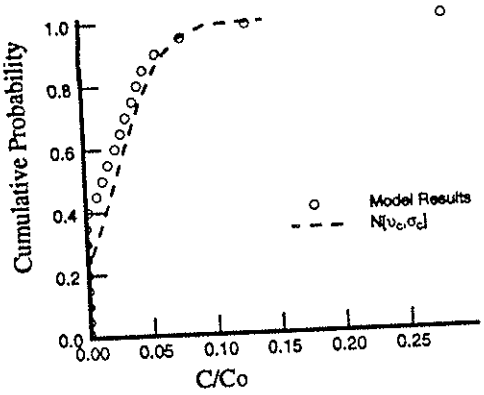

(e) CDF for ω=1

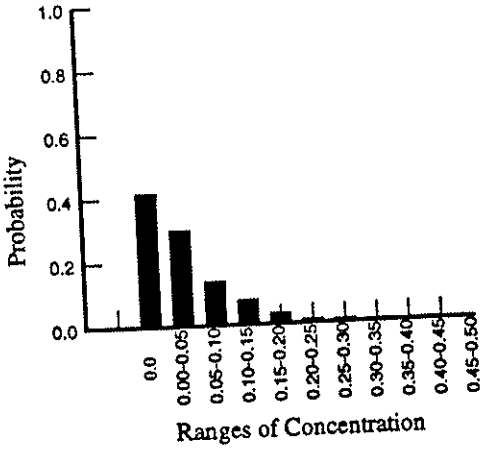

(c) PDF for ω=10

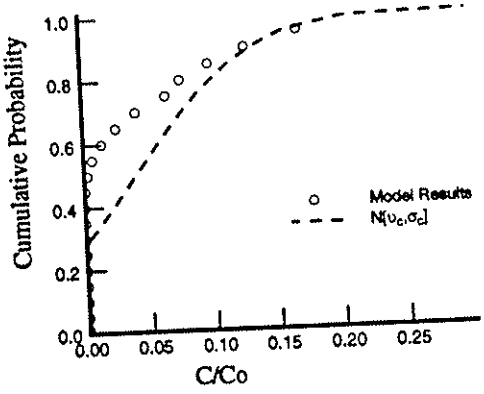

(f) CDF for ω=10

Figure 4-8: PDF and CDF of Local Solute Concentration at x = 4 $I_{Y,H}$ for Statistically Isotropic Formation

by taking the derivative of eqn 4-3 with respect to time (see Appendix B.2). In all three cases, there is a high probability of a zero concentration. The scenario with characteristic times of the same order (ω=1) appears to be the most Gaussian in form. The CDFs for the three scenarios are also compared with a truncated normal distribution. These equivalent distributions were generated using the means and variances of the concentrations determined from the simulations. For the first and last cases (Figures 4-8d and 4-8f), the truncated normal distribution underestimates the cumulative probability for lower concentrations and, as a result, overestimates the probability of not exceeding higher concentrations. These two cases are not fully characterized by their mean and variance. Similar results have been found for tracer concentrations in 2-D heterogeneous formations (Bellin et. al., 1994; Rubin et. al., 1994). For the ω=1 scenario, though, the simulated concentration distribution and truncated normal distribution are similar. For this case, the characteristic times of the nonequilibrium processes and advective transport are on the same order. This results in a smoothing of the bimodal distribution typically associated with a tracer compound and a final distribution in a Gaussian form.

Figure 4-9(a-d) compares the CDF for a tracer with the results for the scenario (ω=1) at two locations. The results for the tracer are at the time of its maximum average concentration. The tracer results are characterized by a high probability of zero concentration which increases with distance from the source. The statisitical distribution is clearly different from the truncated normal distribution. These results are similar to those found for tracers in 2-D statistically isotropic formations (Bellin et. al., 1994; Rubin et. al., 1994). For

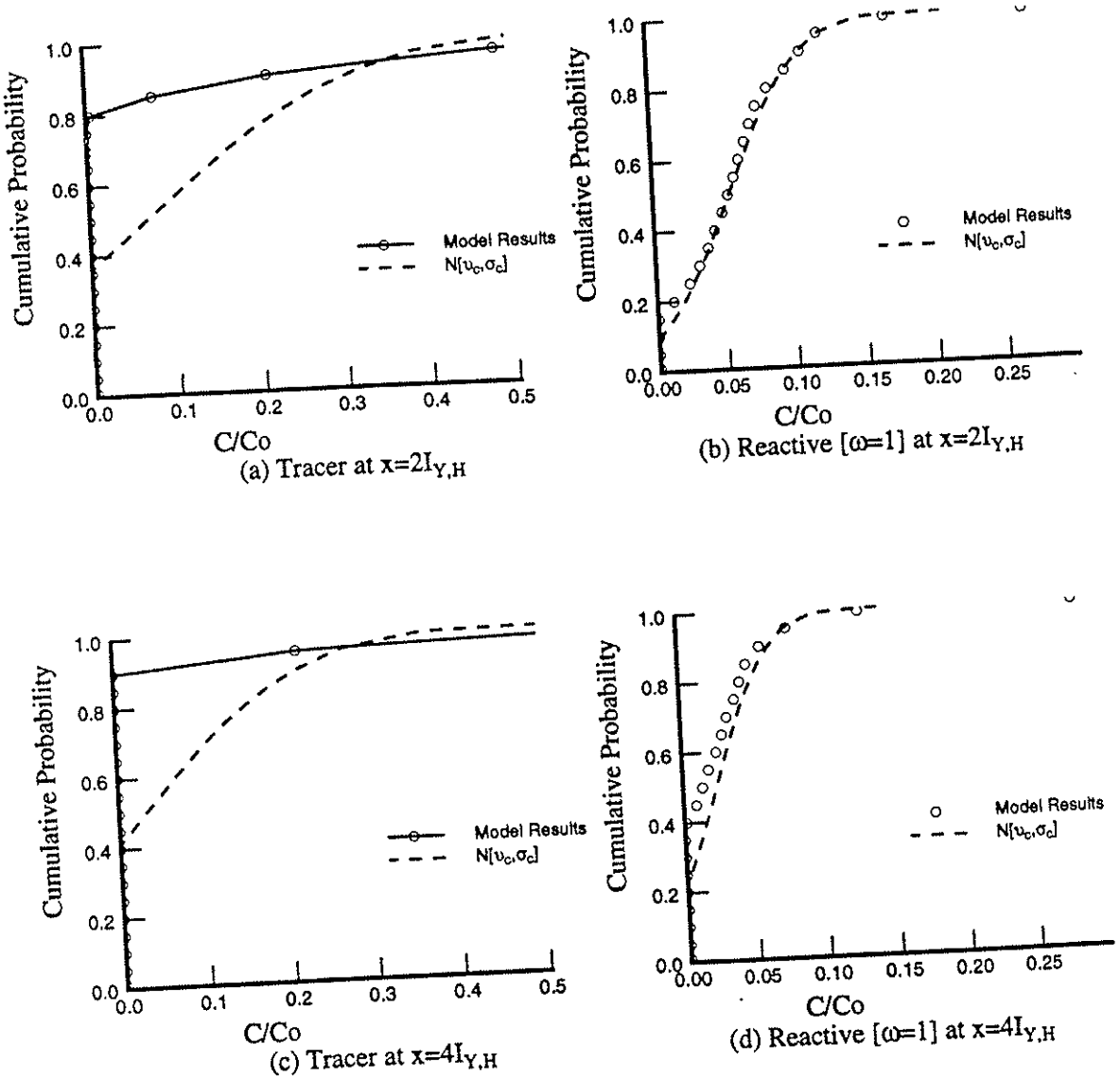

Figure 4-9: Comparison of CDF for Tracer and Solute Concentrations for Statistically Isotropic Formation

the reactive case, the probability of a zero concentration also increases with distance but the magnitude of these probabilities is less than that of the tracer. At both locations, the model results follow a truncated normal distribution.

The consequence of determining only the mean and variance of the solute concentrations as opposed to their full statistical distributions can be demonstrated by comparing the resulting upper confidence bounds. Figure 4-10 illustrates the upper 99% confidence bound for a tracer and reactive solutes (for the scenarios discussed above). The mean and variance of the solute concentration are used with the assumption of a truncated normal distribution to determine the values represented by the white bars. For the tracer, the assumption of a Gaussian distribution results in a significant underestimation of the upper bound concentration. From a regulatory or risk assessment perspective, using only the mean and variance to estimate an upper bound could result in substantially underestimating this value at an exposure point. The model upper bounds are also higher for the reactive compounds but in some instances the differences are less pronounced. For the ω=1 scenario, the difference is minimal and attributable to the model results resembling a truncated normal distribution. Figure 4-11 illustrates this same analysis for the 95% upper confidence bound. For this case, the Gaussian assumption and distributions generated by the model give similar values. In short, the assumption of a truncated normal distribution results in an underestimation of the 99% confidence bounds but not lower bounds. This underestimation is more pronounced for tracers and is reduced for reactive solutes subject to nonequilibrium processes which have characteristic times on the order of that advective transport.

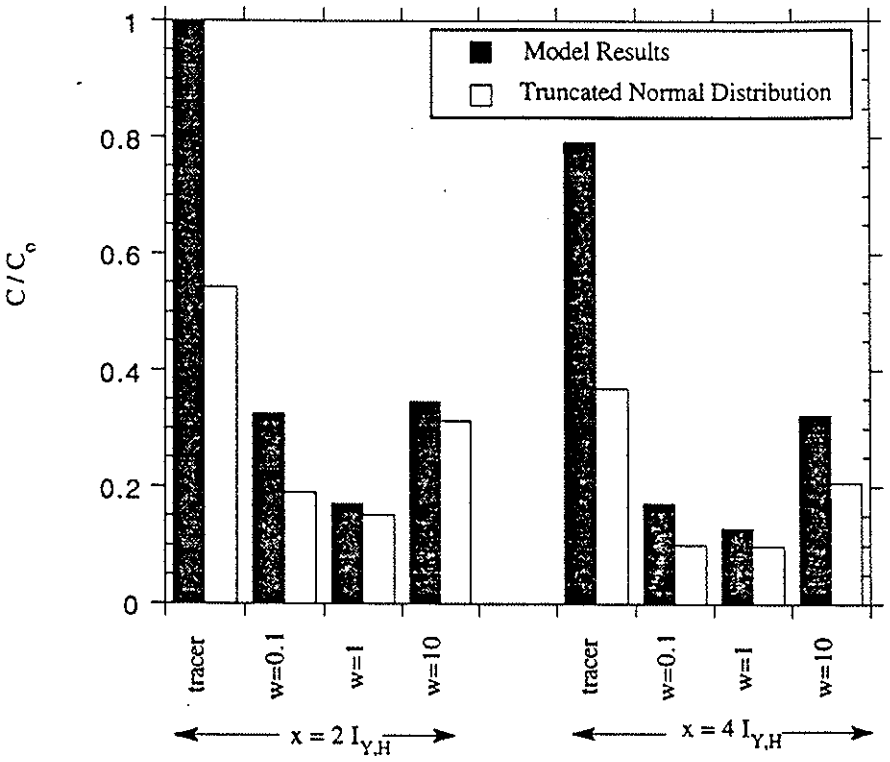

Figure 4-10: Comparison of Upper 99% Confidence Bounds for Statistically Isotropic Formations

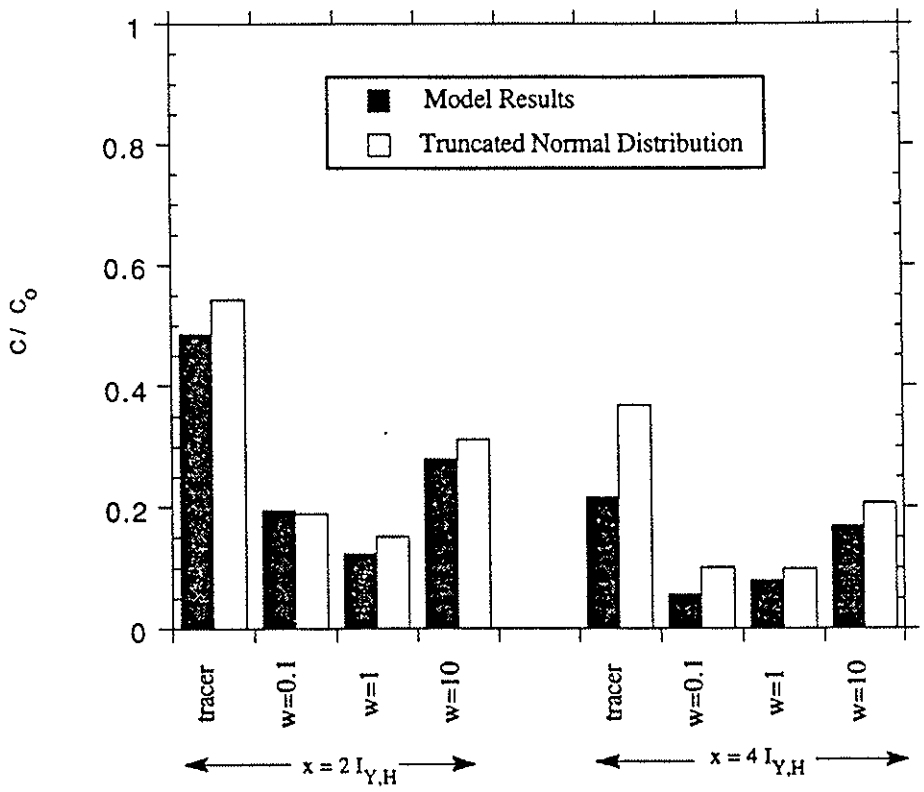

Figure 4-11: Comparison of Upper 95% Confidence Bounds for Statistically Isotropic Formations

4.3.2 *Statistically Anisotropic Formations*

Three hundred and fifty realizations of the flow field in statistically anisotropic (e=0.1) heterogeneous porous media (with σ_Y^2=0.25) were generated for this part of the analysis. Again, the transport of a solute plume through the flow field was simulated for four scenarios (three reactive and a tracer) and local solute concentrations were determined for detection blocks at two locations over time for each realization (as shown in Figure 4-1). The mean and coefficient of variation of the concentrations and their statistical distribution are determined and discussed below.

Average Concentration and Coefficient of Variation

Figure 4-12 (a-b) shows the average concentration and the coefficient of variation (CV) with time at the location x = 4 $I_{Y,H}$, for a statistically anisotropic formation (e=0.1). The integral scale in the vertical direction ($I_{Y,V}$) is only one-tenth as long as the one in the horizontal direction ($I_{Y,H}$). The maximum average concentrations are higher than those for the statistically isotropic formation. The length of time when concentrations are observed at this location is also longer than that for the isotropic case. The CV for all cases reaches its minimum near the time of the maximum average concentration. This is similar to the observations for the 3-D statistically isotropic formations. The magnitude of these minimum CV is also similar to those determined for the statistically isotropic case. The general shape of the curve at later times though is steeper and more comparable to those for tracers and instantly adsorbing solutes.

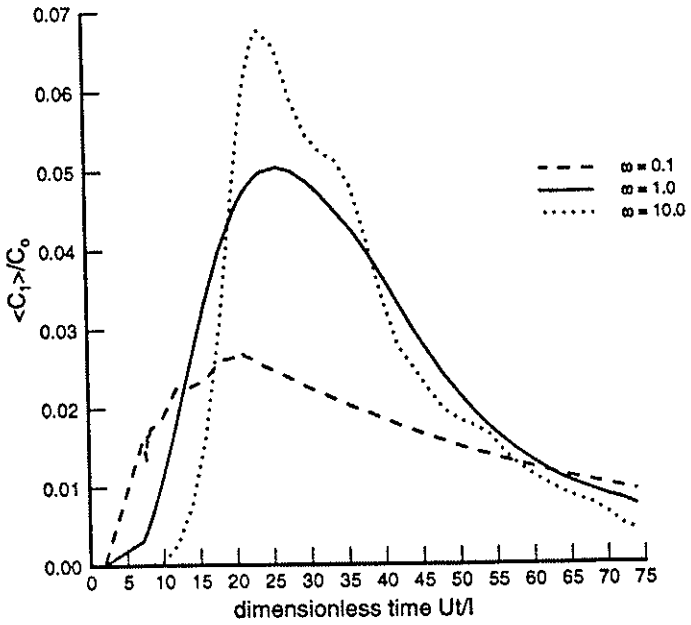

(a) average concentration

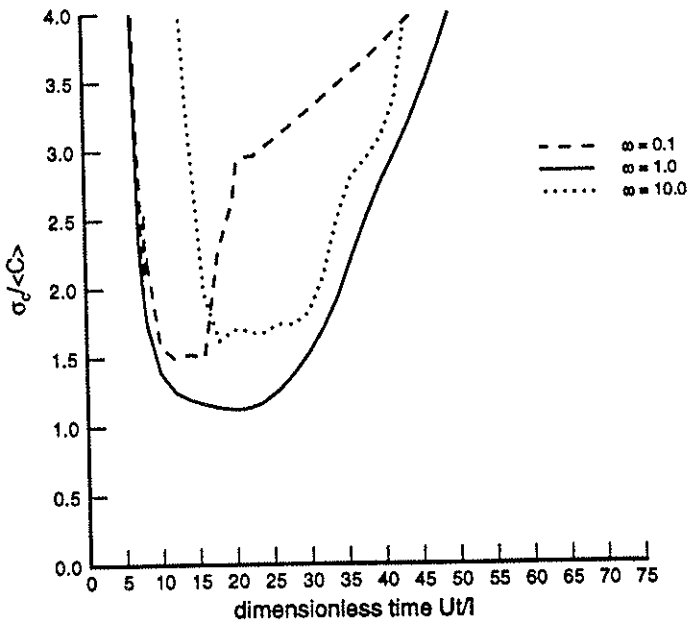

(b) coefficient of variation

Figure 4-12: Average Concentration and Coefficient of Variation at $x = 4\ I_{Y,H}$ for Statistically Anisotropic Formation (e=0.1)

Statistical Distribution of Concentrations

Figure 4-13 (a-f) illustrates the PDF and CDF for reactive compounds at the same location. The distributions shown are at the time which corresponds with the maximum average concentration at that location. The shape of the PDF is more unimodal than for the isotropic formation and the probability of observing a zero concentration is substantially reduced. The CDFs are compared with both a truncated normal distribution and a log-normal distribution. For all three cases, the distributions generated are similar to a log-normal distribution. For the ω=1 case, in particular, the distribution based on the model results is nearly identical to a log-normal distribution. The reduced vertical correlation length for the anisotropic formation results in the plume passing through many layers of the formation which can have substantially different velocities. In addition, for anisotropic formations (e<1), the horizontal length scale over which velocities are correlated is less than in the isotropic case (see Chapter 2). The plume is subjected to groundwater velocities which vary more substantially and are less spatially correlated than in the isotropic case. Through encountering these multiple layers of velocities, the distribution, by the central limit theorem, approaches a Gaussian form. For the last case, w=10, the distribution deviates from a log-normal distribution at lower concentrations due to the probability of zero concentrations (which is always zero for a log-normal distribution).

Figure 4-14 (a-d) compares the CDF for a tracer with the results for the scenario (ω=1) at two locations. The results for the tracer are at the time of its maximum average concentration. For the tracer, the probability of a zero concentration is still elevated but less than in the statistically isotropic case.

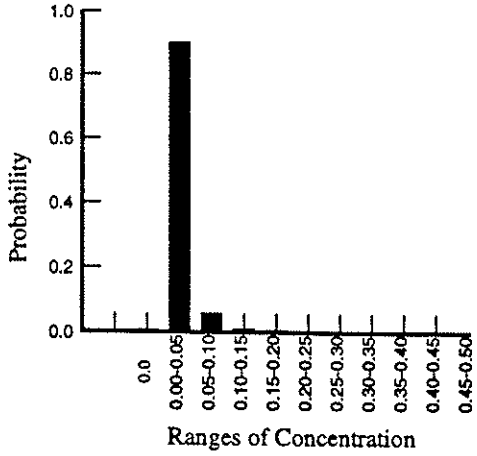

(a) PDF for ω=0.1

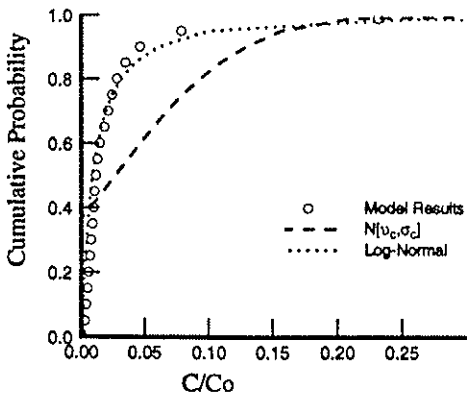

(d) CDF for ω=0.1

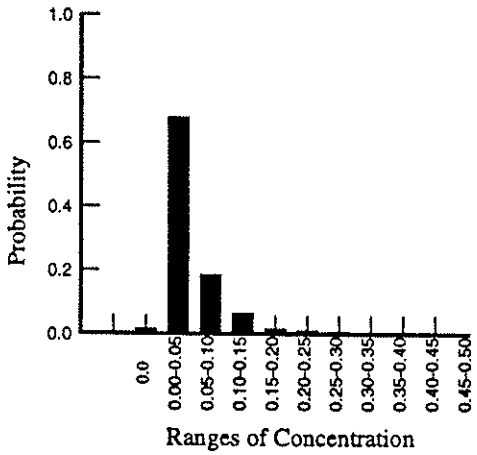

(b) PDF for ω=1

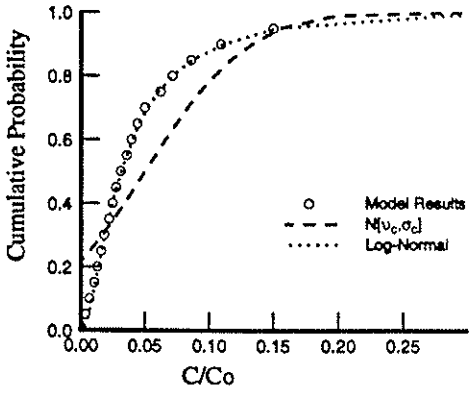

(e) CDF for ω=1

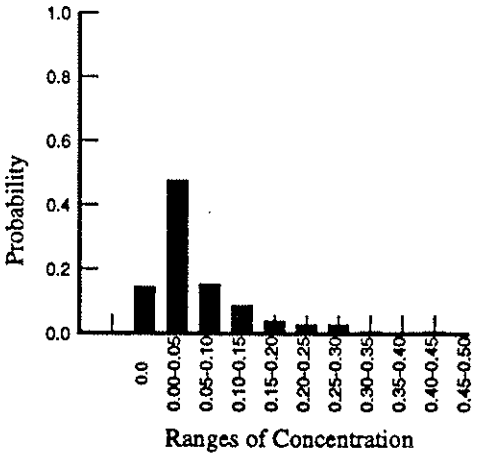

(c) PDF for ω=10

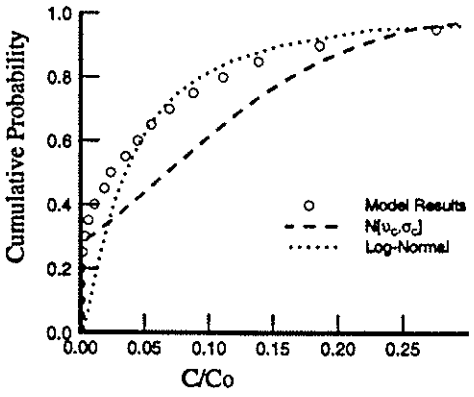

(f) CDF for ω=10

Figure 4-13: PDF and CDF of Local Solute Concentration at x = 4 $I_{Y,H}$ for Statistically Anisotropic Formation (e=0.1)

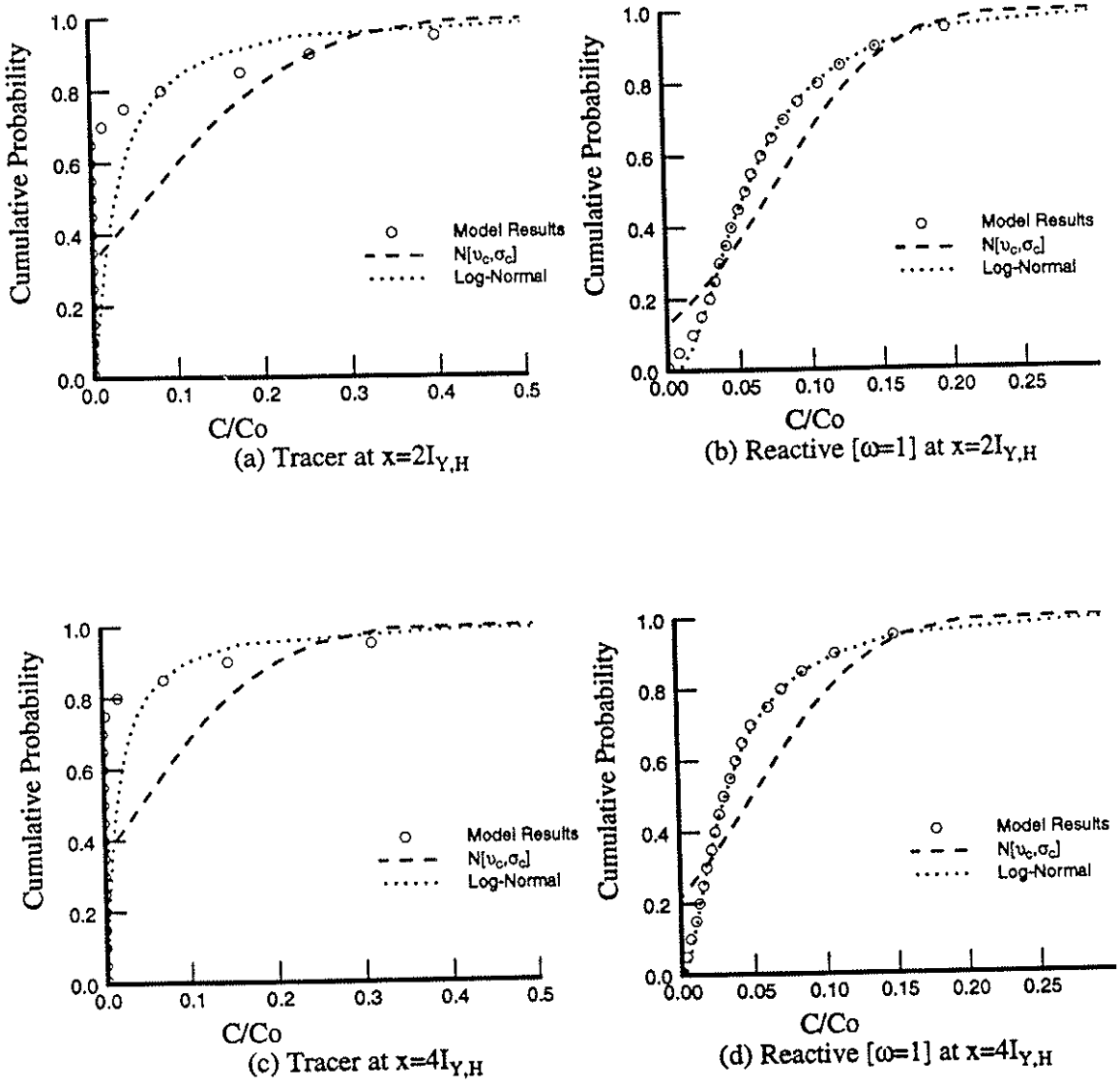

Figure 4-14: Comparison of CDF for Tracer and Solute Concentrations for Statistically Anisotropic Formation (e=0.1)

The statisitical distribution is different from the truncated normal and log-normal distribution. This latter difference is primarily attributable to the probability of zero concentrations. For the reactive case, the concentration distribution follow a log-normal distribution at both locations.

Figure 4-15 compares the resulting estimates for the upper 99% confidence bounds using only the mean and variance of the solute concentrations with the results from the model runs. The mean and variance of the solute concentration are used with the assumption of a truncated normal and log-normal distribution to determine the values represented by the white and cross-hatched bars, respectively. As was found for the statistically isotropic case, the assumption of a truncated normal distribution underestimates this upper bound. The log-normal distribution assumption results in a more accurate estimate. The difference is still significant for the tracer but is fairly small for the reactive solutes.

4.3.3 *Sampling Volumes*

As noted previously, the results shown in the previous subsections are volume-averaged concentrations. The selected volume of the detection block affects the local solute concentration and its statistics. At larger detection volumes, zones where no solute is present are averaged with zones of high concentration resulting in a smoothing of the local fluctuations. The resulting shape of the distribution is also affected by the volume of the detection block (Δ_x by Δ_y by Δ_z). Bellin et. al. (1994) showed that tracer concentration distributions, in 2-D formation, approached a Gaussian form at

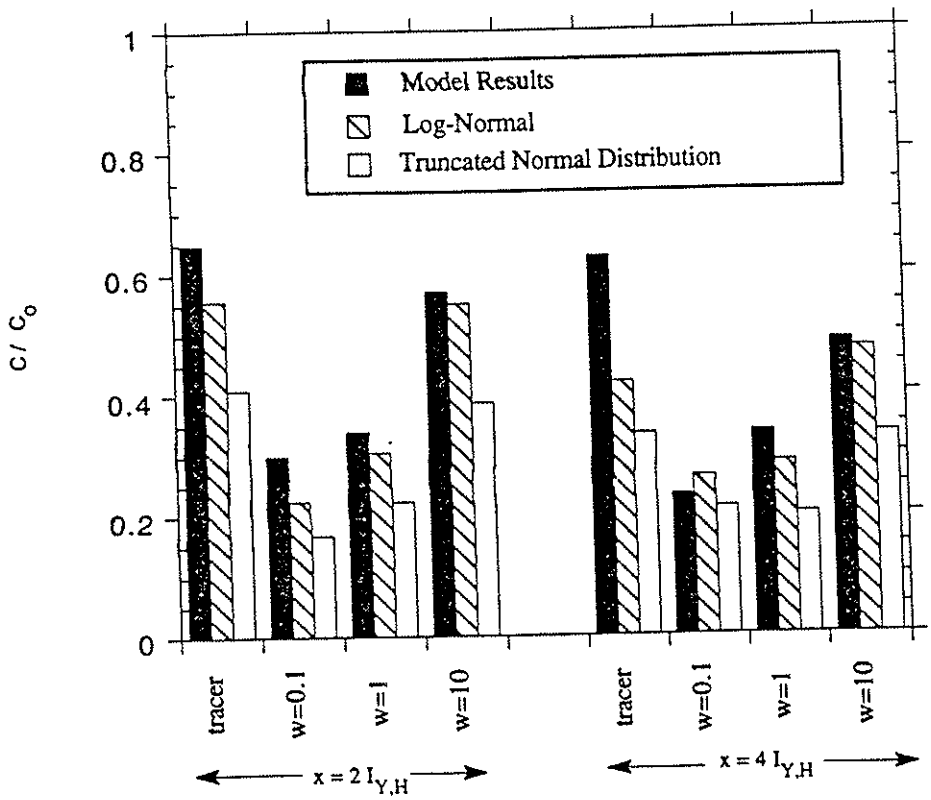

Figure 4-15: Comparison of Upper 99% Confidence Bounds for a Statistically Anisotrpic Formation (e=0.1)

large sampling volumes. Figure 4-16 (a,b) illustrates a similar effect for a reactive solute with a rate parameter $\omega = 0.1$ in a 3-D statistically isotropic formation. Previously, the CDF for a small sampling volume was shown to be non-Gaussian (Figure 4-8d). In Figure 4-16a, the probability of a zero concentration is shown to decrease as the concentration is averaged over larger and larger volumes. Eventually, the distribution will approach a Gaussian form as shown in Figure 4-16b. For many instances, the size of detection volume required may be unreasonable or non-applicable.

4.3.4 *Early and Late Arrival Times*

Estimates of solute concentrations at early arrival times (relative to the expected arrival time) are also of regulatory and research interest. The CDFs shown in the previous subsections were all at the time of the maximum average concentration. The following subsection considers the CDF of solute concentrations at other times.

Figure 4-17 (a,b) shows the CDF for the local solute concentration at the location $x = 4\ I_{Y,H}$ for six different times for the scenario $\omega=1$ in a statistically isotropic formation. The solid line is the CDF at the time of the maximum average concentration which was previously shown in Figure 4-8e. At earlier times, the probability of zero concentration increases and the CDF is steeper. At later times, the CDF, again, becomes steeper but the probability of zero concentration remains the same for the range of times shown. At later times than those shown here, the probability of zero concentration will increase.

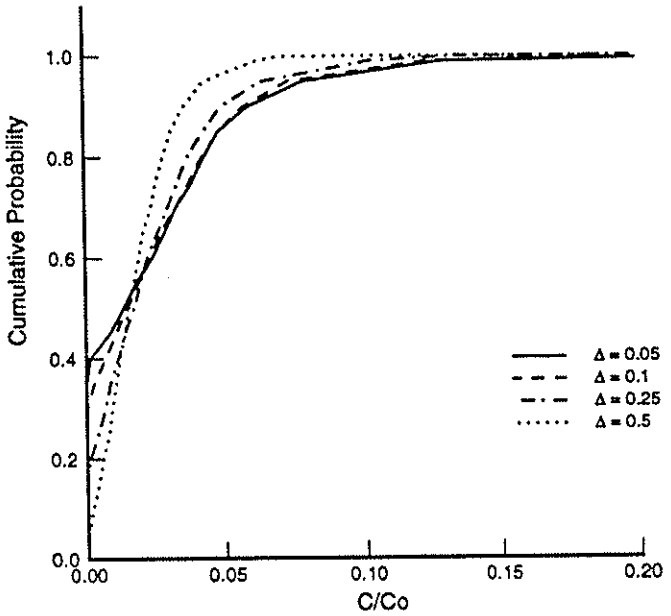

(a) CDF for a Range of Sampling Volumes

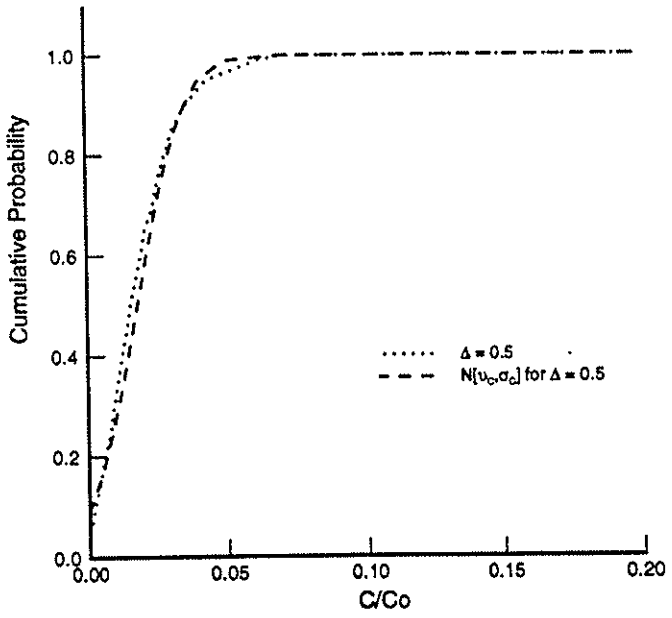

(b) Comparison with a Truncated Normal Dist. for Large Sampling Volume

Figure 4-16: Effect of Sampling Volume on Solute Concentration Distributions at $x = 4\ I_{Y,H}$ for Statistically Anisotropic Formation [with ω=0.1 and σ^2_Y=0.25]

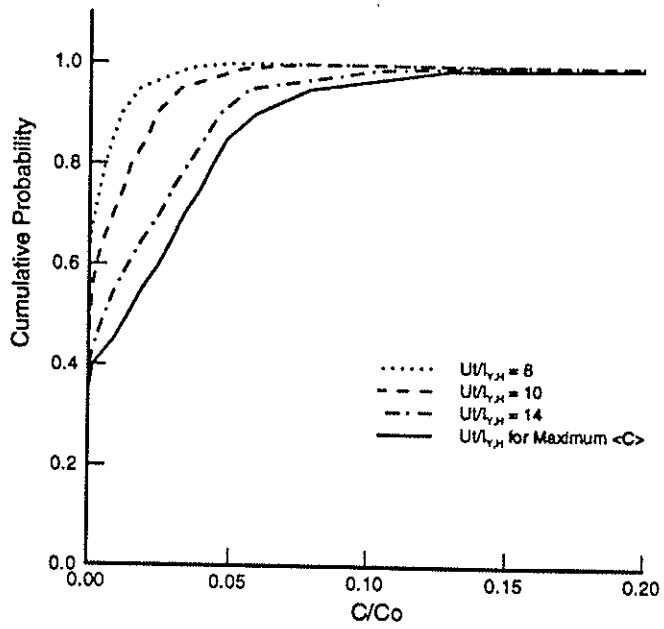

(a) CDF at Earlier Times

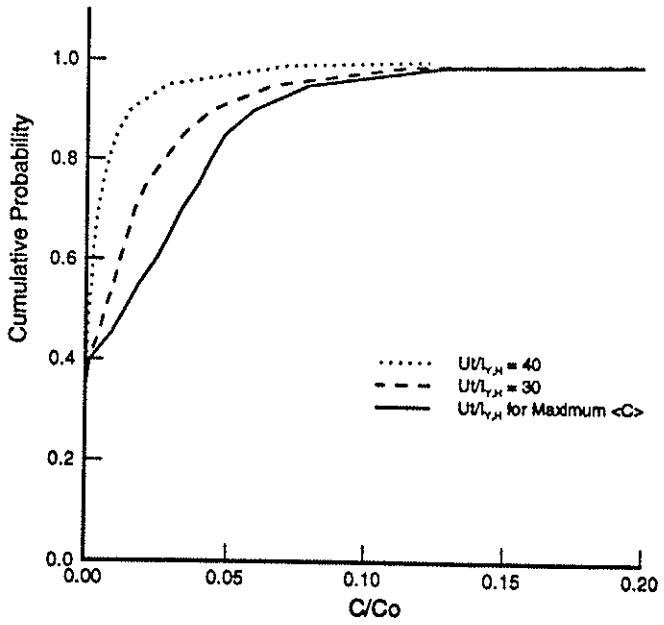

(b) CDF at Later Times

Figure 4-17: Comparison of Solute Concentration Distributions at Early and Late Times at $x = 4\ I_{Y,H}$ [with ω=1.0 and σ^2_Y=0.25]

These CDFs are compared with a truncated normal distribution in Figure 4-18 (a-f). As time increases (Figure 4-18a-d), the CDF becomes flatter and approaches the truncated normal distribution at the time of the maximum average concentration (Figure 4-18d - $Ut/I_{Y,H} = 20.8$). At later times, the CDF becomes steeper again. The results shown for the earlier times represent those portions of the plume which moved through higher flow regions and reached the sampling location quickly. As such, for these portions of the plume, little of the material will have diffused into immobile regions within the soil or undergone surface reactions on the non-equilibrium sites.

Figure 4-19 (a-f) shows the CDF for the same scenario in a statistically anisotropic formation (e=0.1). Again, the probability of zero concentration increases at earlier times. The shape of the CDF is steeper at earlier times but appears to merely shift at later times. Figure 4-20 (a-f) compares these CDFs with truncated normal and log-normal distributions. At both early and late times, the simulated distribution is approximately log-normal. For the statistically anisotropic formation considered, the CDF changes with time but its form remains log-normal.

The upper 99% confidence bounds generated by the model for these early and late times are compared with values calculated using only the concentration mean and variance with an assumed distribution in Figure 4-21. For the statistically isotropic case, the estimates based on an assumed truncated normal distribution are consistently lower than the model results. For the anisotropic case, the model results and calculated values are nearly identical at early times but these values underestimate the upper bound at later times.

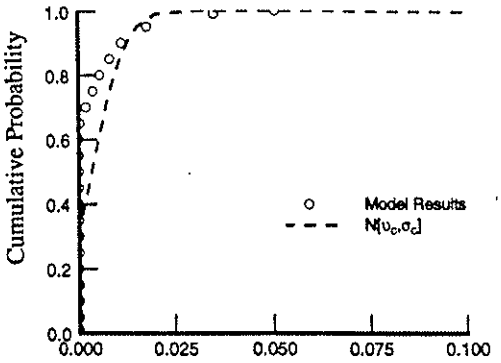

(a) CDF at $Ut/I_{Y,H} = 8$

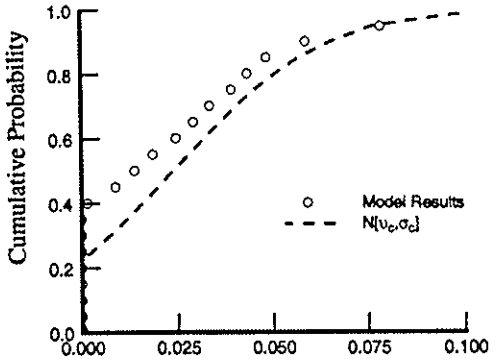

(d) CDF for $Ut/I_{Y,H} = 20.8$

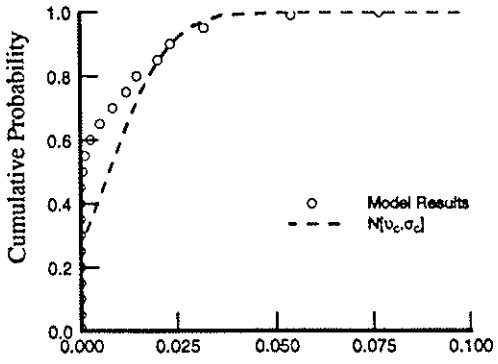

(b) CDF at $Ut/I_{Y,H} = 10$

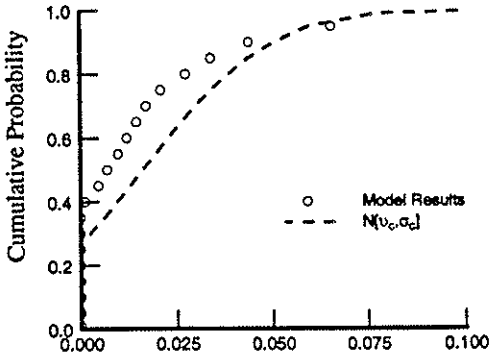

(e) CDF at $Ut/I_{Y,H} = 30$

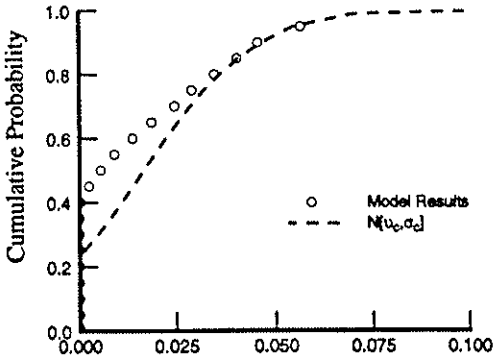

(c) CDF at $Ut/I_{Y,H} = 14$

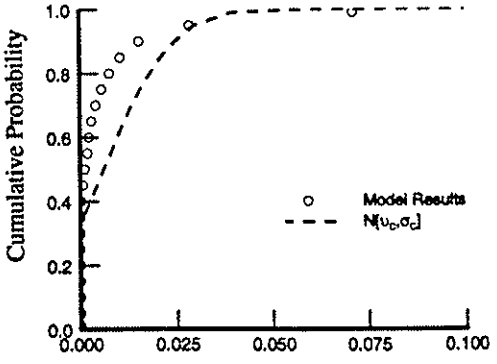

(f) CDF at $Ut/I_{Y,H} = 40$

Figure 4-18: Solute CDFs at Early and Late Times
at $x = 4\ I_{Y,H}$ [with ω=1.0 and σ^2_Y=0.25]

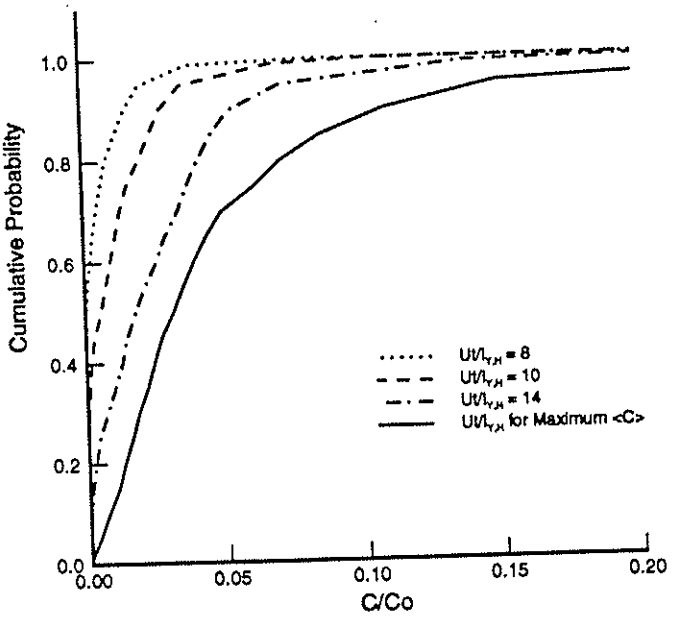

(a) CDF at Earlier Times

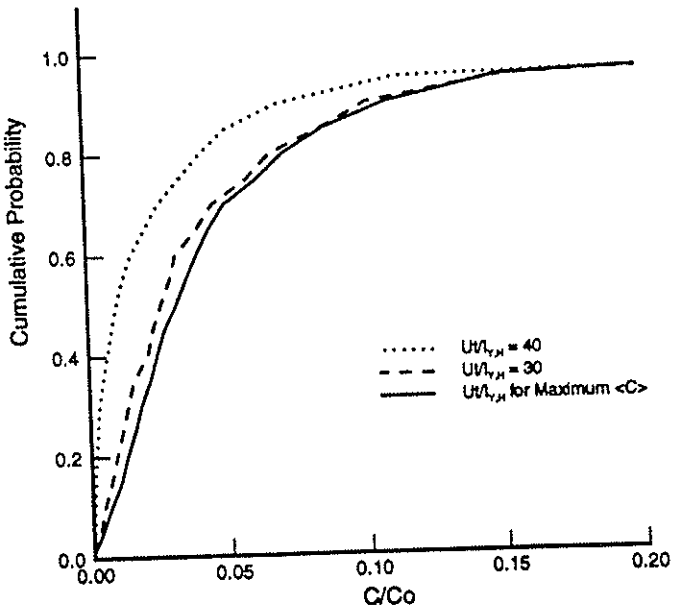

(b) CDF at Later Times

Figure 4-19: Solute CDF for Earlier and Later Times in a Statistically Anisotropic Formation at $x = 4\ I_{Y,H}$ [with ω=1.0 and σ^2_Y=0.25]

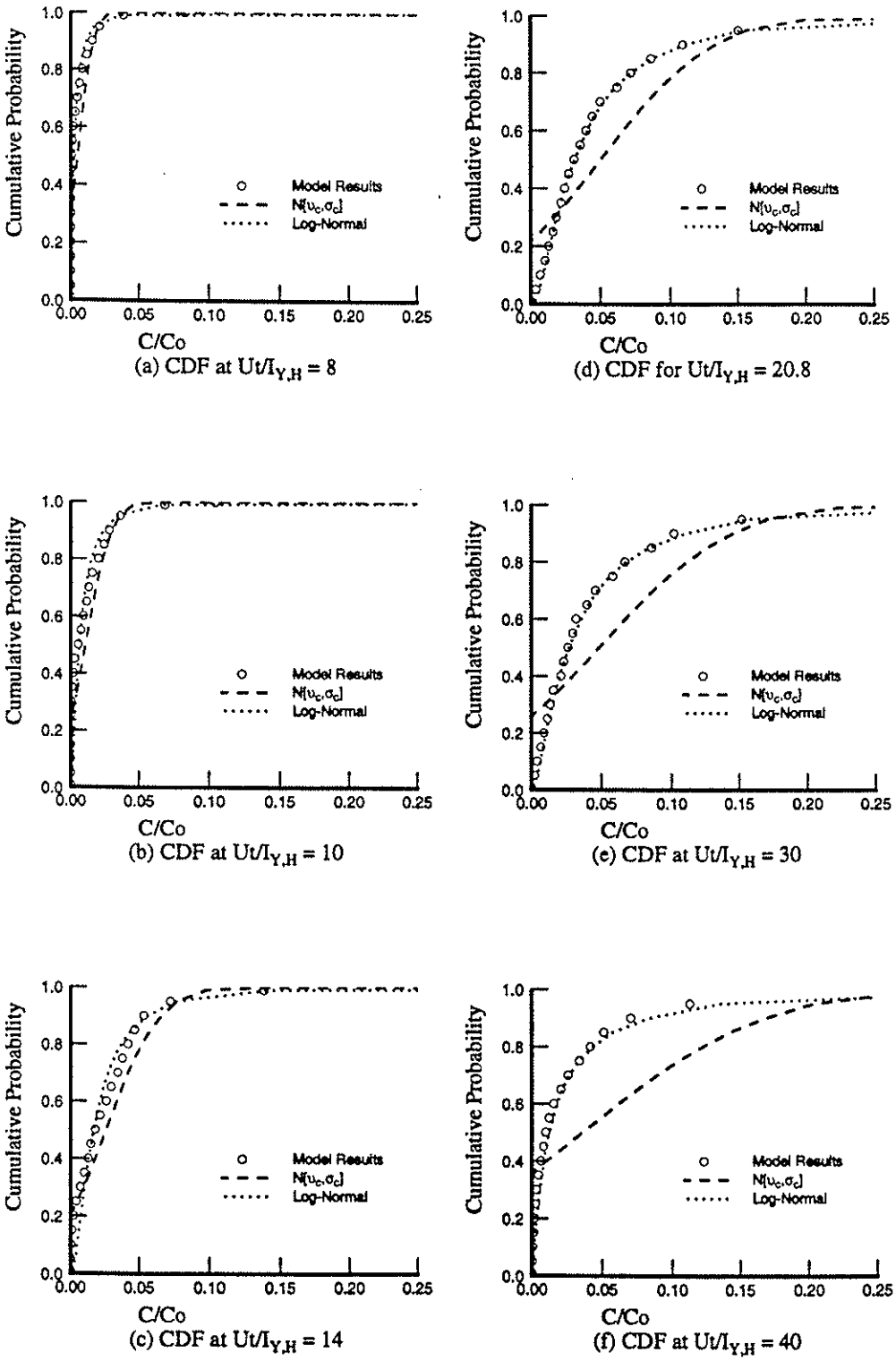

Figure 4-20: Comparison of CDF for Other Times in a Statistically Anisotropic Formation at $x = 4\ I_{Y,H}$ [with ω=1.0 and σ^2_Y=0.25]

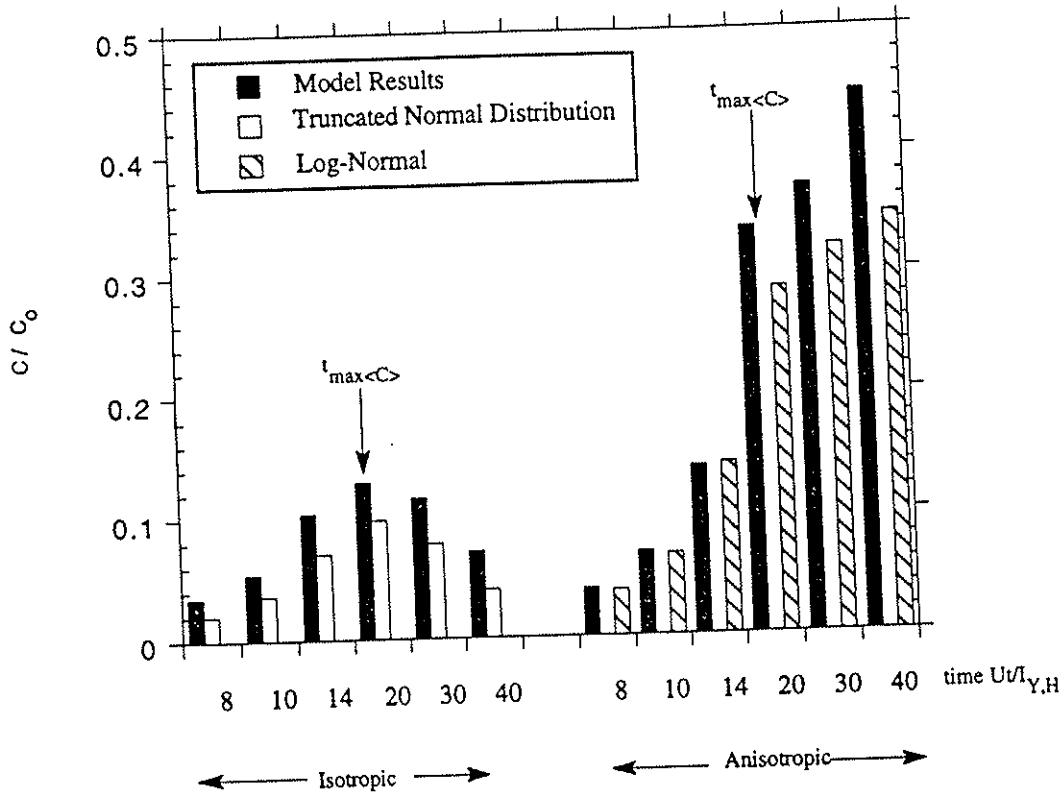

Figure 4-21: Upper 99% Confidence Bound at $x = 4\ I_{Y,H}$ for a Reactive Solute (ω=1) at Various Times

These results are similar to those shown previously at the time of the maximum average concentration.

Lastly, the CDF for a tracer at different times is considered. Figure 4-22 (a,b) shows the CDF for a tracer at the location $x = 4\ I_{Y,H}$ for six different times in a statistically isotropic formation. At earlier and late times, the probability of a zero concentration increases and the CDF becomes flatter. The probability of detecting a tracer at times substantially different than the time of expected maximum concentration is small. Unlike reactive solutes subject to non-equilibrium processes, a tracer only remains at a sampling location for a brief time.

4.4 Conclusions

A series of simulations was completed to investigate the coupled effects of the heterogeneities of subsurface hydraulic properties and nonequilibrium processes on reactive solute concentrations undergoing transport in three-dimensional natural porous formations. Based on the analysis of 350 to 500 realizations for each scenario considered, the following conclusions can be drawn:

- The minimum coefficient of variation (CV) occurs at the time of the maximum average concentration for a majority of the scenarios considered. The minimum CV increases with distance from the injection point.

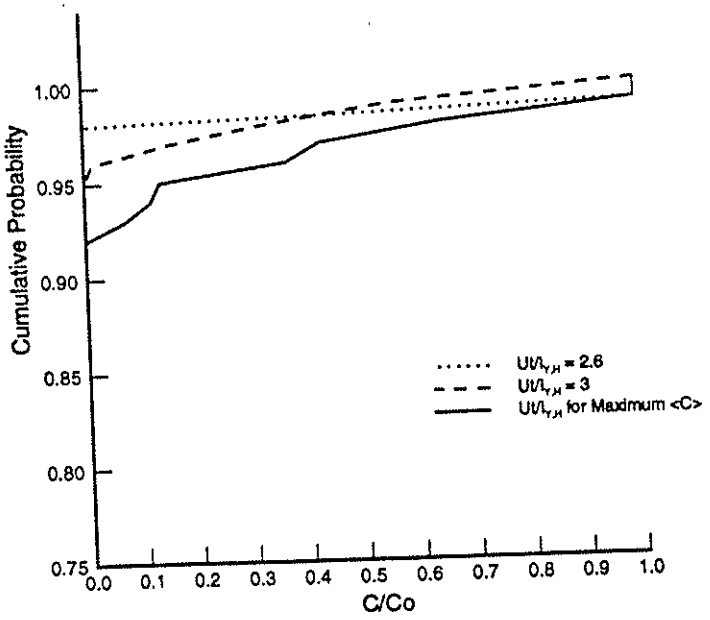

(a) CDF at Earlier Times

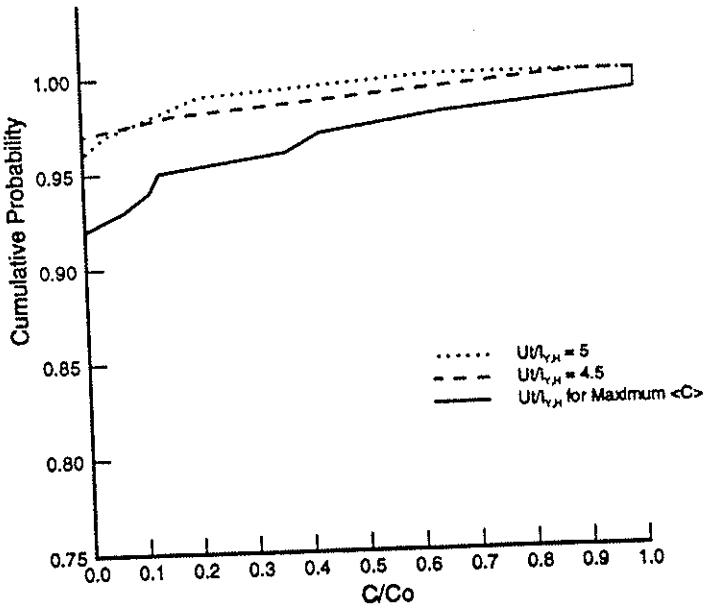

(b) CDF at Later Times

Figure 4-22: Tracer Concentration Distributions at Early and Late Times at $x = 4\ I_{Y,H}$ [σ^2_Y=0.25]

- The CV is less for the reactive solutes subject to non-equilibrium processes than for tracers under the conditions considered.
- The model results presented indicate that the expression derived by Dagan (1982, 1989) for the CV hold for a tracer in a 3-D statistically isotropic formation.
- The statistical distribution for tracer concentrations is non-Gaussian for transport in 3-D statistically isotropic and anisotropic formations and is therefore not fully characterized by its mean and variance.
- For statistically isotropic formations, the statistical distribution for reactive solutes subject to nonequilibrium processes is similar to a truncated normal distribution for cases where ω equals unity. This represents the case where the characteristic time of the nonequilibrium process is on the same order as the characteristic time of advective transport. For the other scenarios and for times other than the time of the maximum average concentration, the distributions are non-Gaussian.
- For the statistically anisotropic formation (e=0.1), the statistical distribution for reactive solutes closely resembles a log-normal distribution. For the ω=1 scenario, the distribution is log-normal for all times considered.
- In general, the combined effects of the subsurface heterogeneities and nonequilibrium processes associated with sorbing solutes are non-additive. Sorption processes are rate-limited and their influence at a particular location depends on the arrival statistics for the solute which can be controlled by the spatial variability of subsurface hydraulic properties.

The analysis presented here indicates the importance of considering the impact of advective and reactive transport mechanisms as coupled processes. Their effects are non-additive and either type can control the transport of reactive solutes depending on the field conditions and time scale of the analysis. The concentration distributions for reactive solutes subject to nonequilibrium processes are found to approach Gaussian forms under less restrictive conditions than tracers or non-reactive solutes. The methodology developed for simulating these type of processes provides a convenient means for analyzing their potential impact on the transport of contaminants in large 3-D geological formations.

CHAPTER 5

Summary and Conclusions

A methodology for simulating 3-D flow and reactive solute transport through statistically anisotropic heterogeneous porous media was developed and demonstrated. First, a method for generating 3-D flow fields in statistically anisotropic heterogeneous porous media was presented. Sample flow fields were generated and analyzed to demonstrate the method and examine the characteristics of 3-D subsurface flow. This stochastic technique was then coupled with a mobile-immobile domain model for simulating the sorption processes. Model results for the spatial moments of the solute plume were shown to capture the major trends observed in the field-scale experiment performed at Borden. These simulations were based on basic site information and independent laboratory data was used to determine the sorption parameters. In a second application of the model, a series of simulations was completed to investigate the coupled effects of heterogeneities of subsurface hydraulic properties and nonequilibrium processes on reactive solute concentrations undergoing transport in three-dimensional natural porous formations. From these analyses, the following observations and conclusions were made:

- The generated velocity fields exhibited the specified spatial correlation structure and mass continuity was observed on a block-by-block level. Cross sectional planes of sample flow fields illustrated the extent and direction of velocity correlations which conformed with previous derivations and theory.

- The method for generating the 3-D flow fields was shown to be computationally efficient in terms of its CPU requirements which increase linearly with the number of velocities or nodes. For the analysis in Chapter 3, 2500 realizations of the flow field were generated whereas previous studies of the site had only reported results from several realizations. In Chapter 4, 350 to 500 realizations of 3-D flow fields were generated for each of the field conditions and parameter settings considered to determine full statistical distributions of local solute concentrations. No other studies at this scale for this number of realizations have been reported in the literature.
- The coupling of the stochastic approach for modeling advective transport with a mobile-immobile model for simulating sorption processes captured the major trends observed in the field data for PCE at the Borden site. This included nearly identical values for the zero and first spatial moments of the plume. The observed second spatial moments were within the predicted 95% confidence intervals. The model results more closely resembled the field data than previous studies reported in the literature.
- The results presented in Chapter 3 also indicate that proper selection of model input parameters is vital. Equilibrium distribution coefficients must be based on experiments were sufficient time was allowed for equilibrium. The assumption of $f=\phi$ for modeling purposes does not appear to be valid. An alternative is to estimate f based on batch equilibrium experiments or surface area measurements.

- The combined effects of subsurface heterogeneities and nonequilibrium processes associated with sorbing solutes were shown to be non-additive. Sorption processes are rate-limited and their influence at a particular location depends on the time that each portion of the solute plume arrives which can be controlled by the spatial variability of subsurface hydraulic properties.
- As has been reported previously for non-reactive solutes in 2-D formations and instantaneously adsorbing solutes, the distributions for non-reactive solute (tracer) concentrations are non-Gaussian in 3-D statistically isotropic and anisotropic formations.
- In statistically isotropic formations, the concentration distribution for reactive solutes subject to nonequilibrium processes which have characteristic times on the order of advective transport processes were found to resemble truncated normal distributions.
- In statistically anisotropic formations (e=0.1), reactive solutes subject to nonequilibrium processes were found to have log-normal distributions under most conditions considered.

As discussed in Chapter 3, the importance of using only laboratory data for the input parameters should be noted. Many of the mechanisms which can influence the transport of reactive contaminants can be modeled in similar mathematical forms. Fitting parameters to these models based on observed data does not confirm that the controlling mechanisms have been identified but merely that the true controlling mechanisms can be represented by a similar mathematical form.

The model, in the form presented here, is designed for the simulation of the field-scale transport of dissolved nonpolar organic solutes. It should be noted that for other types of dissolved contaminants such as ionic and/or polar organic compounds and metals, the sorption process may be limited by other mechanisms such as surface reaction kinetics. If these processes are represented by first-order expressions then the model presented here could be utilized by redefining the nondimensional parameters as discussed in Chapter 4. For incorporating other types of kinetic models, accounting for the presence of nonaqueous phase liquids (NAPL), or including continuous sources, eqn 3-1 would have to be modified and new expressions derived for eqns 3-5 through 3-9 using different boundary conditions, if applicable. The technique though would remain the same.

Finally, the relative importance of the potential controlling mechanisms will depend on the type of solute, the properties of the aquifer material, and the scale of the analysis. For field-scale applications, the utilization of a mobile-immobile domain model within the framework of 3-D stochastic groundwater model was shown to simulate the transport of dissolved nonpolar organic compounds and results corresponded directly with site data. The unmapped heterogeneities of the subsurface hydraulic properties, physical and chemical nonequilibrium processes, and the non-ergodic nature of a plume can all be important factors in assessing the field-scale transport of reactive solutes. In general, the efficiency of the 3-D flow field generator allows for the simulation of the large number of realizations necessary to fully analyze field-scale problems in a probabilistic framework. This combined with the presented approach for modeling reactive nonequilibrium

processes provides a means to investigate the impacts and inter-relationships of advective and reactive transport mechanisms and develop a better understanding of the migration of contaminants in the subsurface.

CHAPTER 6

References

Anderson, E. 1992. *LAPACK Users' Guide.* Society for Industrial and Applied Mathematics. Philadelphia, PA.

Anderson, M. P.; Woessner, W. W. 1992. *Applied Groundwater Modeling: Simulation of Flow and Advective Transport.* Academic Press, Inc. San Diego, CA.

Ball, W. P.; Roberts, P. V. 1991a. Long-term sorption of halogenated organic chemicals by aquifer material: 1. Equilibrium. *Environ. Sci. Technol.* 25(7): 1223-1236.

Ball, W. P.; Roberts, P. V. 1991b. Long-term sorption of halogenated organic chemicals by aquifer material: 2. Intraparticle diffusion. *Environ. Sci. Technol.* 25(7): 1237-1249.

Bellin, A.; Rubin, Y.; Rinaldo, A. 1994. Eulerian-Lagrangian approach for modeling of flow in heterogeneous geological formations. *Water Resour. Res.* 30(11): 2913-2924.

Bellin, A.; Salandin, P.; Rinaldo, A 1992. Simulation of dispersion in heterogeneous porous formations: statistics, first-order theories, convergence of computations. *Water Resour. Res.* 28(9): 2211-2227.

Bellin, A.; Valocchi, A. J.; Rinaldo, A. 1991. *Double Peak Formation in Reactive Solute Transport in One-Dimensional Heterogeneous Porous Media.* Dipartimento di Ingegneria Civile ed Ambientale, Universita Degli Studi di Trento. IDR 1/1991.

Bosma, W. J. P.; Bellin, A.; van der Zee, S. E. A. T. M.; Rinaldo, A. 1993. Linear equilibrium adsorbing solute transport in physically and chemically heterogeneous porous formations: 2. Numerical results. *Water Resour. Res.* 29(12): 4031-4043.

Brusseau, M. L. 1992. Transport of rate-limited sorbing solutes in heterogeneous porous media: application of a one-dimensional multifactor nonideality model to field data. *Water Resour. Res.* 28(9): 2485-2497.

Brusseau, M. L. 1994. Transport of reactive contaminants in heterogeneous porous media. *Reviews in Geophysics*. 32(3):285-313.

Brusseau, M. L.; Gerstl, Z.; Augustijn, D.; Rao, P. S. C. 1994. Simulating transport in an aggregated soil with the dual-porosity model: measured and optimized parameter values. *J. Hydrol.* 163:187-193.

Brusseau, M. L.; Rao, P.S.C. 1989. Sorption nonideality during organic contaminant transport in porous media. *CRC Critic. Rev. Environ. Control.*. 19(1):33-99.

Burr, D. T.; Sudicky, E. A.; Naff, R. L. 1994. Nonreactive and reactive solute transport in three-dimensional heterogeneous porous media: Mean displacement, plume spreading, and uncertainty. *Water Resour. Res.* 30(3), 791-815.

Cameron, D. K.; Klute, A. 1977. Convective-dispersive solute transport with a combined equilibrium and kinetic adsorption model. *Water Resour. Res.* 13(1): 183-188.

Campbell, J. E.; Cranwell, R. M. 1988. Performance assessment of radioactive waste repositories. *Science*. 239: 1389-1392.

Carrick, R. L. 1987. *Surviving Proposition 65 - a Basic Guidebook to the Safe Drinking Water and Toxic Enforcement Act of 1986*. Nossaman, Guthner, Knox, and Elliot, Los Angeles.

Chen, W.; Wagenet, R. 1995. Solute transport in porous media with sorption-site heterogeneity. *Environ. Sci. Technol.* 29: 2725-2734.

Chin, D. A.; Wang, T. 1992. An investigation of the validity of first-order stochastic dispersion theories in isotropic porous media. *Water Resour. Res.* 28(6): 1531-1542.

Chiou, C. T. and D. E. Kile. 1994. Effects of polar and nonpolar groups on the solubility of organic compounds in organic matter. *Environ. Sci. Technol.* 28:1139-1144.

Curtis, G. P.: Roberts, P. V.; Reinhard, M. 1986. A natural gradient experiment on solute transport in a sand aquifer: 4. Sorption of organic solutes and its influence on mobility. *Water Resour. Res.* 22(13): 2059-2067.

Cushey, M. A.; Bellin, A.; Rubin, Y. 1995. Generation of three-dimensional flow fields for statistically anisotropic heterogeneous porous media. *Stoch. Hydrol. Hydraul.* 9(1): 89-104.

Cvetkovic, V.; Dagan, G. 1994. Transport of kinetically sorbing solute by steady random velocity in heterogeneous porous formations. *J. Fluid Mech.* 265: 189-215.

Dagan, G. 1982. Stochastic modeling of groundwater flow by unconditional and conditional probabilities: 2. The solute transport. *Water Resour. Res.* 18(4): 835-848.

Dagan, G. 1984. Solute transport in heterogeneous porous formations. *J. Fluid Mech.* 145: 151-177.

Dagan, G. 1986. Statistical theory of groundwater flow and transport: pore to laboratory, laboratory to formation, and formation to regional scale. *Water Resour. Res.* 22(9): 120S-134S.

Dagan, G. 1987. Theory of solute transport by groundwater. *Ann. Rev. Fluid Mech.* 19: 183-215.

Dagan, G. 1989. *Flow and Transport in Porous Formations.* Springer-Verlag. Berlin.

Dagan, G. 1990. Transport in heterogeneous porous formations: spatial moments, ergodicity, and effective dispersion. *Water Resour. Res.* 26(6): 1281-1290.

Dagan, G. 1991. Dispersion by passive solute in non-ergodic transport by steady velocity fields in heterogenous formations. *J. Fluid Mech.* 233: 197-210.

Dagan, G. 1996. The influence of pore-scale dispersion on concentration statistical moments in transport through heterogeneous aquifers: 1. Theory. (under review)

Dagan, G.; Cvetkovic, V. 1993. Spatial moments of a kinetically sorbing solute plume in a heterogeneous aquifer. *Water Resour. Res.* 29(12): 4053-4061.

Davis, J. A.: Fuller, C. C.; Coston, J. A.; Hess, K. M.; Dixon, E. 1993. Spatial heterogeneity of geochemical and hydrologic parameters affecting metal transport in groundwater. *Environmental Research Brief.* U.S. Environmental Protection Agency. EPA/600/S-93/006.

Denny, R. J.; Monahan, M. A.; Hickok, M.L., editors. 1989. *California Environmental Law Handbook* by the attorneys of McCutchen, Black, Verlager, and Shea. 3rd Edition. Government Institutes, Inc.

Fiori, A.; Dagan, G. 1996. The influence of pore-scale dispersion on concentration statistical moments in transport through heterogeneous aquifers: 2. Applications. (under review)

Freyberg, D. L. 1986. A natural gradient experiment on solute transport in a sand aquifer: 2. Spatial moments and the advection and dispersion of nonreactive trascers. *Water Resour. Res.* 22(13): 2031-2046.

Gelhar, L. W. 1986. Stochastic subsurface hydrologyt from theory to application. *Water Resour. Res.* 22(9): 135S-145S.

Glimm, J; Lindquist, W.B.; Pereira, F.; Zhang, Q. 1993. A theory of macrodispersion for the scale-up problem. *Transp. Porous Media.* 13: 97-122.

Goltz, M. N.; Roberts, P. V. 1988. Simulations of physical nonequilibrium solute transport models: application to a large-scale field experiment. *J. Contam. Hydrol.* 3: 37-63.

Griffin, H. E.; North, D. W., editors. 1987. *Determination of No Significant Risk Under Proposition 65.* Proceedings of One-Day Workshop of the Risk Assessment Subpanel of the Governor's Scientific Advisory Panel for Proposition 65. Health and Welfare Agency, State of California, December 16, 1987.

Haggerty, R.; Gorelick, S. M. 1995. Multiple-rate mass transfer for modeling diffusion and surface reactions in media with pore-scale heterogeneoty. *Water Resour. Res.* 31(10): 2383-2400.

Hahn, G.J.; Shapiro, S.S. 1967. *Statistical Methods in Engineering.* John Wiley & Sons. New York.

Halket, R. M.; Allen-King, R. M.; Gaylord, D. R. 1995. Correlation of hydraulic conductivty and PCE sorption in the Borden aquifer: a sedimentary facies based approach. AGU Fall Meeting. San Francisco. December, 1995.

Hallenback, W. H.; Cunningham, K. M. 1986. *Quantitative Risk Assessment for Environmental Health and Occupational Health.* Lewis Publishers, Inc. Chelsea, Michigan.

Hamaker, J. W.; Thompson, J. M. 1972. Chapter 2: Adsorption in *Organic Chemicals in the Soil Environment.* Volume 1. ed. Goring, C. A. I. and J. W. Hamaker. Marcel Dekker, Inc. New York.

Helton, J. C. 1991. Risk uncertainty in risk, and the EPA release limits for radioactive waste disposal. *Nuclear Technology.* 101: 18-39.

Hinz, C.; Gaston, A.; Selim, H. M. 1994. Effect of sorption isotherm type on prediction of solute mobility in soil. *Water Resour. Res.* 30(11):3013-3021.

Hoeksema, R. J.; Kitanidis, P. K. 1985. Analysis of spatial structure of properties of selected aquifers. *Water Resour. Res.* 21(4): 563-572.

Hubert, J.; Lenda, A.; Zuber, A. 1971. A solution of the dispersion-adsorption equation with linear adsorption isotherm. *Nukleonika.* 16: 271-278.

Indelman, P.; Rubin, Y. 1995. Flow in heterogeneous media displaying a linear trend in logconductivity. *Water Resour. Res.* 31(5): 1257-1265.

Israelachvilli, J.N. 1985. *Intermolecular and Surface Forces.* Academic Press. London.

Jang, Y-S.; Sitar, N.; Der Kiureghian, A. 1994. Reliability analysis of contaminant transport in saturated porous media. *Water Resour. Res.* 30(8):2435-2448.

Jennings, B.H. 1990. *California's Experience with Proposition 65: Implementing the Safe Drinking Water and Toxic Enforcement Act of 1986.* Senate Office of Research.

Journel, A.G.; Hujibregts, C.J. 1978. *Mining Geostatistics.* Academic Press. London.

Kabala, Z. J.; Sposito, G. 1994. Statistical moments of reactive solute concentration in a heterogeneous aquifer. *Water Resour. Res.* 30(3): 759-768.

Kapoor, V.; Gelhar, L. W. 1994a. Transport in three-dimensionally heterogeneous aquifers: 1. Dynamics of concentration fluctuations. *Water Resour. Res.* 30(6): 1775-1788.

Kapoor, V.; Gelhar, L. W. 1994b. Transport in three-dimensionally heterogeneous aquifers: 2. Predictions and observations of concentration fluctuations. *Water Resour. Res.* 30(6): 1789-1801..

Karickhoff, S. W.;Brown, D. S.; Scott, T. A. 1979. Sorption of hydrophobic pollutants on natural sediments. *Water Research.* 13: 241-248.

Karickhoff, S.W. 1984. Organic pollutant sorption in aquatic systems. *J. Hydraulic Eng.* 110(6): 707-735.

Kile, D. E., Chiou, C. T.; Zhou, H.; Li, H.; Xu, O. 1995. Partition of nonpolar organic pollutants from water to soil and sediment organic matters. *Environ. Sci. Technol.* 29: 1401-1406.

Kinniburgh, D.G. 1986. General purpose adsorption isotherm. *Environ. Sci. Technol.* 20: 895-904.

Larsen, T.; Christensen, T. H.; Brusseau, M. L. 1992. Predicting nonequilibrium transport of naphthalene through aquifer materials using batch determined sorption parameters. *Chemosphere.* 24(2): 141-153.

Lassey, K. R. 1988. Unidimensional solute transport incorporating equilibrium and rate-limited isotherms with first-order loss: 1. Model conceptualizations and analytic solutions. *Water Resour. Res.* 24(3): 343-350.

Lee, L. S., Rao, P. S. C.; Brusseau, M. L.; Ogwada, R. A. 1988. Nonequilibrium sorption of organic contaminants during flow through columns of aquifer materials. *Environ. Toxic. Chem.* 7: 779-793.

Levin, O; Zhang, D.; Neuman, S. P. 1992. Statistical properties of steady-state 3-D Eulerian and Lagrangian velocity fields. *Supplement to EOS,* October 27, 1992.

Mackay, D. M.; Freyberg, D. L.; Robert, P. V. 1986. A natural gradient experiment on solute transport in a sand aquifer: 1. Approach and overview of plume movement. *Water Resour. Res.* 22(13): 2017-2019.

Massmann, J.; Freeze, R.A. 1987a. Groundwater contamination from waste management sites: the interaction between risk-based engineering design and regulatory policy: 1. Methodology. *Water Resour. Res.* 23(2): 351-367.

Massmann, J.; Freeze, R.A. 1987b. Groundwater contamination from waste management sites: the interaction between risk-based engineering design and regulatory policy: 2. Results. *Water Resour. Res.* 23(2): 368-380.

Massmann, J.; Freeze, R.A.; Smith, L.; Sperling, T.; James, B. 1991. Hydrological decision analysis: 2. Applications to ground-water contamination. *Ground Water.* 29(4): 536-548.

McBean, E.A.; Rovers, F. A. 1992. Estimation of the probability of exceedance of contaminant concentrations. *Ground Water Monitoring Review*. 12(1): 115-119.

McBride, M.B. 1994. *Environmental Chemistry of Soils*. Oxford University Press. New York.

McComb, W. D. 1990. *The Physics of Fluid Turbulence*. Oxford University Press. New York.

Mood, A. M. F.; Graybill, F. A. 1963. *Introduction to the Theory of Statistics*. 2nd ed. McGraw-Hill: New York.

National Research Council. 1990. *Ground Water Models: Scientific and Regulatory Applications*. National Academy Press. Washington, D.C.

Nkedi-Kizza, P.; Biggar, J. W.; Selim, H. M.; van Genuchten, M. T.; Wierenga, P. J.; Davidson, J. M.; Nielsen, D. R. 1984. On the equivalence of two conceptual models for describing ion exchange during transport through an aggregated oxisol. *Water Resour. Res.* 20(8): 1123-1130.

Patrick, R.; Ford, E.; Quarles, J. 1987. *Groundwater Contamination in the United States*. 2nd ed. University of Pennsylvania Press. Philadelphia.

Pedit, J. A.; Miller, C. T. 1994. Heterogeneous sorption processes in subsurface systems: 1. Model formulations and applications. *Environ. Sci. Technol.* 28: 2094-2104.

Prausnitz, J. M.; Lichtenthaler, R. N.; Gomes de Azevedo, E. 1986. *Molecular Thermodynamics of Fluid-Phase Equilibria*. Second Edition. Prentice-Hall, Inc. Englewood Cliffs, N.J.

Ptacek, C. J.; Gillham, R. W. 1992. Laboratory and field measurements of non-equilibrium transport in the Borden aquifer. *J. Contam. Hydrol.* 10:119-158.

Quinodoz, H. A. M.; Valocchi, A. J. 1993. Stochastic analysis of the transport of kinetically sorbing solutes in aquifers with randomly heterogeneous hydraulic conductivity. *Water Resour. Res.* 29(9): 3227-3240.

Rautman, C. A.; Treadway, A. H.. 1991. Geological uncertainty in a regulatory environment; an example from the potential Yucca Mountain nuclear waste repository site. *Environmental Geology and Water Sciences*. 18: 171-184.

Reichard, E.; Cranor, C.; Raucher, R.; Zapponi, G. 1990. *Groundwater Contamination Risk Assessment.* International Association of Hydrological Sciences. Publication No. 196. Wallingford, UK.

Roberts, G.E.; Kaufman, H. 1966. *Table of Laplace Transforms.* W. B. Sanders Company, Philadelphia.

Roberts, P. V.; Goltz, M. N.; Mackay, D. M. 1986. A natural gradient experiment on solute transport in a sand aquifer: 3. Retardation estimates and mass balances for organic solutes. *Water Resour. Res.* 22(13): 2047-2058.

Roberts, P.V.; Mackay, D. M., editors. 1986. *A Natural Gradient Experiment on Solute Transport in a Sand Aquifer.* Technical Report No. 292. Department of Civil Engineering, Stanford University. Stanford, CA.

Robin, M. J. L.; Gutjahr, A. L.; Sudicky, E. A.; Wilson, J. L. 1993: Cross-correlated random field generation with the direct fourier transform method. *Water Resour. Res.* 29(7): 2385-2397.

Robin, M. J. L.; Sudicky, E. A.; Gilham, R.; Kachanoski, R. 1991. Spatial variability of strontium distribution coefficients and their correlations with hydraulic conductivity in the Canadian Air Forces Base Borden aquifer. *Water Resour. Res.* 27(10): 2619-2632.

Rubin, Y. 1990. Stochastic modleing of macrodispersion in heterogeneous porous media. *Water Resour. Res.* 26(1): 133-141.

Rubin, Y. 1991a. Prediction of tracer plume migration in disordered porous media by the method of conditional probabilities. *Water Resour. Res.* 27(6): 1291-1308.

Rubin, Y. 1991b. Tranpsort in heterogeneous porous media: prediction and uincertainty. Water Resour. Res. 27(7): 1723-1738.

Rubin, Y.; Bellin, A. 1994. The effects of recharge on flow nonuniformity and macrodispersion. *Water Resour. Res.* 30: 939-948.

Rubin, Y.; Cushey, M. A.; Bellin, A. 1994. Modeling of transport in groundwater for environmental risk assessment. *Stoch. Hydrol. Hydraul.* 8(1): 57-77.

Rubin, Y.; Dagan, G. 1988. Stochastic analysis of boundaries effects on head spatial variability in heterogeneous aquifers: 1. Constant head boundary. *Water Resour. Res.* 24(10): 1689-1697.

Rubin, Y.; Dagan, G. 1992a. Conditional estimation of solute travel time in heterogeneous formations: impact of transmissivity measurements. *Water Resour. Res.* 28(4):1033-1040.

Rubin, Y.; Dagan, G. 1992b. A note on head and velocity covariances in three-dimensional flow through heterogeneous porous media. *Water Resour. Res.* 28(5): 1463-1470. (Correction, *Water Resour. Res.* 31(6):1613).

Rubin, Y.; Seong, K. 1994. Investigation of flow and transport in certain cases of nonstationary conductivity fields. *Water Resour. Res.* 30(11): 2901-2911.

Schafer-Perini, A. L.; Wilson, J. L. 1991. Efficient and accurate front tracking for two-dimensional groundwater flow models. *Water Resour. Res.* 27(7): 1471-1485.

Schwarzenbach, R. P.;Gschwend P. M.; Imboden, D. M. 1993. *Environmental Organic Chemistry.* John Wiley & Sons, Inc. New York.

Selim, H.M.; Davidson, J. M.; Mansell, R. S. 1976. Evaluation of a two-site adsorption-desorption model for describing solute transport in soils. In Proceedings of the 1976 Summer Computer Simulation Conference. Washington, D.C. Simulation Councils, Inc. La Jolla, CA. pp. 444-448.

Selroos, J.; Cvetkovic, V. 1992. Modeling solute advection coupled with sorption kinetics in heterogeneous formations. *Water Resour. Res.* 28(5): 1271-1278.

Simmons, C. S. 1982. A stochastic-convective transport representation of dispersion in one-dimensional porous media systems. *Water Resour. Res.* 18(4): 1193-1214.

Sitar, N.; Cawlfield, J.D.; Der Kiureghian, A. 1987. First-order reliability approach to stochastic analysis of subsurface flow and contaminant transport. *Water Resour. Res.* 23(5): 794-804.

Thorbjarnarson, K. W.; Mackay, D. M. 1994. A forced-gradient experiement on solute transport in the Borden aquifer: 3. Nonequilibrium transport of the sorbing organic compounds. *Water Resour. Res.* 30(2): 401-419.

Tompson, A.F.B.; Gelhar, L.W. 1990: Numerical simulation of solute transport in three-dimensional, randomly heterogeneous porous media. *Water Resour. Res.* 29(7): 2385-2397.

Tompson, A. F. B.; Schafer-Perini, A. L.; Smith, R. W. 1995. *Impacts of physical and chemical heterogeneity on co-contaminant transport in a sandy porous medium.* Lawrence Livermore National Laboratory. LLNL Report No. UCRL-JC-120685.

Travis, C. C.; Etnier, E. L. 1981. A survey of sorption relationships for reactive solutes in soil. *J. Environ. Qual* . 10(1): 8-17.

Turcke, M.A.; Kueper, B.H. 1996. Geostatistical analysis of the Borden aquifer hydraulic conductivity field. *J. Hydrol.* 178: 223-240.

U. S. Environmental Protection Agency (U.S. EPA). 1986a. Guidelines for estimating exposures. *Federal Register.* v51. no 185. pp. 34042-34054.

U. S. Environmental Protection Agency (U.S. EPA). 1986b. *Superfund Public Health Evaluation Manual.* Washington, D.C. EPA/540/1-86/060.

U. S. Environmental Protection Agency (U.S. EPA). 1988. *Methods Used in the United States for the Assessment and Management of Health Risk due to Chemicals.* Washington, D.C. EPA/600/D-89/070.

Valocchi, A.J. 1989. Spatial moment analysis of the transport of kinetically adsorbing solutes through stratified aquifers. *Water Resour. Res.* 25(2): 273-279.

van Genuchten, M. Th.; Wierenga, P. J. 1976. Mass transfer studies in sorbing porous media: 1. Analytical solutions. *Soil Sci. Soc. Am. J.* 40: 473-480.

Varshney, P.; Tim, U. S.; Anderson, C. E. 1993. Risk-based evaluation of ground-water contamination by agricultural pesticides. *Ground Water.* 31: 356-62.

Vomvoris, E. G.; Gelhar, L. W. 1990. Stochastic analysis of the concentration variability in a three-dimensional heterogeneous aquifer. *Water Resour. Res.* 26(10): 2591-2602.

Weber, W.J., P.M. McGinley, and L.E. Katz. 1991. Sorption phenomena in subsurface systems - concepts, models, and effects on contaminant fate and transport. *Water Resour. Res* . 25(5): 499-528.

Wood, W.W., T.F. Kraemer, PP. Hearn. 1990. Intragranular diffusion: An important mechanism influencing solute transport in clastic aquifers? *Science.* 247: 1569-1572.

Woodbury, A. D.; Sudicky, E. A. 1991. The geostatistical characteristics of the Borden aquifer. *Water Resour. Res.* 27(4): 533-546.

Wu, S-C, Gschwend, P. M. 1986. Sorption kinetics of hydrophobic organic compounds to natural sediments and soils. *Environ. Sci. Technol* . 20(7): 717-725.

Zhang, D.; Neuman, S.P. 1992. Comment on "A note on head and velocity covariances in three-dimensional flow through heterogeneous porous media" by Y. Rubin and G. Dagan, *Water Resour. Res.* 28(12): 3343-3344.

APPENDIX A

Additional Information: Modeling 3-D Flow Fields

This appendix contains supplemental information regarding the procedures utilized to generate the groundwater velocity fields. Section A.1 provides a description of the system of equations utilized to calculate the conditioning coefficients in eqns 2-1 and 2-2 and Section A.2 lists the step-by-step procedures for generating coarse and refined grids.

A.1 Building and Solving the System of Equations for Calculating Conditioning Coefficients

As discussed in Chapter 2, the conditional mean and variance of the components of the velocity vector at a generic node N are calculated using eqns 2-1 and 2-2, respectively. These equations include conditioning coefficients ($\lambda^i_{k,j}$) which are the solutions of a linear system of equations (eqn 2-3):

$$\sum_{k=1}^{m}\sum_{j=1}^{N-1}\lambda^i_{k,j}(\mathbf{x}_N)v_{k,p}(\mathbf{x}_j,\mathbf{x}_q)=v_{ip}(\mathbf{x}_N,\mathbf{x}_q) \quad \text{for i, p} = 1,\ldots,\text{m and q} = 1,\ldots,\text{N}-1 \qquad \text{(A-1)}$$

where m = number of dimensions

N = number of conditioning nodes in the search neighborhood

$\lambda^i_{k,j}$ = conditioning coefficient (conditions velocity i on velocity k at node j)

$\mathbf{x}_j$ = vector of coordinates of node j

v_{ip} = unconditional variance – covariance tensor

The superscript i denotes the component of the velocity vector. In matrix notation, eqn A-1 for a three-dimensional formation becomes:

$$\underline{\underline{A}}\,\underline{\Lambda^i} = \underline{\Gamma^i} \text{ for i} = 1,2,3 \tag{A-2}$$

The matrix A consists of sub-matrices B:

$$\underline{\underline{A}} = \begin{bmatrix} \underline{\underline{B_{11}}} & \underline{\underline{B_{12}}} & \underline{\underline{B_{13}}} \\ \underline{\underline{B_{21}}} & \underline{\underline{B_{22}}} & \underline{\underline{B_{23}}} \\ \underline{\underline{B_{31}}} & \underline{\underline{B_{32}}} & \underline{\underline{B_{33}}} \end{bmatrix} \tag{A-3}$$

Each of these sub-matrices B consists of velocity covariance tensors:

$$\underline{\underline{B_{pk}}} = \begin{bmatrix} v_{pk}(x_1,x_1) & \cdots & v_{pk}(x_1,x_{N-1}) \\ \vdots & \ddots & \vdots \\ v_{pk}(x_{N-1},x_1) & \cdots & v_{pk}(x_{N-1},x_{N-1}) \end{bmatrix} \tag{A-4}$$

The vector Λ^i contains the conditioning coefficients:

$$\underline{\Lambda^i} = \begin{bmatrix} \lambda^i_{1,1} \\ \vdots \\ \lambda^i_{1,N-1} \\ \lambda^i_{2,1} \\ \vdots \\ \lambda^i_{2,N-1} \\ \lambda^i_{3,1} \\ \vdots \\ \lambda^i_{3,N-1} \end{bmatrix} \tag{A-5}$$

The vector Γ^i consists of velocity covariance tensors:

$$\underline{\Gamma^i} = \begin{bmatrix} v_{i1}(x_N, x_1) \\ \vdots \\ v_{i1}(x_N, x_{N-1}) \\ v2(x_N, x_1) \\ \vdots \\ v_{i2}(x_N, x_{N-1}) \\ v_{i3}(x_N, x_1) \\ \vdots \\ v_{i3}(x_N, x_{N-1}) \end{bmatrix} \tag{A-6}$$

Expressions for the velocity variance-covariance tensors in eqns A-4 and A-6 have been derived for steady state conditions (Rubin and Dagan, 1992b; Zhang and Neuman, 1992), for a uniformly-recharged field (Rubin and Bellin, 1994), and for a nonstationary logconductivity field (Rubin and Seong, 1994; Indelman and Rubin, 1995). The appropriate expressions for these covariances are selected based on the conditions applicable to the site. The values for the velocity covariances are calculated to build matrix A and vector Γ^i (for i=1,2,3). Equation A-1 is then solved for vector Λ^i using the subroutine DPPSV from the application package LAPACK (Anderson, 1992). These conditioning coefficients are used in eqns 2-1 and 2-2 to generate the 3-D flow field. The development and utilization of this system of linear system of equations is discussed further in Bellin et. al., (1994).

A.2 Step-by-Step Procedure for Generating Coarse and Refined Grids

The following steps are utilized to generate the 3-D flow fields:

Step 1 - Calculate Conditioning Coefficients:

Based on the selected size and spatial arrangement of the search neighborhood, the conditioning coefficients for each component of the velocity vector are calculated using eqn 2-3.

Step 2 - Generate Outer Grid:

An outer grid of unconditional velocities is generated around the primary grid to provide values for conditioning for nodes along the edges. These outer values are generated using the unconditional mean and a random deviate based on the unconditional variance.

Step 3 - Calculate conditional means and variance at node:

The conditional mean and variances of the three components of the velocity vector are determined at the first node on the grid. The velocities are conditioned on other velocities using the conditioning coefficients.

Step 4 - Calculate and add random deviates:

Multivariate normal random deviates are determined based on the conditional variance-covariance tensors and the assumed velocity distribution. These deviates are corrected by the conditional standard deviation and added to the conditional mean to generate values for the current realization. This procedure is discussed in more detail below.

Step 5 - Repeat steps 3 and 4 for the entire grid:

The values for the remaining modes are calculated using the same method. The order is sequential moving along the x, then y, and lastly z direction. This is illustrated in Figure A-1. Each row of nodes is filled in moving left to right (along the x direction) until the entire plane has been generated. Then, the next plane above is generated and the process moves up through the grid.

Step 6 - Grid refinement:

Once the entire grid is generated, it can be refined to reduce the block size using the method discussed below.

Step 7 - Repeat steps 2 to 6 for each realization:

The generated coarse or refined grid represents a realization of the flow field. Steps 2 to 6 are repeated to generate multiple realizations of the field.

The discussion below provides further details for steps 4 and 6.

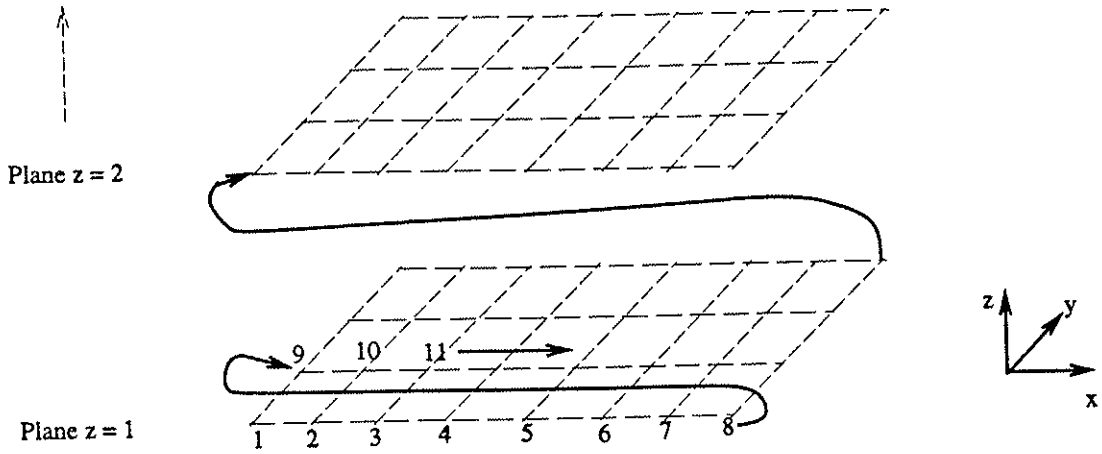

Figure A–1: Sequence of Grid Movement for Velocity Calculations
(z direction is exaggerated for illustration purposes)

Random Deviates (step 4)

Generating values for the velocity vector for a given realization requires adding random deviates to the calculated conditional means. If the velocity is assumed to follow a normal distribution, the value is calculated as follows (Hahn and Shapiro, 1967):

$$v_i(x_N) = U_i^c(x_N) + R_i\left[v_{ii}^c(x_N)\right]^{1/2} \text{ for } i = 1,2,3 \qquad \text{(A-7)}$$

where the superscript i is the component of the velocity vector, U_i^c is the conditional mean, R_i is the multivariate normal random deviate, and v_{ii}^c is the conditional variance for the velocity vector component i. For a lognormal distribution, the expected value and standard deviation are calculated first using the conditional statistics:

$$\mu_i^c(x_N) = \ln\left\{\frac{\left[U_i^c(x_N)\right]^2}{\left(\left[U_i^c(x_N)\right]^2 + v_{ii}^c(x_N)\right)^{1/2}}\right\} \qquad \text{(A-8)}$$

$$\sigma_{ii}^c(x_N) = \left[\ln\left\{1 + \frac{v_{ii}^c(x_N)}{\left[U_i^c(x_N)\right]^2}\right\}\right]^{1/2} \qquad \text{(A-9)}$$

The multivariate normal random deviate is then utilized as follows:

$$v_i^c(x_N) = \exp\left\{\mu_i^c(x_N) + R_i\sigma_i^c(x_N)\right\} \qquad \text{(A-10)}$$

Typically, in the analyses shown in the previous chapters, the longitudinal velocity (v_1) is assumed to have a lognormal distribution while the

transverse and vertical transverse velocities (v_2 and v_3) are assumed to have normal distributions.

The multivariate normal random deviates are calculated using LU decomposition. This accounts for the correlation between the components of the velocity vector at the given node. For a three-dimensional velocity vector with all components assumed to have a normal distribution, R_i is calculated as follows:

$$R_1 = r_1 \tag{A-11}$$

$$R_2\sqrt{v_{22}^c} = r_1\frac{v_{12}^c}{\sqrt{v_{11}^c}} + r_2\sqrt{v_{22}^c - \frac{\left(v_{12}^c\right)^2}{v_{11}^c}} \tag{A-12}$$

$$R_3\sqrt{v_{33}^c} = r_1\frac{v_{13}^c}{\sqrt{v_{11}^c}} + r_2\frac{v_{23}^c - \left(\frac{v_{12}^c v_{13}^c}{v_{11}^c}\right)}{\sqrt{v_{22}^c - \frac{\left(v_{12}^c\right)^2}{v_{11}^c}}} + r_3\sqrt{v_{33}^c - \frac{\left(v_{13}^c\right)^2}{v_{11}^c} - \frac{\left[v_{23}^c - \left(\frac{v_{12}^c v_{13}^c}{v_{11}^c}\right)\right]^2}{v_{22}^c - \frac{\left(v_{12}^c\right)^2}{v_{11}^c}}} \tag{A-13}$$

where r_1 ,r_2 , and r_3 are uncorrelated normal random deviates with zero mean and standard deviation of unity. If the longitudinal velocity is assumed to have a lognormal distribution, eqns A-11 through A-13 are modified. The v_{11}^c is replaced with σ_{11}^c (eqn A-9) and cross-covariances v_{12}^c and v_{13}^c are divided by the conditional mean U_1^c.

Grid Refinement (step 6)

Once a coarse grid is generated (step 5), subsequent levels of refinement can be performed to reduce the block size of the grid (step 6). Each level of refinement requires three passes over the grid. A different set of conditioning coefficients is required for each of these passes for each level of refinement. The additional nodes added to the original search neighborhood for each pass are illustrated in Figure A-2. The first pass entails generating velocities between the coarse grid values along the longitudinal or x direction. The search neighborhood consists of the original spatial configuration plus the two adjacent coarse grid nodes. The second pass fills in every other row of nodes in the y direction. The search neighborhood includes the original configuration plus seven additional nodes -- the six nearest nodes from the coarse grid and first pass of refinement and the last node calculated. The last pass fills in every other plane in the vertical or z direction. In addition to the original search neighborhood, the nearest nine nodes in the planes above and below and the nearest two nodes in the current plane are utilized (20 additional nodes). Once a refined grid has been generated, the process can be repeated to further reduce the grid size.

Pass 1

2 additonal nodes

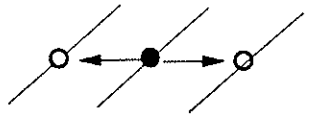

Pass 2

7 additional nodes

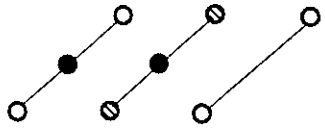

Pass 3

20 additional nodes

(z direction is exaggerated)

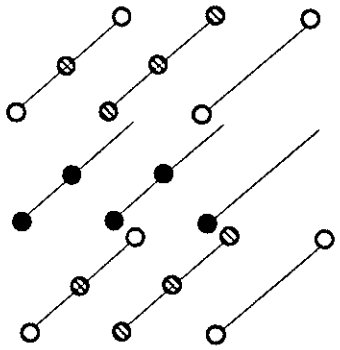

● – node where value is being calculated

● – node determined with current pass

⊘ – node from previous pass

○ – coarse grid node (or previous refinement level node)

Figure A–2: Additional Conditioning Nodes Included for Grid Refinement

APPENDIX B

Additional Information: Advective and Reactive Transport Modeling

This appendix provides additional information regarding the development of the techniques and approaches used in the modeling of advective and reactive transport as presented and utilized in Chapters 3 and 4. For advective transport, the particle tracking methodology is discussed and model results are compared with analytical solutions. For reactive transport, the derivation of the function γ and its derivative with respect to time are presented.

B.1. Advective Transport

The modeling of advective transport is discussed in Chapter 3. The Lagrangian approach is utilized and the solute body is represented by a large number of solute particles. Single solute particles are larger than the pore scale, to ensure the applicability of Darcy's law, but much smaller than $I_{Y,V}$ and $I_{Y,H}$ which enables it to accurately capture the media heterogeneity. The displacement of these particles is simulating utilizing a particle tracking approach. This section of the appendix discusses the techniques used to perform the particle tracking (section B.1.1) and presents comparisons of results for tracer transport with analytical solutions (section B.1.2).

B.1.1 Particle Tracking

The approach used here consists of simulating a large number of solute particles which together constitute the solute body. Hence, the displacement of a plume is performed by moving the particles through a 3-D grid of velocities computed a priori according to the methodology described in Chapter 2. The particle is displaced using a relatively small time steps. To minimize the error incurred, a fourth-order Runge-Kutta integration method is used (Anderson and Woessner, 1992). The velocity of the particle is calculated at four intermediate points -- the beginning point, two mid-points, and an estimated endpoint. Figure B-1 and the equations shown below illustrate the technique for the x direction (Anderson and Woessner, 1992);

$$
\begin{aligned}
& x_{t+\Delta t} = x_t + \tfrac{1}{6}\left(d_1 + 2d_2 + 2d_3 + d_4\right) \\
& \text{where } d_1 = \mathrm{v}_{1,x_0}\Delta t \\
& \qquad d_2 = \mathrm{v}_{1,x_1}\Delta t \\
& \qquad d_3 = \mathrm{v}_{1,x_2}\Delta t \\
& \qquad d_4 = \mathrm{v}_{1,x_3}\Delta t
\end{aligned}
\qquad \text{(B-1)}
$$

The three dimensional movement of the particle is simulated by applying eqn B-1 for each of the velocity vector components.

The particle velocity at each of the above locations is determined using a linear interpolation scheme to conserve mass locally (Anderson and Woessner, 1992; Schafer-Perini and Wilson, 1991). First, the point is located within a block on the volumetric grid. The velocities perpendicular to each face of the block are determined by averaging the corresponding velocity

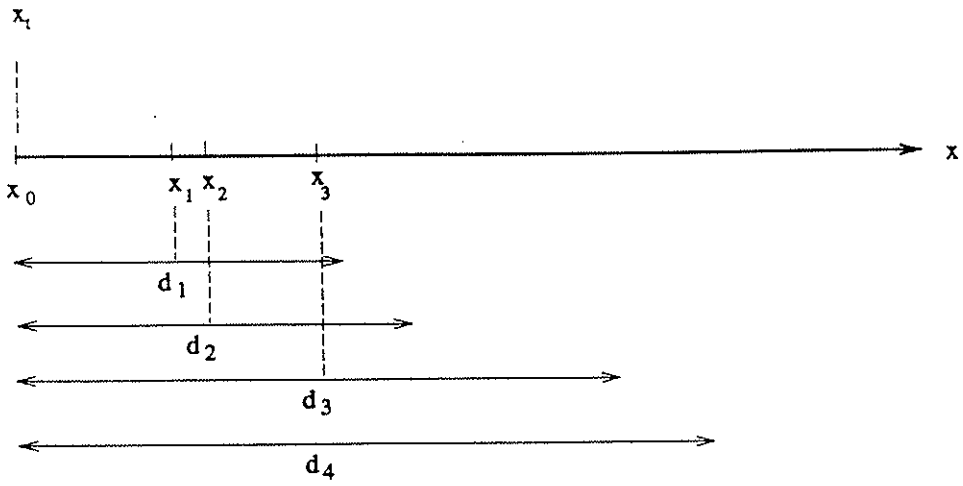

Figure B–1: Schematic diagram for the Runge–Kutta method

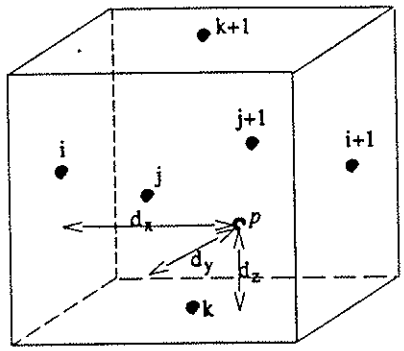

Figure B–2: Schematic for determining point velocities at location p

vector components at the four grid nodes defining the face. Each component of the velocity vector at the point of interest is only a function of one direction. Figure B-2 shows a schematic defining the variables utilized in determining the point velocity. The equations utilized to determine the point velocities are listed below:

$$
\begin{aligned}
v_1(x_p, y_p, z_p) &= (1 - d_x)v_{1,i} + d_x v_{1,i+1} \\
v_2(x_p, y_p, z_p) &= (1 - d_y)v_{2,j} + d_y v_{2,j+1} \\
v_3(x_p, y_p, z_p) &= (1 - d_z)v_{3,k} + d_x v_{3,k+1} \\
d_x &= \frac{x_p - x_i}{\Delta x} \\
d_y &= \frac{y_p - y_j}{\Delta y} \\
d_z &= \frac{z_p - z_k}{\Delta z}
\end{aligned}
\qquad \text{(B-2)}
$$

This approach corresponds directly with the technique used to check the mass balance on a block-by-block basis (see Chapter 2). The particle tracking scheme therefore maintains the same mass continuity as determined in the flow field analysis.

B.1.3 Comparison with Analytical Solutions

The model presented in Chapters 2 and 3 can be used to directly determine the variance of a plume about its mean trajectory ($S_{11}(t)$) and the variance of the centroid trajectory ($R_{11}(t)$). Analytical and numerical solutions have been proposed for these moments for non-reactive solutes. Dagan (1990, 1991)

proposed the relationship for a line source of length l, normal to the flow direction:

$$\langle S_{11}(t)\rangle = S_{11}(0) + X_{11}(t,0) - R_{11}(t,l) \tag{B-3}$$

Under ergodic conditions, $R_{11}(t,l)$ is assumed to be zero. For non-ergodic conditions, the variance of the centroid trajectory in a 2-D formation is given by (Dagan, 1991):

$$R_{11}(t,l) = \frac{1}{A_o^2}\int_{A_o}\int_{A_o} X_{11}(t,\mathbf{b})d\mathbf{a}'d\mathbf{a}'' \qquad \text{where } \mathbf{b} = \mathbf{a}' - \mathbf{a}'' \tag{B-4}$$

and

$$X_{11}(t,\mathbf{b}) = \int_0^t\int_0^t u_{11}\left[\mathrm{U}(t'-t'') + b_1, b_2\right]dt'dt'' \tag{B-5}$$

Analytical solutions for u_{11} have been reported in the literature (Rubin and Dagan, 1992b; Zhang and Neuman, 1992). Using these expressions, eqns B-3 and B-4 can numerically integrated. Figure B-3 compares this integration results with a 2-D model simulation. For 3-D formations and sources, eqn B-4 can be utilized by replacing A_o with V_o and utilizing the appropriate expressions for u_{11}.

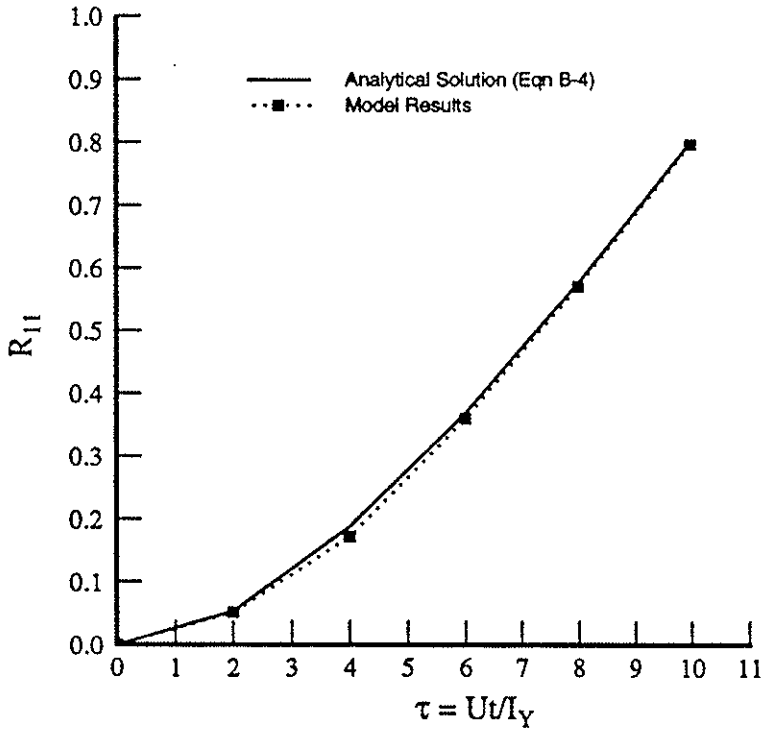

Figure B-3: Comparison of Model Results with Analytical Solution for R_{11} [2-D analysis : the source width normal to flow is 2 I_Y and σ^2_Y=0.1]

B.2 Reactive Transport

As discussed in Chapter 3, the mobile-immobile model (eqn 3-2) is reformulated in a Lagrangian framework by defining a curvilinear coordinate system along a streamline. The resulting eqn 3-7 is solved for a single solute particle using Laplace transforms and the solution is given in eqns 3-8 and 3-9. Section B.2.1 gives the details of this derivation using Laplace transforms. Section B.2.2 presents the time derivative of this expression which can be used to estimate the expected arrival time of maximum concentration.

B.2.1 *Derivation of Solution Along a Streamline*

The mobile-immobile model can be expressed in a Lagrangian framework as follows (eqns 3-7a and b):

$$\beta \frac{\partial C_2}{\partial T} + \frac{\partial C_1}{\partial T} = -\frac{\partial C_1}{\partial \tau} \tag{B-6}$$

$$\frac{\partial C_2}{\partial T} = \omega (C_1 - C_2) \tag{B-7}$$

The final solution for a single particle is expressed as (eqn 3-8):

$$C_1(\tau, T) = \frac{m}{\theta_m v_{1,m}} \gamma(\tau, T) \delta(s_2) \delta(s_3) \tag{B-8}$$

Coupled equations, similar to eqns B-6 and B-7, were solved by Hubert et. al. (1971) and later adapted by Lassey (1988) for instantaneous injection and a

two-site kinetic model. The expression for γ can be derived in a similar manner. The solution shown is for the case of an instantaneous source and assuming that the initial aqueous and soil concentrations are zero. Taking the Laplace transforms gives the following expression for γ:

$$\overline{\gamma}(s,\tau) = \exp\left[-s\tau\left(1+\frac{\omega\beta}{s+\omega}\right)\right] \tag{B-9}$$

Taking the inverse Laplace transform of the right hand side gives the solution. This involves a number of steps. First rearranging,

$$\gamma(t,\tau) = L^{-1}\left\{e^{-s\tau}e^{-\left(\frac{s\omega\beta\tau}{s+\omega}\right)}\right\} \tag{B-10}$$

using the relationship $L^{-1}\left\{e^{-sh}\overline{\Phi}(s)\right\} = \Phi(t-h)\cdot U(t-h)$ (Hubert et. al., 1971):

$$\begin{aligned}\gamma(t,\tau) &= \Phi(t-\tau)U(t-\tau)\\ \text{where } \Phi(t') &= L^{-1}\left\{e^{-\left(\frac{s\omega\beta\tau}{s+\omega}\right)}\right\}\end{aligned} \tag{B-11}$$

where U(t-r) is the unit step function. Solving for $\Phi(t')$:

$$\Phi(t') = L^{-1}\left\{\exp\left(\frac{\omega^2\beta\tau-(s+\omega)\omega\beta\tau}{s+\omega}\right)\right\} \tag{B-12}$$

by frequency shift:

$$\Phi(t') = e^{-\omega t'} L^{-1}\left\{\exp\left(\frac{\omega^2\beta\tau - s\omega\beta\tau}{s}\right)\right\} \qquad \text{(B-13)}$$

by rearranging:

$$\Phi(t') = e^{-\omega t'} L^{-1}\left\{e^{-\omega\beta\tau}\exp\left(\frac{\omega^2\beta\tau}{s}\right)\right\} = e^{-\omega(t'+\beta\tau)} L^{-1}\left\{\exp\left(\frac{\omega^2\beta\tau}{s}\right) - 1 + 1\right\} \qquad \text{(B-14)}$$

and using tables of inverse Laplace transforms (Roberts and Kaufman, 1966)

$$\Phi(t') = e^{-\omega(t'+\beta\tau)}\left[\omega^2\beta\tau\ \tilde{I}_1\left(\omega^2\beta\tau t'\right) + \delta(t')\right] \qquad \text{(B-15)}$$

where,

$$\tilde{I}_1(z) = \frac{I_1\left(2\sqrt{z}\right)}{\sqrt{z}}$$

I_1 is a modified Bessel function of the first kind of order one; and δ is the Dirac functions. Replacing t' with $(t\text{-}\tau)$ gives:

$$\Phi(t-\tau) = e^{-\omega(t-\tau+\beta\tau)}\left[\omega^2\beta\tau\ \tilde{I}_1\left(\omega^2\beta\tau(t-\tau)\right) + \delta(t-\tau)\right] \qquad \text{(B-16)}$$

Substituting back into eqn B-11 gives the final solution (eqn 3-9):

$$\gamma(t,\tau) = e^{-\omega\beta t}\delta(t-\tau) + \left(\omega^2\beta\tau\right)e^{-\omega(t-\tau+\beta\tau)}\tilde{I}_1\left[\omega^2\beta\tau(t-\tau)\right]H(t-\tau) \qquad \text{(B-17)}$$

For equations B-10 to B-17, the symbol t is dimensionless time and is equivalent to the symbol T in Chapters 3 and 4.

B.2.2 Expected Arrival Time for Maximum Concentrations

By setting the time derivative ($\delta/\delta T$) of eqn B-17 to zero, the expected arrival time for the peak concentrations can be estimated. Two solutions are found:

$$T = \tau \quad \text{or} \quad t = R_m \tau \left(\frac{I_{Y,H}}{\mathrm{U}} \right) \tag{B-18}$$

and for $T > \tau$

$$\omega^2 \beta \tau e^{-\omega(T-\tau+\beta\tau)}(-\omega)\left(\frac{I_1\left(2\sqrt{z}\right)}{\sqrt{z}} \right) + \omega^2 \beta \tau e^{-\omega(T-\tau+\beta\tau)}(2)\left(\frac{-I_2\left(2\sqrt{z}\right)}{2\sqrt{z}} \right)\left(\frac{-1}{\sqrt{z}} \right)\left(\omega^2 \beta \tau \right) = 0$$

$$-\omega\left(\frac{I_1\left(2\sqrt{z}\right)}{\sqrt{z}} \right) + \left(\frac{I_2\left(2\sqrt{z}\right)}{\sqrt{z}} \right)\left(\frac{\omega^2 \beta \tau}{\sqrt{z}} \right) = 0$$

$$\frac{I_1\left(2\sqrt{z}\right)}{I_2\left(2\sqrt{z}\right)} = \frac{\omega \beta \tau}{\sqrt{z}} \tag{B-19}$$

where

$$z = \omega^2 \beta \tau (t - \tau)$$

Eqn B-19 can be solved numerically. Bellin et. al. (1991) found a similar expressions for reactive solute transport in one-dimensional homogeneous porous media.

APPENDIX C

Modeling Sorption Processes for Nonpolar Organic Compounds in Saturated Soils

The theoretical basis for the sorption of organic compounds within natural soils and the development of empirical models representing these processes are reviewed and their applicability is discussed. The sorption of nonpolar organic compounds is identified as an instantaneous process at the soil-water interface. Observed nonequilibrium behavior is attributable to the aqueous phase mass transfer resistances within soil aggregates or pores. These physical nonequilibrium processes can be represented by mobile-immobile domain models.

C.1 Introduction

The presence of organic compounds in groundwater is a primary concern due to their potential toxicity . Organic compounds can enter the environment as the result of leaks or spills at industrial facilities, service stations, or waste disposal facilities. Efforts to determine where contamination will spread and the time required to clean-up contaminated groundwater are important in assessing the overall risk to drinking water supplies and the environment. The mobility of these compounds is controlled by a number of physical, chemical and biological processes. One of the primary processes is sorption by soil constituents. Modeling of the sorption process can enable the prediction of the transport of organics given a release or the time required to remove the organics from the subsurface using technologies such as pump-and-treat systems. This appendix reviews some of the current efforts to model the sorption of nonpolar organics.

The following appendix is divided into four sections. First, a theoretical basis is discussed for the sorption of organic compounds onto soils. Second, the various empirical models which have been used to model these processes are presented. Next, these theoretical and empirical approaches are then combined in the analysis of the modeling of nonpolar compound sorption. The last section presents conclusions based on this review.

C.2 Organic Chemical Interactions at the Water-Mineral Interface

C.2.1 Bonding Forces

The primary bonding forces of interest for the adsorption of organics on soils are summarized below (Weber et. al., 1991) :

Chemical interactions

- covalent bonding
- hydrogen bonding

Electrostatic interactions

- ion-ion
- ion-dipole

Physical interactions

- dipole-dipole (Coulombic)
- dipole-dipole (Keesom energy)
- dipole-induced dipole (Debeye energy)
- instantaneous dipole-induced dipole (London dispersion forces)

Hydrogen bonding is sometimes considered a special case of dipole-dipole bonding (McBride, 1994). Some of the entries under physical interactions are sometimes collectively referred to as van der Waals forces. These can include the last three entries (Israelachvilli, 1985; McBride, 1994) or only the London dispersion forces (Hamaker and Thompson, 1972). The bonding forces are listed in decreasing order of strength except that electrostatic interactions are typically stronger than hydrogen bonding. The strongest forces are covalent bonding with energies greater than 200 kJ/mole and the weakest are the London forces which are typically less than 10 kJ/mole (McBride, 1994).

It should be noted that organic compounds themselves are relatively stable in the ambient environment. This is due to the strength of the single, double, and triple covalent bonds as well as hydrogen bonds. For example, more than 800 kJ/mole of energy is required to reduce methane to carbon dioxide and water (Schwarzenbach et. al., 1993). As such, kinetics controls the reactivity of organic compounds rather than thermodynamics (Schwarzenbach et. al., 1993).

The bonding forces active in adsorption processes, though, are much weaker. In general, the primary forces for the adsorption of organics onto soil are van der Waals forces. For the adsorption of nonpolar organic compounds, the van der Waals forces, and in particular the London dispersion forces, are the most important (Hamaker and Thompson, 1972; McBride, 1994). For the adsorption of polar compounds the primary interaction forces are van der Waals forces, hydrogen bonding, and other dipole-dipole interactions (Chiou and Kile, 1994).

C.2.2 Hydrophobic Interactions

The attraction between nonpolar hydrocarbons and surfaces is often stronger in water than in free space. Predictions of this interaction energy based solely on van der Waals forces are on the order of 100 times less than observed experimental values (Israelachvilli, 1985). This increased interaction is attributable to an entropic phenomenon rather than a bonding mechanism (Israelachvilli, 1985).

When a nonpolar hydrocarbon dissolves in water, heat is released. The entropy of the solution, though, is negative. When the nonpolar hydrocarbon sorbs to a surface, the water returns to original structure and the entropy of the system increases. As such, sorption is thermodynamically favorable (Hamaker and Thompson, 1972).

The hydrophobic interaction can be referred to as an enhanced attraction between surface and sorbate. It is attributable to the solvent-sorbate attraction being weaker than the solvent-solvent attraction. In other words, the organic compound has less affinity for water than water has for itself (McBride, 1994).

C.2.3 Thermodynamics of the Adsorption Process

Adsorption processes can also be evaluated utilizing a thermodynamics framework. This typically includes analysis of the fugacity[1] of a compound in each phase and the total free energy of sorption. These are discussed individually in the following two subsections.

---

[1] from the Latin word *fuga* , meaning flight or escape

C.2.3.1 Fugacity

From a thermodynamic perspective, sorption equilibrium can defined as an equality of fugacities between phases:

$$f^s = f^w$$

$$f^s = \text{fugacity in the sorbed phase} \qquad \text{(C-1)}$$

$$f^w = \text{fugacity in the aqueous phase}$$

Fugacity or *escaping tendency* can be expressed in terms of mole fractions and activity coefficients:

$$f^i = x_{ai}\gamma_{ai}f_o^i$$

$$f_o^i = \text{reference fugacity in phase } i \qquad \text{(C-2)}$$

$$x_{ai} = \text{mole fraction of } a \text{ in phase } i$$

$$\gamma_{ai} = \text{activity coefficients of } a \text{ in phase } i$$

Fugacity corrects for the nonidealities of the system and is sometimes referred to as a *corrected pressure* (Prausnitz, 1986). The relationship between fugacity and mole fraction is nonlinear because the activity coefficients are also dependent on the mole fraction. An example is illustrated in Figure C-1 with the subscript 2 referring to the solute. The two most common normalizations are also shown. For the ideal mixture, the activity coefficients approach unity with the mole fraction. For the ideal dilute mixture, the activity coefficient approaches unity as the solute mole fraction approaches zero (Prausnitz, 1986).

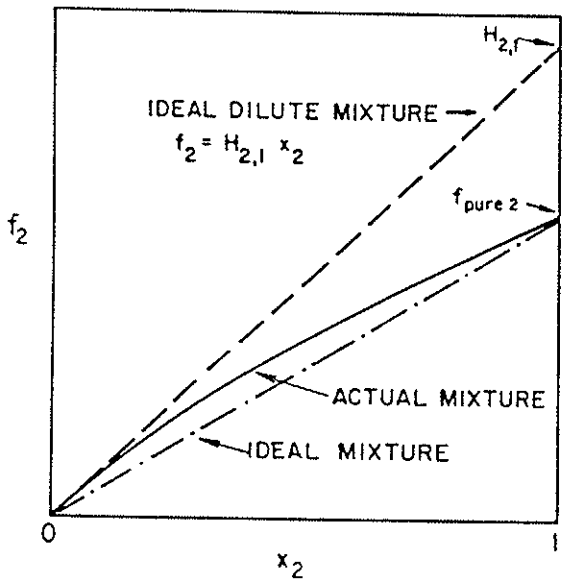

Figure C-1: Normalization of activity coefficients (from Prausnitz, 1986)

Substituting (C-2) into (C-1) and rearranging, the mole fraction in either phase can be expressed as a ratio of activity coefficients corrected by the mole fraction:

$$\begin{aligned} x_{as}\gamma_{as}f_o^s &= x_{aw}\gamma_{aw}f_o^w \\ x_{as}\gamma_{as}P_a^o &= x_{aw}\gamma_{aw}P_a^o \\ x_{as} &= \frac{\gamma_{aw}}{\gamma_{as}}x_{aw} \end{aligned} \qquad \text{(C-3)}$$

The resulting distribution between the aqueous and sorbed phase depends on the ratio of the activity coefficients which are concentration-dependent. For dilute systems, however, activity coefficients approach limiting values and the relationship becomes linear (Karickhoff, 1984). A constant activity coefficient over a range of solute concentrations indicates that the solute-solvent interactions remain of constant character over that range (Brusseau and Rao, 1989a). Environmental systems are typically dilute. This linear relationship has been used to explain experimental observations as discussed in the Section C-3.

C.2.3.2 Total Free Energy

By evaluating the terms that contribute to the total free energy of sorption from aqueous solutions, the most important interactions can be identified. The total energy of sorption (ΔE_T) as a function of the relevant energy terms is given by (McBride, 1994):

$$\Delta E_T = E_{S-W} + E_{A-W} - E_{W-W} - E_{S-A}$$

E_{S-W} = surface hydration energy

E_{A-W} = adsorbate hydration energy (C-4)

E_{W-W} = water - water bonding energy

E_{S-A} = surface adsorption energy

These energies represent the surface-water, organic compound-water, water-water, and surface-organic compound interactions, respectively. The importance of each of these is summarized in the Table C-1.

Table C-1: Important Energy Terms (McBride, 1994)

Adsorbate	Surface	E_{S-W}	E_{A-W}	E_{W-W}	E_{S-A}
Polar	Hydrophilic	x	x	x	x
Nonpolar	Hydrophilic	x		x	
Polar	Hydrophobic		x	x	
Nonpolar	Hydrophobic			x	

For the last case (nonpolar adsorbate onto hydrophobic surface), the water-water bonding energy is the only large term. This indicates that the sorption

process is controlled by the attraction forces between water molecules which coincides with the hydrophobic interaction discussed in the previous section.

C.3 Sorption Models for Organic Compounds

Many models for sorption have been developed based on experimental observations. Some of these have been combined with theoretical analysis to include particular relationships. The first subsection below presents the types of isotherms which have been observed experimentally. The second subsection discusses a number of models which have been developed to utilize isotherm data.

C.3.1 Adsorption Isotherms

Adsorption isotherms represent the equilibrium concentrations of a compound in the aqueous and sorbed phase. In general, there are four types of isotherms as illustrated in Figure C-2. The L-type reflects an adsorbate's high affinity for the adsorbent but with a limited sorbent capacity or single layering of adsorbate. The S-type represents adsorbates which are more strongly attracted to each other than the surface and can indicate multiple layering of adsorbate on the surface. The C-type represents a constant affinity which is independent of the adsorbate concentration on the surface. This type of isotherm is usually limited to low concentrations. The H-type represents a very high affinity for the adsorbent and is an extreme case of the L-type (McBride, 1994).

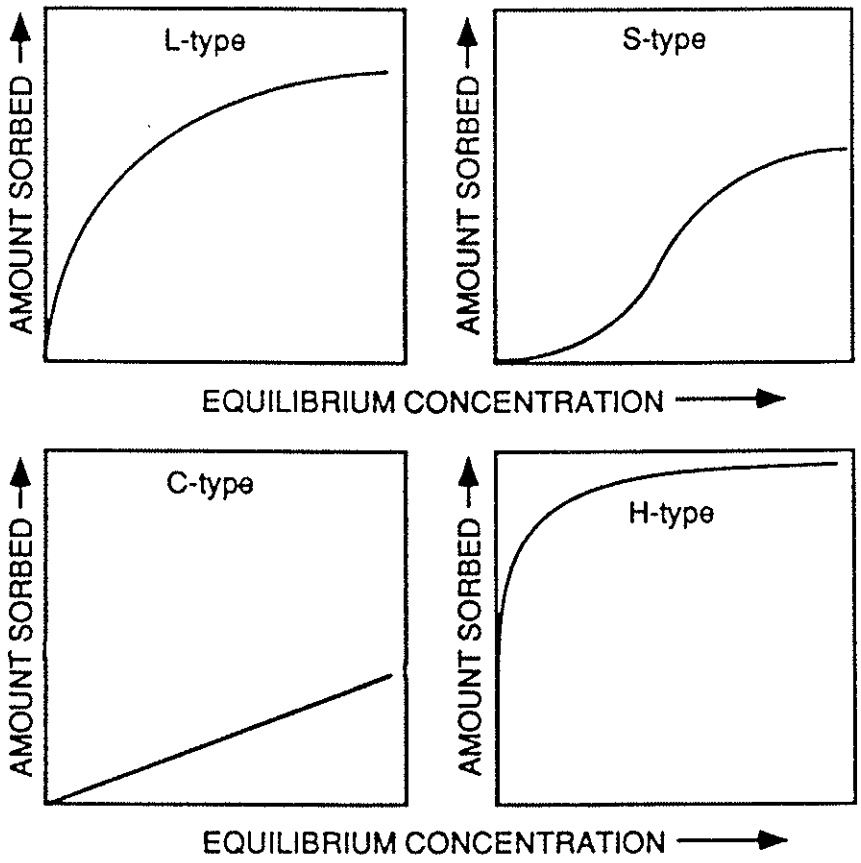

Figure C-2: Classification of adsorption isotherms (from McBride, 1994)

The isotherm type and apparent affinities for nonpolar and polar (uncharged) compounds are listed in Table C-2.

Table C-2: Sorption Affinities (adapted from McBride, 1994)

Molecule Type	Affinity for	Isotherm Type
Nonpolar	hydrophobic organic phases in humid acid	C or S
Polar	humid polar groups	L

C.3.2 Types of Models

The two assumptions which define most models used for analyzing the sorption of organic compounds onto soils are 1) whether or not the sorption process is assumed to be instantaneous (equilibrium or non-equilibrium) and 2) whether the relationship between the soil and aqueous concentration is assumed to be linear or non-linear. The most utilized equilibrium models are (Travis and Etnier, 1981):

Equilibrium Adsorption Isotherms

$$\text{linear adsorption} \qquad S = K_d C$$

$$\text{Freundlich} \qquad S = KC^N$$

$$\text{Langmuir} \qquad S = \frac{kbC}{1+kC}$$

The latter two are nonlinear models. The Langmuir is analogous with the L-type isotherm shown previously in Figure C-2. Other variations include the

two-site and competitive Langmuir (Travis and Etnier, 1981). The Langmuir represents a monolayer of adsorbate on the surface. Other models represent multiple layers of adsorbate on the surface. One of the more common forms of multiple layering models is the BET (Brunaer, Emmett, and Teller) model. The resulting isotherm is similar to the S-type.

The most common nonequilibrium models represent first-order kinetics (list adapted from Travis and Etnier, 1981):

First-Order Kinetic Sorption Models

reversible linear	$\frac{dS}{dt} = k_1 \frac{\theta}{\rho} C - k_2 S$
reversible nonlinear	$\frac{dS}{dt} = k_1 \frac{\theta}{\rho} C^N - k_2 S$
bilinear adsorption	$\frac{dS}{dt} = k_1 C(b - S) - k_2 S$
two - domain / mass transfer	$\frac{dS}{dt} = k\left(S^* - S\right)$ or $\frac{dC}{dt} = \alpha\left(C^* - C\right)$
two - site kinetic	$\frac{\partial S}{\partial t} = f\left(k_1 \frac{\theta}{\rho} C - k_2 S\right) + (1-f) k_3 \frac{\theta}{\rho} \frac{\partial C}{\partial t}$

For the two domain model, if the mass transfer resistance is within the sorbed phase then the first expression is used and (S^*-S) is the driving force with S^* being the solute concentration at the soil-water interface (commonly set to $K_d C$). If the mass transfer resistance is within the aqueous phase then the second expression is used. The two-site kinetic model listed above was first used by Cameron and Klute (1977). A nonlinear version was independently introduced by Selim et. al. (1976). Other variations of the two-site model include box and bicontinuum models (as well as multiple site models). Other

variations of the above models are the kinetic product, Elovich, Fava and Erying models (Travis and Etnier, 1981).

Most sorption data exhibits two stages -- an initial rapid rate followed by a much slower rate. This initial rate typically accounts for approximately 50% of the total sorption (Lee et. al., 1988; Brusseau and Rao, 1989a) This type of phenomenon has lead to the development of two-site and two-domain models. For the two-site models, one type of site represents an instantaneous equilibrium site while the other represents a nonequilibrium site. For two-domain models, the sorption process is assumed to be effectively instantaneous at the water-sorbent interface and its rate is controlled by the rate at which the solute is transported to and from the interface. Van Genutchen and Wierenga (1976) were one of the first to develop a conceptual and mathematical model for this phenomenon. The premise is that flow occurs only in mobile water regions where the contaminant is transported by advection. The contaminant can only enter or exit the immobile water regions only by diffusion. These immobile regions are located within soil aggregates or dead-end pores. In both the mobile and immobile regions, the contaminant will undergo adsorption and desorption into the soil matrix. Assuming that the adsorption-desorption process is instantaneous, the rate of sorption will be controlled by the transfer of solute into and out of the immobile regions. This model of the sorption process has been typically referred to as the mobile-immobile domain model.

The concept of the two-site and two-domain models has been expanded to include multiple sites and/or more complex processes. There are

bicontinuum models where the two sites or domains are interconnected (Lee et. al., 1988;Brusseau and Rao, 1989a;Larsen et. al., 1992); dual-porosity models (Brusseau et. al., 1994) and two-box models (Wu and Gschwend, 1986).

C.3.3 Utilization of Isotherms and Models

There are a number of difficulties in fitting experimental data to any of the above mentioned isotherm models. A good fit does not necessarily indicate that the selected model is the most appropriate. For example, a model which assumes a small number of high affinity sites can often fit the data as well as a model which assumes a large number of low affinity sites (Kinniburgh, 1986). In general, models which much different theoretical basis can be mathematical analogous. For example, the *reversible linear* and *mass transfer* models listed above are mathematical analogous.

Slight differences can be amplified when these isotherms are used in conjunction with a transport model. Hinz et. al. (1994) fit a number of different isotherms to the same set of experimental data and then utilized these in a simulation model. Isotherms which fit the lab data with approximately the same level of accuracy gave substantial different results. In particular, some of the isotherms did not produce the tailing of concentrations which is typically observed in the field. With this in mind, only isotherms with some level of theoretical basis should be utilized.

C.4 Selecting Sorption Models for Nonpolar Organic Compounds in Saturated Soils

Chemical Interactions

The primary bonding forces for the adsorption of nonpolar organic compounds onto mineral surfaces of soils are van der Waals forces (McBride, 1994). These weak bond forces are complemented by the hydrophobic effect. In many cases, the sorption process is dominated by these hydrophobic interactions (Karickhoff, 1984). For these instances, the sorption process is controlled by water-water interactions (see Table C-1) and is independent of the aqueous and soil concentration of the organic compound since the energies of the organic-sorbent and organic-water interactions are relatively insignificant. As such, the sorption of nonpolar organic compounds can often be modeled by a linear relationship.

Linear Equilibrium Models

The adsorption isotherm observed experimentally for nonpolar organic compounds is typically linear or of the C-type (Karickhoff, 1979; McBride, 1994). This linear relationship can be expressed in a linear, equilibrium model in terms of concentrations and a linear coefficient, referred to as a partition coefficient (K_p):

$$S = K_p C \tag{C-5}$$

S = sorbed concentration

C = aqueous concentration

The partition coefficient K_p has units of soil concentration over aqueous concentration. These units can vary from study to study but are most often L/kg which represents parts per million for both phases[2].

For nonpolar organic compounds, sorption onto soils has been found to be controlled by the amount of organic carbon present in the soil (Karickhoff, 1984; Weber et. al., 1991;Chiou and Kile, 1994). Figure C-3 illustrates this relationship for a soil before and after it has been stripped of organic matter. As can be seen, the sorption onto the soil is orders of magnitude greater when the organic matter is present. For this reason, the sorption process is often modeled as sorption onto soil organic matter or carbon rather soil mineral surfaces. The partition coefficient (K_p) in (7) is replaced $f_{oc}K_{oc}$ where f_{oc} is the fraction of organic carbon in the soil and K_{oc} is the partition coefficient for organic carbon and water:

$$S = f_{oc} K_{oc} C \tag{C-6}$$

This expression can also be derived from a thermodynamic prospective. The partitioning of a nonpolar organic compound between organic carbon (oc) and water(w) can be represented as follows (using the vapor pressure P^o for the reference fugacity):

$$\begin{aligned} f_a^{oc} &= f_a^w \\ x_{aoc}\gamma_{aoc} f_o^{oc} &= x_{aw}\gamma_{aw} f_o^w \\ x_{aoc}\gamma_{aoc} P_a^o &= x_{aw}\gamma_{aw} P_a^o \\ x_{aoc} &= \frac{\gamma_{aw}}{\gamma_{aoc}} x_{aw} \end{aligned} \tag{C-7}$$

[2]units of [(mg of a)/(kg of soil)] / [(mg of a)/(L of water)] = (L of water) / (kg of soil).

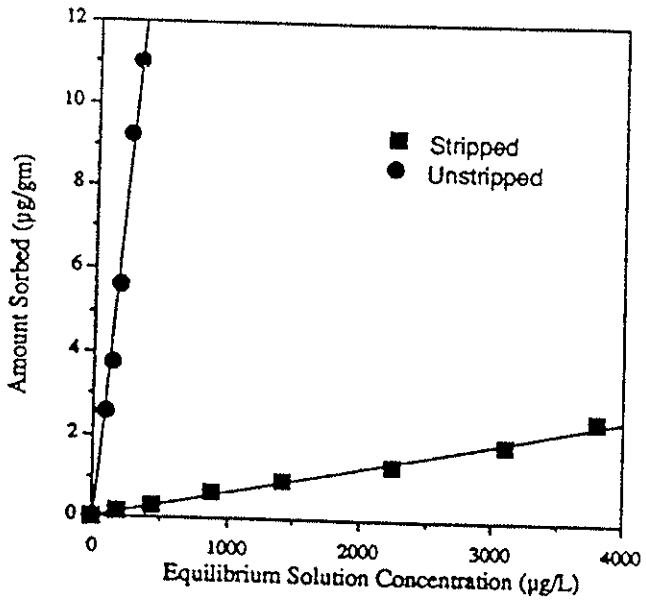

Figure C-3: Sorption of lindane on soil before (unstripped) and after (stripped) removal of soil organic matter (from Weber et. al., 1991)

The mole fraction of the compound in the organic carbon can be related to mole fraction in soil by f_{oc} and the mole fractions can be expressed in concentrations.

$$x_{as} = f_{oc} x_{oc} = f_{oc} \frac{\gamma_{aw}}{\gamma_{aoc}} x_{aw}$$
$$C_{as} = f_{oc} \frac{\gamma_{aw}}{\gamma_{aoc}} C_{aw} \qquad \text{(C-8)}$$

For a dilute system, the ratio of activity coefficients can be replaced with a constant and the result is identical to eqn C-6.

$$C_{as} = f_{oc} K_{oc} C_{aw} \qquad \text{(C-9)}$$

Efforts have been undertaken to relate K_{oc} to K_{ow} (the octanol-water partition coefficient). Both represent a distribution of a solute monomer between an aqueous and hydrophobic phase (Karickhoff, 1984). K_{ow} values are much more readily available in the literature and provide a convenient means to predict the expected aqueous and sorbed concentration. Figure C-4 illustrates the observed relationship for K_{oc} and K_{ow}. Karickhoff (1979) found that the ratio of K_{oc} to K_{ow} is approximately 0.6. The soil concentration can then be expressed as:

$$C_{as} = 0.6\, f_{oc} K_{ow} C_{aw} \qquad \text{(C-10)}$$

It should be noted that this expression is only valid in systems where the aqueous concentration is less than half of its solubility and an adequate amount of organic carbon is present. The threshold where the organic carbon

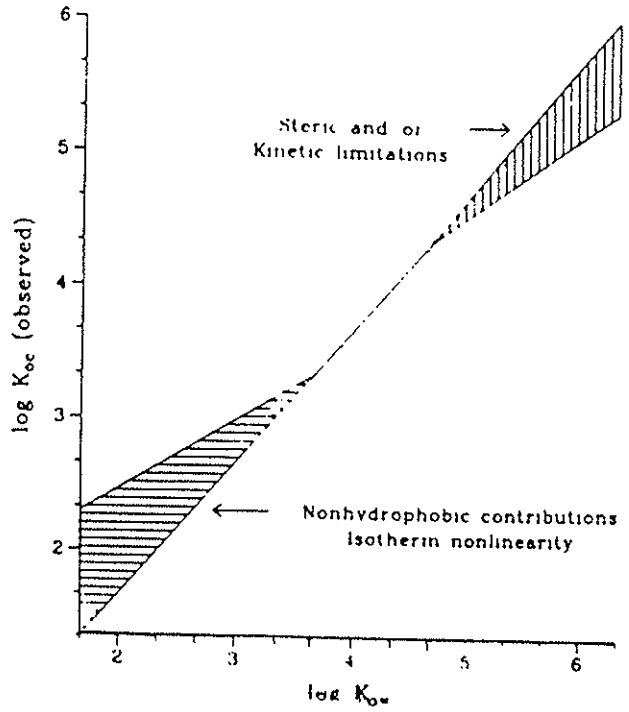

Figure C-4: K_{oc} extrapolation from K_{ow} (from Karickhoff, 1984)

content is too low and mineral surfaces begin to play a partial role varies from system to system (Karickhoff, 1984). In general, this relationship is usually within an order of magnitude with experimental measurements and can often provide an adequate preliminary estimate of expected soil concentrations.

More recent studies have suggested that organic compounds which have been previously deposited in soils do not follow this relationship and that the K_{oc} value is much higher. Kile et. al. (1995) found that K_{oc} values were invariant for series of soils analyzed but were twice as high for river bed sediments.

Despite these concerns, eqn C-10 is still widely used in engineering applications. For example, eqn C-10 is typically utilized in risk assessment analysis to determine the mobility of an organic contaminant (U.S. EPA, 1986a; 1986b). The Superfund Public Health Evaluation Manual (U.S. EPA, 1986b) includes K_{oc} values based on reported K_{ow} values from the literature for a large number of compounds.

Karickhoff (1979) also attempted to relate K_{oc} to aqueous solubility. This relationship would be expected since the activity coefficient γ_{aw} is equal to the inverse of the mole fraction solubility for hydrophobic liquids. Experimentally, though, this relationship has not been adequately established.

Linear Equilibrium-Nonequilibrium Models

As mentioned in Section C.3.2, most sorption data exhibits two stages -- an initial rapid rate followed by a much slower rate. This type of phenomenon

has lead to the development of two domain and two-site models. For nonpolar organic compounds, the two domain approach is the more appropriate since the sorption process at the water-sorbent interface is expected to be relatively instantaneous.

Wood et. al. (1990) utilized a scanning electron microscopy technique to show that there were interior reaction sites with grains that were only reachable by diffusion within the pore. Their results suggest that it is necessary to include a mass transfer diffusion term in a transport model to adequately model the system. Wu and Gschwend (1986) found that sediments that were sonicated approached equilibrium faster than the original undisturbed sediments. The authors concluded that the increase in sorption rate was the result of the reduced diffusive path length.

C.5 Conclusions and Additional Considerations

This appendix has presented a review on the modeling of sorption of nonpolar organic compounds onto soils. Based on this analysis the following conclusions can be made. For the sorption of nonpolar compounds onto soils, the primary bonding forces are van der Waals forces (London dispersion forces) which are complemented by hydrophobic interactions. When hydrophobic interactions dominate, sorption can be modeled as a linear process since these interactions are not concentration dependent. In certain instances, equilibrium models are adequate while under other circumstances, sorption modeling should also include a nonequilibrium component to

account for mass transfer limitations within the aqueous phase. The most appropriate model is a linear mobile-immobile domain model.

Though there have been many studies examining the sorption of specific nonpolar organic compounds onto particular soils, there are still many areas of research which have not been thoroughly investigated. These include, but are not limited to:

- The sorption of nonpolar organic compounds onto soils with a low organic content deserves more study. The point at which mineral surfaces begin to play a role in the sorption process needs to be better understood.
- Correlations between chemical and physical heterogeneities can enhance or reduce the spreading of solute plumes. Field-scale studies addressing the type and magnitude of these correlations have been limited. Some research has suggested that chemical heterogeneities are negatively correlated with physical heterogeneities. Tompson et. al. (1995) suggested that the distribution K_d is inversely proportional to the square root of the permeability of the soil. There have been several field studies involving metals. Robin et. al. (1991) found a correlation coefficient r of -0.13 between the distribution coefficient for strontium ($K_{d,Sr}$) and the hydraulic conductivity (K). Davis et. al. (1993) found a r = -0.29 between $K_{d,Pb}$ and K and r = -0.089 between $K_{d,Zn}$ and K. These negative correlations would result in enhance plume spreading in the field (Valocchi, 1989; Bosma et. al., 1993). On the other hand,

preliminary findings by Halket et. al. (1995) indicate that $K_{d,PCE}$ and K at the Borden site have a slightly positive correlation. There is still much uncertainty regarding the magnitude and sign of any correlation between sorption and hydraulic conductivity and this area warrants further study.

- The aging process also needs further investigation. Contaminants which have been present in soils for an extended period of time are often more resistant to desorption. Further investigation and understanding of this phenomena are necessary to better predict the time required to remove contaminants from the subsurface.

Lastly, a major constraint in developing sorption models is the inability to observe sorption processes on the microscopic scale. As such, it is necessary to use indirect techniques to test hypothesis. Macroscopic analysis can only suggest that the hypothesis can not be refuted but can not be used to prove it.

References

The references for this appendix are listed in Chapter 6 with the other references for this dissertation.

APPENDIX D

Estimating Sorption Parameters for the Borden Site

In Section 3.4.3, the input sorption parameters used to model the Borden site are presented and discussed. This appendix includes the additional computations performed to determine these sorption parameters. Tables D-1 lists the subsurface hydraulic properties used in these calculations. Table D-2 lists the input sorption parameters (K_d, α , and f).

Table D-1: Selected Subsurface Hydraulic Properties for Borden

Parameter	Value	Source
average linear velocity (U)	0.91 m/d	Mackay et. al. (1986)
porosity (θ)	0.33	Mackay et. al. (1986)
soil bulk density (ρ_b)	1.81 g/cm^3	Mackay et. al. (1986)
horizontal integral scale of Y ($I_{Y,H}$)	5.1 m	Woodbury and Sudicky (1991)
fraction of water in the mobile zone (ϕ)	0.87	Goltz and Roberts (1988)

Table D-2: Sorption Parameters for PCE and Borden Soil

Parameter	Value	Source
SCENARIO 1:		
mass transfer coefficient (α)	0.0046 / day	estimated used data from Ptacek and Gilham (1992)
distribution coefficient (K_d)	0.76 mL/g	Ball and Roberts (1991a)
fraction of sorption sites in the mobile zone (f)	0.32	estimated using data from Curtis et. al. (1986)
SCENARIO 2:		
mass transfer coefficient (α)	0.0076 / day	estimated using data from Ball and Roberts (1991b)
distribution coefficient (K_d)	0.76 mL/g	Ball and Roberts (1991a)
fraction of sorption sites in the mobile zone (f)	0.25	calculated using data from Ball and Roberts (1991a)

The non-dimensional parameters required are R_m, R_{im}, β, and ω. Their definitions are as follows:

$$R_m = 1 + \frac{\rho_b f K_d}{\theta_m} = 1 + \frac{\rho_b f K_d}{\phi\theta} \tag{D-1}$$

$$R_{im} = 1 + \frac{(1-f)\rho_b K_d}{\theta_{im}} = 1 + \frac{(1-f)\rho_b K_d}{(1-\phi)\theta} \tag{D-2}$$

$$\beta = \frac{1-\phi}{\phi}\frac{R_{im}}{R_m} \tag{D-3}$$

$$\omega = \frac{\alpha}{\theta(1-\phi)R_{im}}\frac{R_m I_{Y,h}}{U} \tag{D-4}$$

Scenario 1

For the first scenario, f was estimated based on the ratio between the sorption which occurs almost instantaneously during batch equilibrium tests and the asymptotic values. The assumption is that only sorption sites within the mobile zones of the soil would be immediately available. The results from Curtis et. al. (1986) indicate that the K_d would be approximately 0.24 mL/g after the initial contact period (less than 2 hours of equilibration time). Given that the true K_d is 0.76 mL/g, f was estimated to be 0.32.

$$f = \frac{0.24 ml/g}{0.76 ml/g} = 0.32$$

Using eqns D-1 and D-2 and the values in Tables D-1 and D-2, R_m and R_{im} are 2.53 and 22.8, respectively.

$$R_m = 1 + \frac{\left(1.81 g/cm^3\right)(0.32)(0.76 mL/g)}{(0.87)(0.33)} = 2.53$$

$$R_{im} = 1 + \frac{\left(1.81 g/cm^3\right)(0.68)(0.76 mL/g)}{(0.13)(0.33)} = 22.8$$

Using eqn D-3, β is 1.35.

$$\beta = \frac{(0.13)}{(0.87)}\frac{(22.8)}{(2.53)} = 1.35$$

The mass transfer parameter for the first scenario was selected using the results from the two low flow column tests performed by Ptacek and Gilham (1992). The column flow rate and length were 18 cm/d and 10 cm, respectively. Their results were reported as fitted parameters to a two-site kinetic model but these can be adapted to a mobile-immobile model due to the mathematical similarities between the models (Nkedi-Kizza et. al., 1984). The definition of the mass transfer parameter ω used in eqn D-4 is different from that defined by Nkedi-Kizza et. al. (1984). Rearranging eqn D-4 and multiplying by (ϕ/ϕ) gives the relationship between the two different definitions:

$$\omega = \frac{\alpha I_{Y,h}}{\phi\theta U}\frac{\phi R_m}{(1-\phi)R_{im}} = \frac{\alpha I_{Y,h}}{\theta_m U}\frac{\phi R_m}{(1-\phi)R_{im}} = \omega'\frac{\phi R_m}{(1-\phi)R_{im}} \qquad \text{(D-5)}$$

where ω' is the parameters as defined by Nkedi-Kizza et. al. (1984). In analyzing the data from Ptacek and Gilham (1992), the first step is to convert their results from a 2-site model to the mobile-immobile model. The fitted rate coefficient from their two experiments were 1.5 and 1.7 day^{-1}. The average value was used to calculate the equivalent parameter ω'.

$$\omega' = \frac{(1.6/d)(10cm)}{18cm/d} = 0.89$$

Then using eqn D-5 the parameter ω is found to be 0.661.

$$\omega = (0.89)\frac{(0.87)(2.53)}{(0.13)(22.8)} = 0.661$$

The equivalent mass transfer coefficient α can be calculated by rearranging eqn D-4 and is found to be 0.0046/day.

$$\alpha = (0.661)(0.33)(0.13)(22.8)\frac{0.091m/d}{(2.53)(5.1m)} = 0.0046/d$$

Scenario 2

For the second scenario, surface area measurements from Ball and Roberts (1991a) were used to estimate f. The measured surface area for the bulk sample was 0.42 m^2/g and for the pulverized soil was 1.7 m^2/g. The resulting estimation for f is 0.25.

$$f = \frac{0.42m^2/g}{1.7m^2/g} = 0.25$$

Using eqns D-1 and D-2 and the values in Tables D-1 and D-2, R_m and R_{im} are 2.2 and 25.05, respectively.

$$R_m = 1 + \frac{\left(1.81 g/cm^3\right)(0.25)(0.76 mL/g)}{(0.87)(0.33)} = 2.2$$

$$R_{im} = 1 + \frac{\left(1.81 g/cm^3\right)(0.75)(0.76 mL/g)}{(0.13)(0.33)} = 25.05$$

Using eqn D-3, β is 1.7.

$$\beta = \frac{(0.13)}{(0.87)}\frac{(25.05)}{(2.2)} = 1.7$$

For the second scenario, the selection of the α is more direct than in the first scenario. Ball and Roberts (1991b) estimated a form of mass transfer coefficient from their series of batch equilibrium experiments. Their estimated coefficient of 1.8 x 10^{-7}/s was a lumped parameter accounting for intraparticle diffusivity, tortuosity, constrictivity, and interior grain retardation and is referred to here as α'. These additional processes are accounted for separately in eqn D-4. The relationship between this parameter and the parameter α is shown below:

$$\alpha' = \alpha \frac{R_m}{\theta(1-\phi)R_{im}} \qquad \text{(D-6)}$$

The parameter α' is equivalent to a dimensional form of the parameter ω.

The mass transfer coefficient α is found to be 0.0076/day.

$$\alpha = \left(1.8\times10^{-7}\ /\ s\right)\left(\frac{(0.33)(0.13)(25.05)}{2.2}\right)\left(\frac{86400s}{d}\right) = 0.0076\ /\ d$$

Using eqn D-4 and D-6, ω is 0.872.

$$\omega = \frac{\alpha}{\theta(1-\phi)R_{im}}\frac{R_m I_{Y,h}}{U} = \alpha'\frac{I_{Y,h}}{U} = \left(1.8\times10^{-7}\ /\ s\right)\left(\frac{5.1m}{0.091m\ /\ d}\right)\left(\frac{86400s}{d}\right) = 0.872$$

As noted previously, all of the selected model input sorption parameters are based on laboratory experiments and none have been fitted to field observations. This approach to selecting input parameters is necessary since many of the rate-limited sorption processes can be modeled in a mathematically analogous manner (Nkedi-Kizza et. al., 1984).